MASTER´S THESIS

TURKU AMK
TURKU UNIVERSITY OF APPLIED SCIENCES

Andrei Hudik

Study on buckling behavior and strength of typical bulkhead structures under compressive pillar loads using nonlinear finite element techniques.

Thesis submitted for examination for the degree of Master of Engineering in Technology.

THESIS SUPERVISORS:
Andreas Baumgart (D.Sc) Jari Lahtinen (D.Sc)

THESIS ADVISORS:
Heikki Lammi (M.Sc) Ari Niemelä (M.Sc)

Turku University of Applied Sciences
Faculty of Engineering and Business

Joukahaisenkatu 3,
20520 Turku, Finland.
Abstract of the master´s thesis

Author: Andrei Hudik

Title of thesis: Study on buckling behavior and strength of typical bulkhead structures under compressive pillar loads using nonlinear finite element techniques

Degree Programme: Master of Engineering, Marine Technology	**Degree programme language:** English
Thesis supervisors: Andreas Baumgart (D.Sc), Jari Lahtinen (D.Sc)	
Thesis advisors: Heikki Lammi (M.Sc), Ari Niemelä (M.Sc)	

Date: 22.12.2021	**Number of pages:** 113	**Thesis language:** English

Abstract

The main aim of the present Master´s thesis is to study the behavior and failure mechanisms of typical bulkhead structures under compressive pillar loads and to check if the actual behavior of the structures is adequately taken into account in current prevalent simplified analytical loading capacity verification procedures.

To take different sources of nonlinearities, essential for the buckling problems, into account Materially and Geometrically Non-Linear Finite Element Method with Imperfections (GMNIA) was selected as the main research tool. The research was conducted in several phases, where each phase was related to the different relevant structural behavior aspects. Such aspects as the impact of the boundary conditions existing in real ship structures, eccentricity in load application, the impact of various initial imperfections, global buckling- and localized failure modes were addressed. Multiple models with different structural member sizes and arrangements were analyzed, providing extensive coverage on the behavior of typical bulkheads that exist in ship hulls in the way of pillar lines.

The validation study found a good correlation between the analytical solutions and numerical simulations for the idealized columns. However, small systematic deviations were observed for certain types of the columns. The deviation was minimized by replacing the Johnson-Ostenfield plasticity correction in the analytical method with that by European buckling curves in accordance with Eurocode 3. The study discusses the simplifications and limitations of the analytical method when applied to the realistic bulkhead structures. During the imperfection sensitivity study, realistic continuous bulkhead structures showed relatively low imperfection sensitivity when distortion magnitudes being within the manufacturing tolerances. The low imperfection sensitivity was explained by the constraint provided by the continuous bulkhead plate and by the inherent eccentricity, which guide the deformation in a certain direction, and, also, by the fact that some of the studied structures experience failure governed by the material yielding. Localized failure modes, which are not accounted in the common systematic capacity checking procedure, were detected during the analyses on the realistic bulkhead structures. Recommendations on the current checking procedure supplementation are given and structural solutions are proposed to decrease the risks of the occurrence of localized failures.

Keywords: Ship structural design, bulkhead, pillar, buckling, strength, Finite Element Analysis, failure modes, imperfections

Turun Ammattikorkeakoulu Joukahaisenkatu 3,
Tekniikka ja liiketoiminta -sektori 20520 Turku, Finland.
YAMK opinnäytetyön tiivistelmä

Työn nimi: Tutkimus tyypillisten laipiorakenteiden nurjahdus- ja lujuuskäyttäytymisestä puristuvien pilarikuormien alaisina käyttämällä epälineaarisen elementtimenetelmän		
Koulutusohjelma: Master of Engineering, Marine Technology		**Opiskelukieli:** Englanti
Työn valvojat: Andreas Baumgart (D.Sc), Jari Lahtinen (D.Sc)		
Työn ohjaajat: Heikki Lammi (M.Sc), Ari Niemelä (M.Sc)		
Päivämäärä: 22.12.2021	**Sivumäärä:** 113	**Opinnäytetyön kieli:** Englanti

Tiivistelmä

Opinnäytetyön päätavoitteena oli tutkia tyypillisten laipiorakenteiden käyttäytymistä ja murtumismekanismeja puristavien pilarikuormien alaisina sekä tarkistaa onko rakenteiden käyttäytyminen riittävästi huomioitu nykyisissä vallitsevissa analyyttisissä kuormituskapasiteetin tarkistusmenetelmissä.

Erilaisten epälineaarisuuksien huomioon ottaminen on tärkeää stabiliteettiongelmia ratkaistaessa. Siksi tutkimuksen päätyökaluksi valittiin geometrisesti ja materiaalisesti epälineaarinen alkuhäiriöitä sisältävä elementtimenetelmä (GMNIA). Riittävän kattavuuden saavuttamiseksi tutkimus jaettiin useaan vaiheeseen, joissa tutkittiin erilaisten tekijöiden vaikutusta rakenteen käyttäytymiseen. Tutkittavia osakokonaisuuksia olivat reunaehtojen vaikutus, kuormituksen epäkeskeisyys, alkumuodonmuutosten vaikutus, globaali nurjahdus ja paikalliset vauriomuodot. Tutkimuksessa tarkasteltavista laipiorakenteista tehtiin useita variaatioita. Tavoitteena oli saavuttaa kattava kuva laivojen rungoissa pilareiden alla olevien laipiorakenteiden käyttäytymisestä.

Validointitutkimuksessa havaittiin hyvä korrelaatio analyyttisten ratkaisujen ja idealisoituen pystypalkkien käyttäytymisen numeeristen simulaatioiden välillä. Tuloksissa havaittiin kuitenkin pieniä systemaattisia poikkeamia tietyntyyppisten pystypalkkien kohdalla. Poikkeamat minimoitiin korvaamalla Johnson-Ostenfieldin plastisuuskorjauksen analyyttisessä menetelmässä Eurocode 3:n vastaavalla. Työssä on pohdittu tarkasteltavan analyyttisen menetelmän yksinkertaistuksia ja rajoituksia realistisiin laipiorakenteisiin sovellettuna. Alkuhäiriöherkkyystutkimuksessa realistiset jatkuvat laipiorakenteet osoittivat suhteellisen alhaista herkkyyttä alkumuodonmuutoksille niiden ollessa valmistustoleranssien sisällä. Alhainen alkuhäiriöherkkyys selittyi jatkuvan laipiolevyn tuella sekä epäkeskeisyydellä, jotka ohjaavat deformaation määrättyyn suuntaan sekä sillä, että osa tutkituista rakenteista vaurioitui materiaalin plastisoitumisen seurauksena. Analysoitaessa realistisia jatkuvia laipiorakenteita havaittiin paikallisia vauriomuotoja, joita esiintyy standardisoitujen pilari-laipio-liitosten rakenteesta johtuen ja joita ei ole huomioitu yleisessä systemaattisessa laipiorakenteiden kapasiteetin tarkistusmenettelyssä. Sen perusteella annettiin suosituksia tarkastusmenettelyn täydentämiseksi ja ehdotettiin rakenteellisia ratkaisuja, jotka vähentävät paikallisten vaurioiden esiintymisriskiä.

Asiasanat: Laivan rakennesuunnittelu, laipio, pilari, nurjahdus, lujuustekniikka, elementtimenetelmä, vauriomuodot, alkuhäiriöt

CONTENTS

LIST OF FIGURES

LIST OF TABLES

ABBREVIATIONS

CFM	Closed form method
DOF	Degree of freedom
DNV	Det Norske Veritas
EUGLI	Equivalent Unique Global and Local Imperfection
GL	Germanischer Lloyd
GMNIA	Geometrically and Materially Nonlinear Analysis with Imperfections
GT	Gross tonnage
HP	Holland Profile
FB	Flat bar
FE	Finite element
FEA	Finite element analysis
FEM	Finite element method
IACS	International Association of Classification Societies
LA	Linear Static Analysis
LDC	Load-Displacement Control
LBA	Linear Buckling Analysis
MNA	Materially Nonlinear Analysis
NA	Nonlinear Analysis
SOL	Solution

SYMBOLS

Frequently used symbols are defined below. Symbols not defined here are explained in the text.

A	Area of the member cross-section
b_e, b_{em}	Width of the effective flange and its minimum value
Δ, δ	Imperfection amplitude
E	Young's Modulus
ε	Strain
F	Pillar load
η	Buckling utilization factor
λ	Slenderness parameter
l	Length of column
ν	Poisson's ratio
s	Stiffener spacing
σ	Normal stress
σ_{cr}	Minimum critical buckling stress
σ_E	Minimum elastic buckling stress
σ_{VM}	Von-Mises stress
σ_{yield}, R_eH	Minimum yield stress of material of the considered member
τ	Shear stress
t	Thickness (of the bulkhead plating)

1 INTRODUCTION

1.1 Background

Modern cruise ship designs include a considerable amount of large open areas in machinery and public spaces as well as in accommodation. In such open areas, pillars are placed to provide support to the decks, reduce deck beam spans, and tie the structure together in a vertical direction.

Pillars carry the weight of the decks vertically down to the ship's bottom structure where loads are supported by the upward buoyant forces (Eyres, 2001).

Most of the pillars in ship structure primarily experience compression loading, while some pillars also experience high tensile loadings. Pillars are very effective structural members and are capable of carrying relatively high loads. Loads with a magnitude of a few thousand kilonewtons per pillar are common in cruise ship structures.

The most common shape of the pillar in cruise ship hulls is a circular-tubular section, which is also the most effective shape for handling the compressive loading. Rectangular pillars are common in superstructure and are used to maximize the efficiency of the interior space arrangement, mostly in the cabin areas. Pillars made of solid sections or built-up open sections are used in tanks, as hollow sections are not allowed inside tanks (DNV GL, 2018a, Pt.3 Ch.3. Sec 6, [4.1.5]).

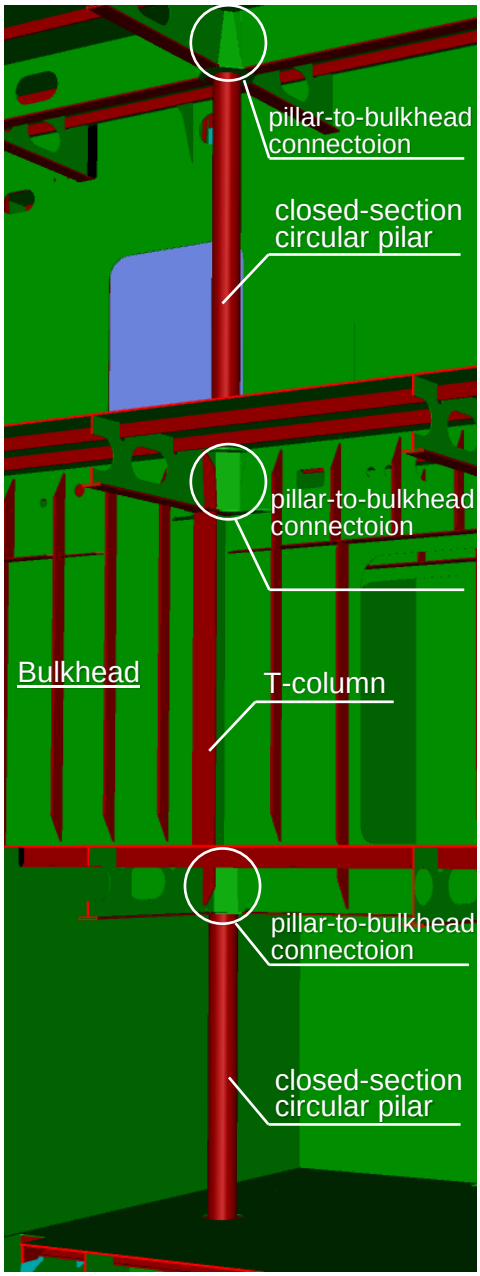

Figure 1. Typical bulkhead structure with T-shaped column in a way of pillar

Pillar lines are mostly continuous, starting from the top and continuing down to the ship´s bottom; however, continuous pillar lines are interrupted by the bulkheads (Figure 1). These bulkheads are of two types: “main”

structural, watertight, or fire-bulkheads; and “minor” bulkheads set for a purpose of compartment subdivision (Eyres, 2001). Especially there are quite a few randomly positioned minor bulkheads in the superstructures of cruise ships. Usually, such minor interior bulkheads are of a little structural importance and correspondingly are made of light scantlings. However, in cases where they are positioned in the way of pillars, they must be capable of either transferring the load coming from the pillar to the pillar at another side of the bulkhead or distributing it to the surrounding structure.

For manufacturability reasons, including requirements of automated panel-lines (as continuous panels with stiffeners positioned at one side of the bulkhead plate are preferred), the most common solution is to fit a T-shaped column on top of the bulkhead plate in the way of a pillar (Figure 1). The column with the effective part of the bulkhead plating must be sufficient to carry loads coming from the pillar. In case of high tensile loading, the pillar connection in particular and its welds are considered critical and are subject for checking by structural designers. In case of high compressive loadings, the T-shaped column with attached plating might be prone to buckling; therefore, buckling capacity verification against pillar axial loads is performed. Obviously, also stress in the structure should not exceed the permissible levels, taking into account the safety factors and design acceptance criteria (DNV GL, 2018 a., Pt.3, Ch.1, Sec 2 [5]; DNV GL, 2018 b, Sec. 2.1).

1.2 Motivation for the research

The behavior of the centrically loaded closed section pillars (Figure 1) is relatively simple as these may fail either by flexural buckling or by material failure due to plasticity. Their capacity verification is based on a straightforward procedure and is therefore automated in the shipyard[1]. A simple computer program checks the closed-section pillar´s capacities, utilizing their geometrical characteristics and force data from the global FE-model.

The buckling behavior of bulkhead structures with T-shaped columns under compressive loads is much more complicated compared with closed-section pillars, as the open-section column might experience different failure modes, depending on the structural configuration and scantlings of the column and associated bulkhead (see Figures 2 and 3). A wide variety of cases with different structural configurations and member sizes in

[1] Here and throughout the thesis, “shipyard” refers to Meyer Turku shipyard.

real structures result in different failure modes and, thus, introduce challenges for the verification process automatization. For that reason, the capacity verification of the bulkhead structures under the pillar loads are performed by structural designers on a one-by-one basis using simplified analytical methods.

It was determined that the current prevalent analytical checking practices that are used for the above-mentioned bulkhead structures contain a number of assumptions and simplifications (see Sec. 3.3). Thereby, the need was recognized for a better understanding of the behavior of the structure, along with the need for critically reviewing the current checking procedures.

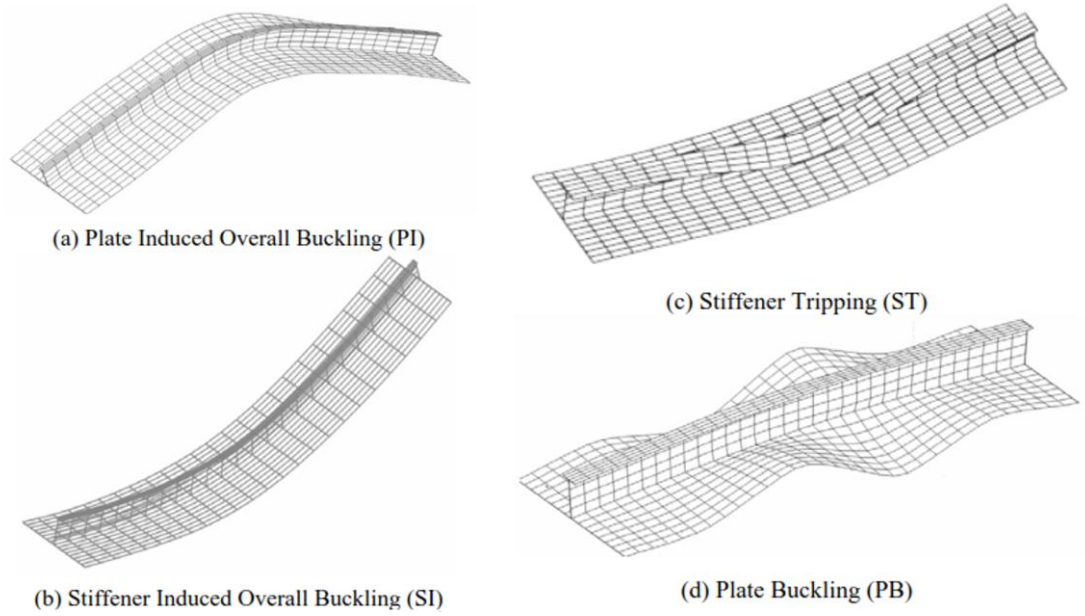

Figure 2. Typical buckling modes of the T-column with effective flange. (Sheikh et al, 2002)

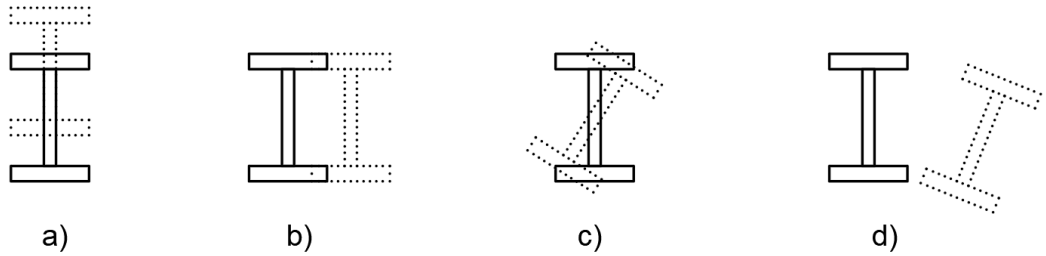

Figure 3. I-shaped column overall buckling modes: a) flexural buckling in plane of web,[2] b) flexural buckling in plane of flange,[3] c) torsional buckling, d) flexural-torsional buckling.

[2] Web: In ship construction, the section of a stiffening member attached perpendicular to the plated surface (DNV GL, 2018a).
[3] Flange: In ship construction, the section of a stiffening member attached to the web or formed by the web bending (DNV GL, 2018a).

A better understanding of the behavior of the structure, as well as understanding of simplifications and limitations of analytical checking methods, will also set a basis for the capacity verification process automatization.

1.3 Limitations of the research

The research is limited to cases with compressive point loadings applied on bulkhead structures with T-shaped columns (see Figure 1) and bulkhead intersections (see chapter 8) positioned in the way of pillars. The buckling behavior and strength will be considered.

Studying fatigue and vibrational behavior does not fall within the scope of the research.

The standard pillar-to-bulkhead connections, as shown on Figure 1, are implemented in the research FE-models as they are. It is not aimed to change or optimize the standardized pillar-to-bulkhead connections.

Welded connections are assumed to have same strength as the base material; the sizing or optimization of welds between the elements of the studied structures are not in scope.

In order to account for the economic implications of the findings and recommendations developed during the research or of implementation of proposed alternative structural solutions, another comprehensive quantitative study is required that focuses on design and manufacturing costs, the shipyard's production processes, as well as the impact on failure risk levels. The thesis research, however, focuses on structural issues, and economic aspects are not covered.

1.4 Outline of the work

The first chapter of the thesis, the introduction, is followed by a chapter that reviews the theoretical background to the thesis. Chapter 3 provides an overview analytical methods that are included in the current capacity verification approach, the applicability of which to the studied structures will be critically evaluated during the research. In Chapter 4, methods used in the research are described in more detail with applied material models, boundary conditions, and selected non-linear solution schemes.

The research part of the thesis consists of several major phases (studies) and is covered in Chapters 5 through 8. The results, findings, and discussion related to each research phase are presented at the end of each chapter. A summary of the major findings and recommendations with references to relevant chapters are provided in Chapter 9.

At the first research phase, a validation study was conducted. The validation study consisted of a two major parts. First, idealized T-columns with effective flanges were modelled and analyzed with Non-Linear Finite Element Analysis (Sec. 5.1). The purpose of this step was to obtain models that are geometrically equivalent with, and have boundary conditions that correspond to, those of idealized structures, which are considered during the capacity verification procedure in accordance with the current prevalent analytical practice (Ch. 3). Results of the non-linear finite element (FE) solutions would thus be directly comparable with those obtained by the analytical method. The comparison served two major goals. The first was to check the validity of the non-linear approach with selected solution scheme, boundary conditions, and settings in the first stage of the research before running time-consuming non-linear analyses for larger models. The second goal was to compare the results obtained with the analytical method against those received with Nonlinear Analysis (NA) and thus to validate the analytical method for idealized columns.

In the second part of the validation study (Sec. 5.2), the same idealized columns as in the first part were studied with decks and pillars included in FE-models in order to represent more realistic boundary conditions existing in real ship structure.

The next major part of the research is the imperfection study (Ch. 6). The imperfection study aimed to check the sensitivity of the structure to different types of geometrical imperfections.

Studies on realistic bulkhead structures were conducted in several phases. First, a continuous bulkhead structure without openings with T-shaped column under pillar was studied (Ch. 7). Next, the impact of openings with different configurations on the behavior of the structure was checked (Sec. 7.2). In Chapter 8, the behavior of the bulkhead intersections was studied. All the analyses in the studies mentioned above were conducted for different sizes of T-columns and different bulkhead thicknesses.

A summary of the models and analyses made during the different phases of the research is given in Table 1. In the table, "*Number of the FE-models"* indicates the number of those with different geometry. "*Number of non-linear FE-analyses conducted"* indicates the minimum number of NAs carried out in each research phase. Several analyses might

be run for a single model - for example, for those with different thicknesses and material grades of structural members. Every non-linear analysis was preceded with linear static FE-analysis and with linear buckling analysis.

Table 1. Phases of the research and local FE-models (continues on the next page)

Phase of the research	**Reference to thesis section**	**Description of FE-models**	**Number of FE-models**	**Number of non-linear FE-analyses conducted**	**Example of FE-model**
Method validation study, idealized column	Sec. 5.1	Idealized T-columns with effective flange with idealized boundary conditions	11	15	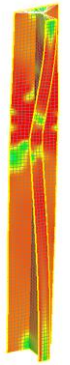
Method validation study, idealized column with more realistic boundary conditions	Sec. 5.2	Idealized T-column with effective flange with decks and pillars included in models to represent more realistic boundary conditions existing in ship structures	10	10	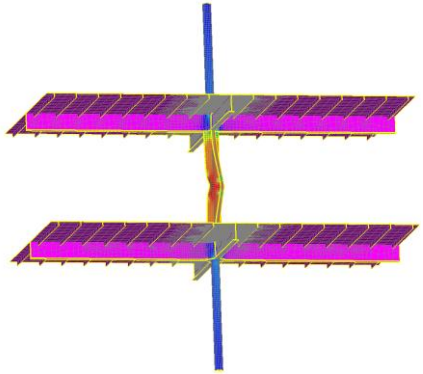
Imperfection study	Ch. 6	Models with different types of initial geometrical imperfections	7	16	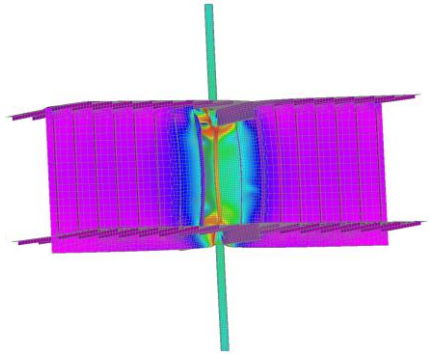

Table 1. Phases of the research and local FE-models (continued)

Study on typical bulkhead structure with T-shaped column	Sec. 7.1	Typical bulkhead structures with T-columns of different sizes	6	15	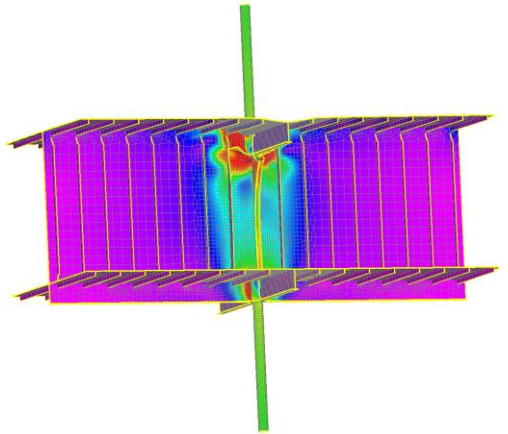
Study on impacts of openings	Sec. 7.2	Models with different bulkhead opening configurations	9	12	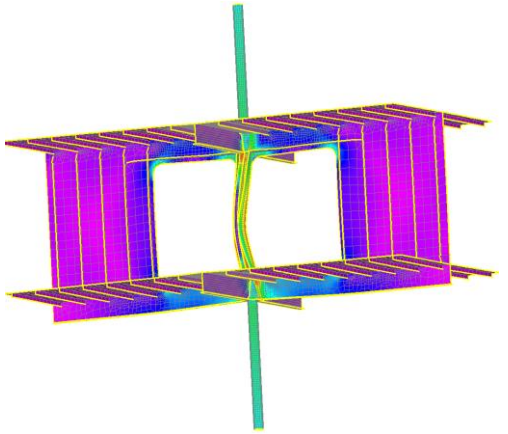
Study on structure of two intersecting bulkheads	Ch. 8	Intersections of bulkheads with different plate and deck beam web thicknesses	1	6	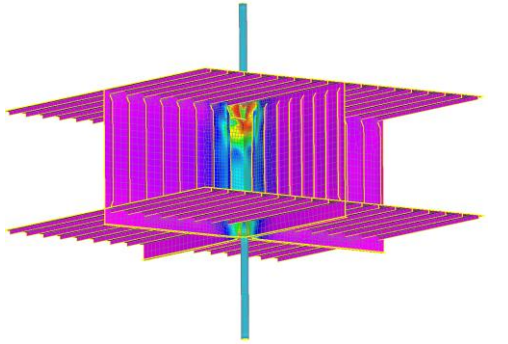

2 THEORETICAL BACKGROUND

2.1 Structural collapse

The term “collapse” refers to the sudden loss of structural integrity and is related to both (a) loss of stability due to loss of structural stiffness within the elastic limit of the material, which is usually referred to as *classical buckling*, and (b) *material failure* due to plasticity or fracture (Falzon & Hitchings, 2006). Slender and thin-walled structures are susceptible to the first type of those while stocky and thicker-walled structures are susceptible to the second one. Structures are considered to be slender if their slenderness parameter $\lambda > 1.4$; moderate slender if $0.6 < \lambda < 1.4$; and stocky if $0.6 > \lambda$ (DNV GL, 2018b).

Slenderness parameter is defined by DNV GL (2018b) as:

$$\lambda = \sqrt{\frac{R\_eH}{\sigma_E}} \tag{1}$$

where R_eH is a minimum yield stress of material of the considered member $\frac{\mathrm{N}}{\mathrm{mm}^2}$ and σ_E is a minimum elastic buckling stress.

Material failure may also take place in a sequence: a thin-walled or slender structure under compressive loading may initially buckle elastically; however, the resulting deformations will cause localized material failure (Falzon & Hitchings, 2006). Thicker-walled or less-slender structures may experience local plastic behavior, which decreases stiffness and leads to buckling.

2.2 Elastic stability and linear eigenvalue buckling analysis

When a perfect slender elastic column is in stable equilibrium along the primary load-deflection path, if the axial load applied on the column is smaller than some critical value, the column will experience axial compression only. If a small lateral force is applied to the column, a small lateral deflection will take place; however, once the lateral force is removed, the lateral deflection will disappear (Falzon & Hitchings, 2006).

If the axial load has reached the critical value, any small perturbation, such as the application of a small lateral force, will cause lateral deflection, which will not disappear

after the lateral load is removed. Such a critical value for the axial load is referred to as a “buckling load.”

Buckling is closely related to the mathematical concept of bifurcation. Bifurcation occurs when the system has reached such a state when a small change made to the system parameter value causes a sudden qualitative change in the system behavior. The term “bifurcation” implies that the structure initially deflecting in one direction, at a specific load, suddenly jumps into a displaced shape orthogonal to the initial displacements (Falzon & Hitchings, 2006). Therefore, linear buckling analysis is also referred as “linear bifurcation analysis” (LBA).

LBA is a Finite Element Analysis (FEA) routine for solving bifurcation problems of an ideally elastic structure.

The main steps of the linear buckling analysis are as follows: (Falzon & Hitchings, 2006):

1. The elastic material stiffness matrix K is assembled.
2. Linear static analysis (LA) is performed to obtain the internal stress distribution.
3. The geometric stiffness matrix K_σ is assembled using internal stress distribution.

Linear buckling analysis comes down to the generalized eigenvalue problem:

$$(K + \lambda_i \cdot K_\sigma)\varphi_i = 0 \qquad (2)$$

The λ_i, being the *i–th* eigenvalue – a scaling factor for the *i-th* buckling load $\lambda_i \cdot f_a$, where f_a is initial applied force. The φ_i – is the corresponding *i-th* eigenvector, which gives the buckling mode shape to the corresponding mode.

4. The eigenvalue problem is solved using an iterative routine.

The common iterative methods for finding eigenvalues and eigenvectors are the *Lanczos* and *subspace iteration methods*.

For buckling, eigenvalues can be positive or negative. A negative eigenvalue indicates that structure will buckle if the load is applied in an opposite direction (Ellobody, 2013). Usually, the lowest (first) eigenvalue is of main interest; however, sometimes multiple eigenvalues and eigenmodes are checked, especially when the lowest eigenvalues are close to each other. The *Sturm sequence method* may be used to calculate how many eigenvalues are below a given value (Falzon & Hitchings, 2006).

Linear buckling analysis requires few computational resources, and it is easy to set up compared with non-linear one. However, buckling loads that are received with linear analysis are usually not reliable and are over-predicted, as LBA cannot take geometric and material non-linearities into account (Figure 4). For structures facing a nonlinear response, relying on linear analysis results may lead to unreliable design.

LBA is usually performed prior to non-linear analyses (NA) in order to check model integrity and get elastic buckling mode shapes that are sometimes utilized in subsequent NA (see Chapter 6).

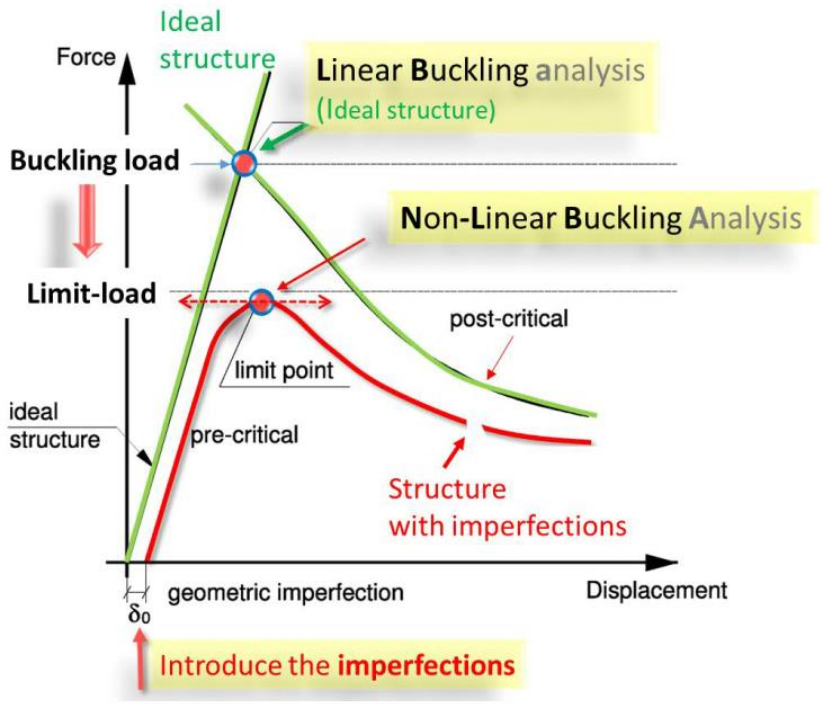

Figure 4. Generic illustration of buckling load by LBA and limit load by NA (Baroudi, 2020).

2.3 Geometrically non-linear buckling analysis

Non-linear analyses are capable of treating geometrical and material nonlinearities as well as those resulting from contact conditions (NX Nastran 11, 2006). Geometrically non-linear FE-analyses are based on incremental solution schemes and second order effects can efficiently be taken into account as each step load is applied on deformed geometry.

During the non-linear FE-analysis, the stiffness of the structure is not constant throughout the simulation. The load is applied in increments and the response of the

structure with corresponding equilibrium configurations is calculated by iterative procedure.

Solution scheme as well as the number of parameters controlling the procedure and output are selected by the analyst.

A convergence criterion is used to determine when the current solution is so sufficiently close to the solution on that iteration process can be terminated. Convergence criterion is usually based on energy, residual forces, or displacements (Hilton, 1992).

External and internal forces (energy parameters) must be balanced at each analysis step. The amount of permissible error is set by convergence tolerances (Titarenko, n.d.).

Table 2 demonstrates the effect of different convergence tolerance magnitudes on analysis accuracy and runtime. EPSP and EPSW parameters denote values of convergence tolerances for load (P) and work (W). Convergence tolerance for displacement (U) is denoted with the EPSU parameter. While the selection of optimum tolerances is always problem-dependent, for most of the practical structural design problems, convergence tolerances that correspond the “Engineering Design” or “High” accuracy levels are sufficient and provide a reasonable balance between analysis accuracy and the runtime.

Table 2. Example of effect of convergence tolerances on analysis accuracy and run time based on a 950,000 DOF´s model study (Siemens, 2017).

Accuracy Type	**Tolerances**		**Run time CPU hours**	**Accuracy for the large model**
	EPSP	**EPSW**		
Very high	0.001	1.0E-7	163.2	Very Good
High	0.01	0.001	10.3	5% or less accurate
Engineering Design	0.01	0.01	7.0	10% or less accurate
Preliminary Design	0.1	0.1	2.9	10% to 20% or less accurate

The load incrimination process is terminated by an analysis termination criterion. Some examples of analysis termination criteria are the maximum number of iterations without the selected convergence criterion being satisfied, rate of dissipated energy, rate of growth of the residual forces, the current stiffness parameter and others (Hilton, 1992).

The general set of equilibrium equations to be solved during non-linear analysis is given by Falzon and Hitchings (2006):

$$^{t+\Delta t}r = {}^{t+\Delta t}\lambda \cdot f_{ext} - {}^{t+\Delta t}f_{int} = 0, \quad (3)$$

where $^{t+\Delta t}\lambda$ is a load scaling factor at time $t + \Delta t$, f_{ext}, is an external reference load vector, $^{t+\Delta t}r$ is a residual out-of-balance force vector. $^{t+\Delta t}f_{int}$ is an internal force vector:

$$^{t+\Delta t}f_{int} = {}^{t+\Delta t}K_t \cdot {}^{t+\Delta t}u \quad , \quad (4)$$

where $^{t+\Delta t}K_t$ is a tangential stiffness matrix and $^{t+\Delta t}u$ is a sum of displacements at time $t + \Delta$t:

$$^{t+\Delta t}u = {}^{t}u + \Delta u \quad (5)$$

If structural response at time Δt is known, then:

$$^{t+\Delta t}f_{int} = {}^{t}f_{int} + \Delta f_{int} \quad (6)$$

It follows that:

$$\Delta f_{int} = {}^{t+\Delta t}K_t \cdot \Delta u \quad (7)$$

By using tangential stiffness matrix $^{t}K_t$, obtained from the previously converged solution, approximation to the evaluation of Δf_{int} may be made:

$$\Delta f_{int} \approx {}^{t}K_t \cdot \Delta u \quad (8)$$

substituting equations (6) and (8) into equation (3), it follows that:

$$^{t}K_t \cdot \Delta u = {}^{t+\Delta t}\lambda \cdot f_{ext} - {}^{t}f_{int} \quad (9)$$

Since $^{t}K_t$ and $^{t}f_{int}$ are known from the previous solution, and $^{t+\Delta t}\lambda \cdot f_{ext}$ is the known externally applied load at $+\Delta$t , then the equation can be solved for Δu. As an approximation with a tangent stiffness matrix from a previous solution was used in equation (8), it will give an approximation for $^{t+\Delta t}u$. An iterative procedure is needed to find a more accurate value for the displacement vector. Different iterative procedures are known; some of them are schematically shown in Figure 5. The generic solution algorithm for non-linear iterative schemes is described below.

Assume that a solution is known for time t and is sought for $t + \Delta t$. Then, the general scheme for the iterative algorithm looks as follows (Falzon & Hitchings, 2006; Hilton, 1992):

- load increment Δf_{ext} is applied
  residual force vector is:

$$ {}^{t+\Delta t}_{0}r = {}^{t+\Delta t}\lambda \cdot f_{ext} - {}^{t}f_{int} \tag{10} $$

- a first approximation for the displacement increment is found using the tangent stiffness matrix of a previous solution:

$$ {}_{1}\delta u = \frac{{}^{t+\Delta t}\lambda \cdot f_{ext} - {}^{t}f_{int}}{{}^{t}K_{t}} \tag{11} $$

  where left lower index *"1"* denotes the iteration number,
- displacements are updated as follows:

$$ {}^{t+\Delta t}_{1}u = {}^{t}u + {}_{1}\delta u \tag{12} $$

- the convergence criterion is checked. If the convergence criterion is achieved within a set tolerance, the procedure stops; otherwise, it continues:
- the new internal force vector ${}^{t+\Delta t}_{1}f_{int}$ is assembled based on new displacements
- new residual force vector is evaluated for ${}^{t+\Delta t}_{1}f_{int}$:

$$ {}^{t+\Delta t}_{1}r = {}^{t+\Delta t}\lambda \cdot f_{ext} - {}^{t}_{1}f_{int} \tag{13} $$

- the new tangential stiffness matrix ${}^{t+\Delta t}_{1}K_{t}$ is assembled
- a second approximation for displacement increment is found:

$$ {}_{2}\delta u = \frac{{}^{t+\Delta t}\lambda \cdot f_{ext} - {}^{t}_{1}f_{int}}{{}^{t+\Delta t}_{1}K_{t}} \tag{14} $$

- total displacements after the second iteration are:

$$ {}^{t+\Delta t}_{2}u = {}^{t}u + {}_{1}\delta u + {}_{2}\delta u = {}^{t}u + {}_{2}\Delta u \tag{15} $$

- the convergence criterion is checked, and the process is repeated until the convergence is achieved within a set tolerance.

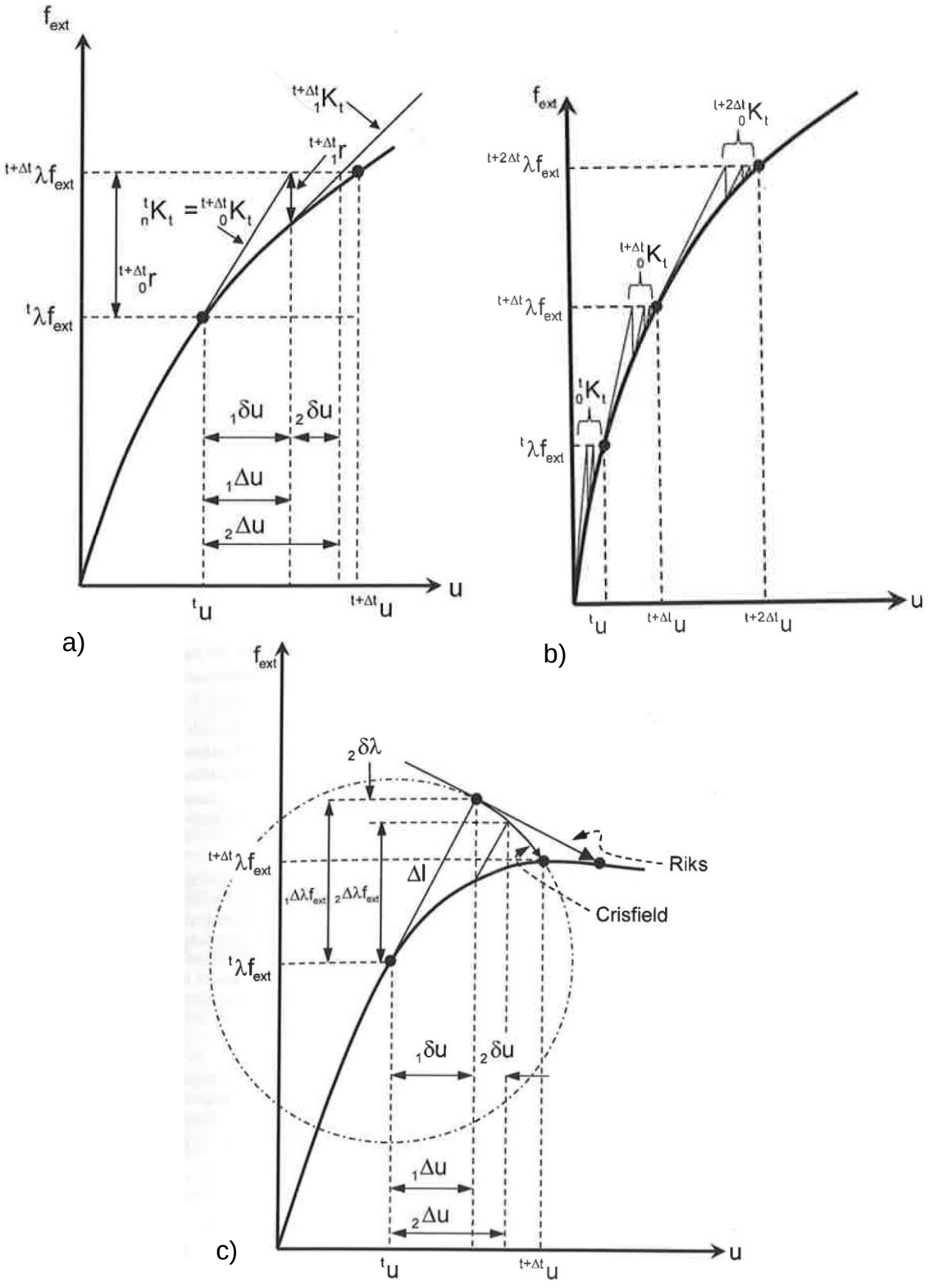

Figure 5. Common iterative routines used for non-linear problems (Falzon & Hitchings, 2006). (a) Full Newton-Rapson method, (b) Modified Newton-Rapson method, (c) Arc-length method.

In the full Newton-Rapson method, the tangential stiffness matrix is updated at every iteration. In the modified Newton-Raphson method, the tangential stiffness matrix is updated only at the start of every increment (NX Nastran 11, 2006).

The Arc-length method was first proposed by Riks, with later modifications proposed by Crisfeld. Arc-length methods make it possible to traverse limit points by using both displacement Δu and scalar load $\Delta\lambda$ increments as unknown variables in incremental iterative schemes. Riks iterates along the hyperplane orthogonal to the tangent of length Δl from the previously converged point along the equilibrium path, while Crisfield's iterates along the hypersphere. Crisfield's method is less likely to fail near the sharp limit points. (Falzon & Hitchings, 2006)

The choice of the solution scheme is central to the analysis effectiveness.

A more detailed description of the methods is not given in the present paper. For details, refer to Falzon and Hitchings (2006), Hilton (1992), and Becker (2001).

The specific solution scheme selected for the research analyses is described in Section 4.2.6.

2.4 Materially non-linear buckling analysis

While slender columns will usually buckle in the elastic regime before reaching the yield stress, practical structures such as those studied in current research (being mostly moderate-slender or stocky) will fail in most cases due to a combination of elastic instability and material plasticity. For such structures, both geometrical as well as material nonlinearities must be taken into account.

If plasticity does occur, then buckling is no longer solely a bifurcation problem; instead, a combined large deflection elastoplastic analysis must be performed (Falzon & Hitchings, 2006).

If the structure is prone to buckling and if plasticity would occur before buckling, the yielding would have a softening effect, lowering the structural stiffness and the buckling load compared to an elastic one.

In order to model elasto-plastic material behavior, a number of analytical relationships are defined (Becker, 2002):

- yield criterion
- yield function
- hardening model
- plastic flow rule

The purpose of the yield criterion to define how the multi-axial behavior of the material is related to the uniaxial one (Becker, 2002).

A widely used criterion for steel is the Von-Mises yield criterion, which relates complex 3D stresses in plasticity to the uniaxial behavior by using the concept of the critical value of shear strain energy stored in the material (Becker, 2002). Its geometric representation is shown in Figure 6. Points that lie inside the cylinder represent the elastic stress states, while those that lie on the surface of the cylinder represent the plastic stress states (Falzon & Hitchings, 2006; Becker, 2002).

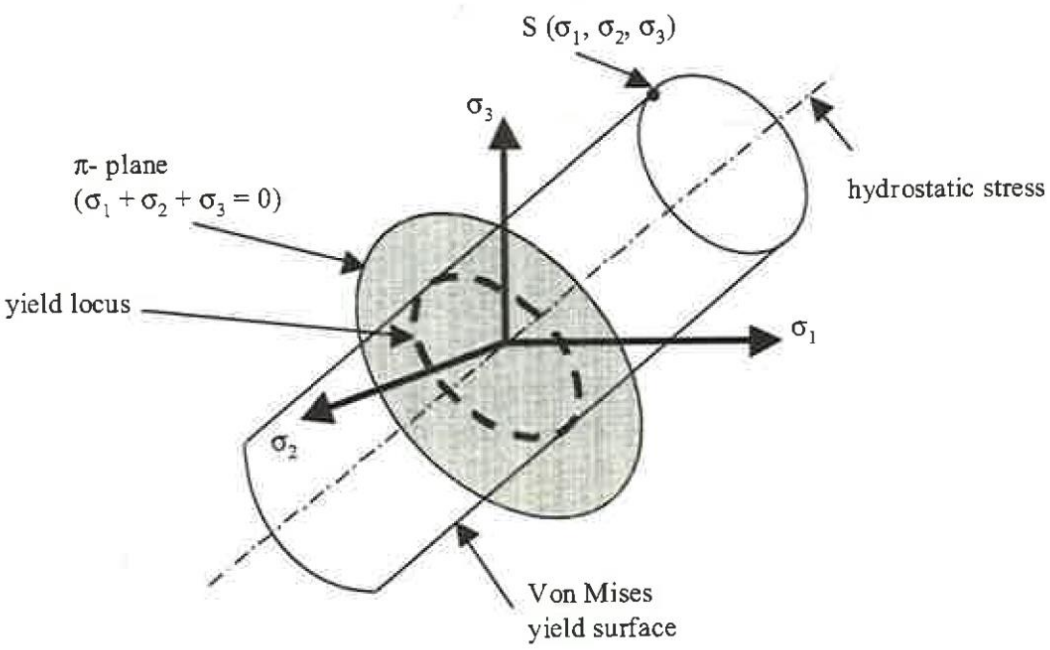

Figure 6. Geometric representation of the Von-Mises yield criterion (Becker, 2002).

The equivalent Von-Mises stress in general form can be written as follows (Becker, 2002):

$$\sigma_{VM} = \sqrt{\frac{(\sigma_{11} - \sigma_{22})^2 + (\sigma_{22} - \sigma_{33})^2 + (\sigma_{33} - \sigma_{11})^2}{2} + 3(\sigma_{12}^2 + \sigma_{23}^2 + \sigma_{31}^2)} \quad (16)$$

In terms of principal stresses:

$$\sigma_{VM} = \sqrt{\frac{(\sigma_1 - \sigma_2)^2 + (\sigma_2 - \sigma_3)^2 + (\sigma_3 - \sigma_1)^2}{2}} \quad (17)$$

In case of two-dimensional loading, the conditions takes the form of:

$$\sigma_{VM} = \sqrt{\sigma_{11}^2 + \sigma_{22}^2 - \sigma_{11} \cdot \sigma_{12} + 3{\sigma_{12}}^2} = \sqrt{\sigma_x^2 + \sigma_y^2 - \sigma_x \cdot \sigma_y + 3\tau^2} \quad (18)$$

where τ is a shear stress in xy plane.

As the plastic strain increases, the yield surface changes with the hardening parameter k. The hardening parameter may be described though strain hardening (Crocombe, 2001):

$$k = \varepsilon_{eq}^{pl} = \int d\varepsilon_{eq}^{pl} \quad (19)$$

or though work hardening (Crocombe, 2001):

$$k = W^{pl} = \int d\sigma_{ij}\varepsilon_{ij}^{pl} \quad (20)$$

where ε_{eq}^{pl} is an equivalent plastic strain and W^{pl} is a dissipated plastic work.

In order to account for strain hardening, either perfectly plastic models or those with isotropic, kinematic, or mixed hardening can be used (see Figure 7).

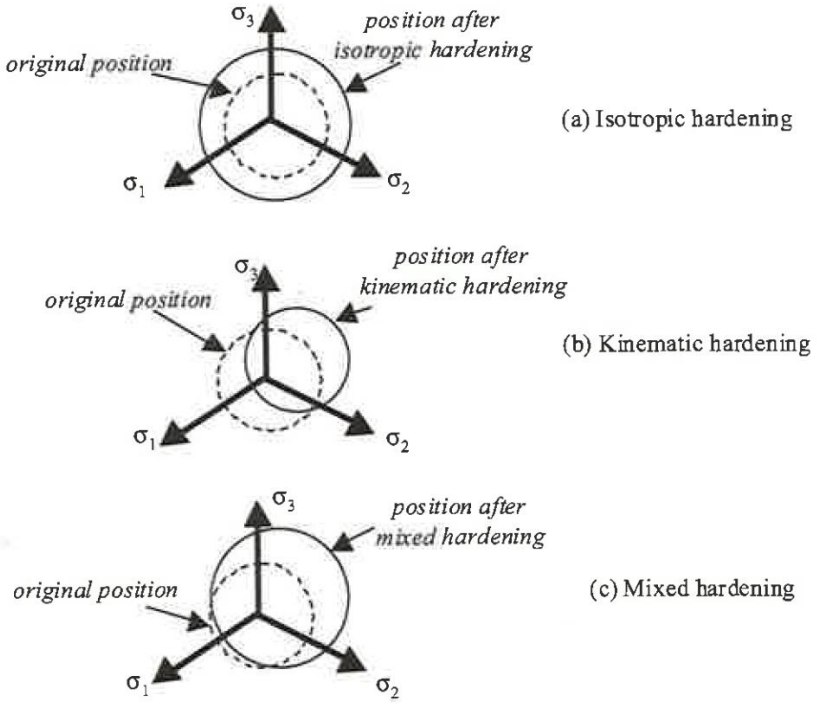

Figure 7. Impact of different hardening rules on von Mises yield surface position after hardening (Becker, 2002).

The yield surface is described by the following functions (Crocombe, 2001):

for isotropic hardening rule:

$$F(\sigma_{ij}) - \sigma_{yield}(k) = 0 \tag{21}$$

for kinematic hardening rule:

$$F(\sigma_{ij} - \alpha_{ij}(k)) = 0 \tag{22}$$

The plastic flow rule defines the interconnection between plastic strain and stress increments under multi-axial loading.

In general form, a plastic flow rule can be written as follows (Kelly, 2013):

$$d\varepsilon_{ij}^{p} = d\lambda \frac{\partial \mathrm{g}}{\partial \sigma_{ij}} \tag{23}$$

where $\partial \mathrm{g}$ is the plastic potential function, and $d\lambda$ is the positive scalar factor of proportionality.

If the yield function $\partial \mathrm{f}$ and plastic potential function $\partial \mathrm{g}$ are identical, which is valid for most metals, the flow rule is called an “associated flow rule” (Kelly, 2013; Becker, 2002):

$$d\varepsilon_{ij}^{p} = d\lambda \frac{\partial \mathrm{f}}{\partial \sigma_{ij}} \qquad (24)$$

For metals, usually the so-called “normality rule” is applied, which states that the plastic strain increment vector is normal to the yield surface (see Figure 8).

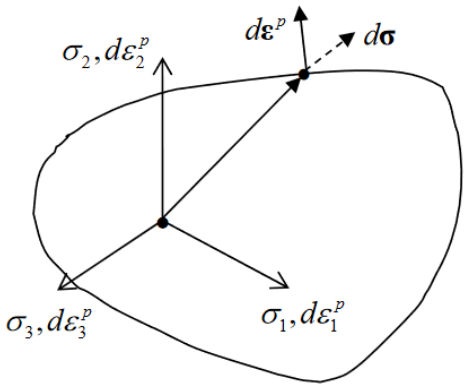

Figure 8. Yield surface and normality rule (Kelly, 2013).

For a description of the material models used in the research analyses, refer to Section 4.2.4.

2.5 Imperfections

2.5.1 Imperfections in ship structures

The ultimate capacity of compressed structural members is reduced due to the presence of imperfections. Imperfections refer to geometrical distortions, load eccentricities, misalignments, and welding residual stresses. In a real structure, members always have initial distortions caused by manufacturing, transporting, handling, and operation. Manufacturing imperfections in ship structures are mostly related to non-homogenous heat caused by welding (Ellobody et al, 2013; Efstein et al, 2016; DNV GL, 2018 b).

The degree of imperfection sensitivity is highest for moderate slender panels and is lower for slender panels. Imperfection sensitivity grows for panels with greater curvature. For stocky structures, the capacity of which is governed by material yielding, non-linear effects due to the imperfections are expected to be small (Ni et al., 2002-2012; DNV GL, 2018 b).

2.5.2 Importance of initial perturbations for numerical buckling simulations

A mathematically perfect structure may not buckle during numerical simulation at a relatively high load. For a perfect column, buckling may not be observed even beyond the elastic buckling load. This would not happen in reality, as real structures are never perfect. Therefore, applying an external perturbation to a model may be necessary in order to observe bifurcation during a numerical analysis (Saha & Culpepper, 2014).

The scenario just described is illustrated with a comparative test by a non-linear FE-analysis performed on perfect column and the same column with an initial geometrical imperfection. As is seen from Figure 9, the column with an initial imperfection reached bifurcation at 730 kN load, while the perfect column at the same load is stable, and bifurcation is not observed until the yield limit.

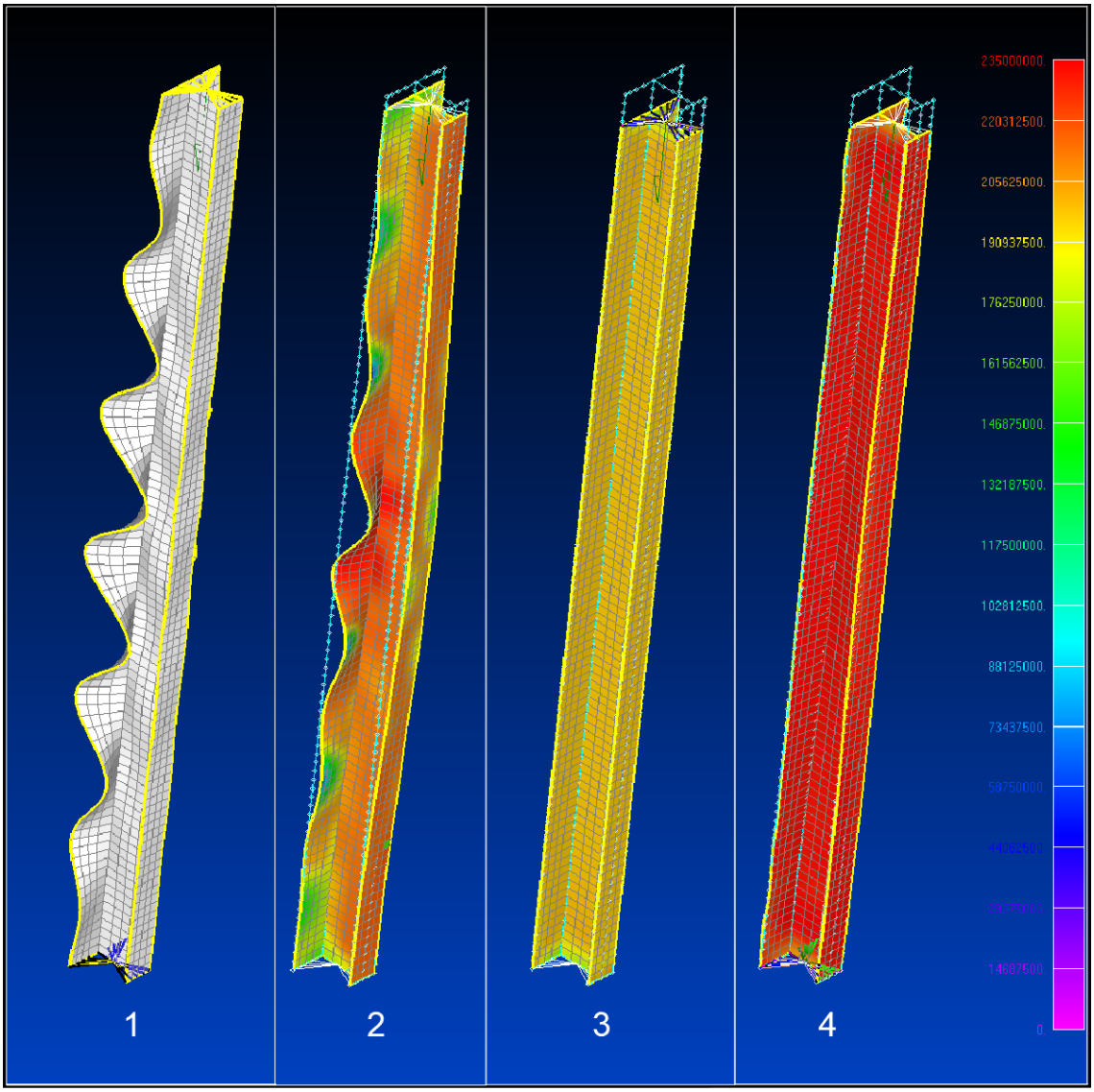

Figure 9. Example of difficulties with reaching bifurcation during numerical analysis of the perfect column:

1. *Linear FEM analysis lowest buckling mode (first eigenmode).*
2. *Non-linear analysis with eigenmode imperfection with amplitude of 3 mm. Step with load factor 0.73 (= 730 kN = critical buckling load).*
3. *Non-linear analysis of a perfect column without imperfections. Step with load factor 0.73 (= 730 kN).*
4. *Non-linear analysis of a perfect column without imperfections. Step with load factor 0.85 (= 850 kN).*

2.6 Loads for pillar and surrounding structure capacity verification

Loads for pillar and surrounding structure capacity verifications are obtained by direct strength calculations using a global FE-model.

The pillar loads are induced by both deck weights as well as hull girder deflections.

In order to obtain pillar loads that correspond to the most severe loading condition of the ship, these are calculated for the following load cases: maximum hogging, maximum sagging, transverse racking PS, transverse racking SB, and docking condition. For each pillar, the axial forces from all load cases mentioned above are compared, and the worst of them is used for checking the pillar and surrounding structure loading capacity.

2.6.1 Calculation of pillar loads for sagging and hogging conditions

Considering a ship as a beam under distributed load, the longitudinal bending moment at location x acting on a ship hull is (Tupper, 1996; Bai, 2003):

$$M = \int_0^x Q dx = \iint_0^x (\rho g A - mg) dx dx \qquad (25)$$

where $\rho \cdot g \cdot A$ is a buoyancy per unit of length, ρ is the density, g is the gravitational constant, and A is the cross-sectional area of immersed section; $m \cdot g$ is the hull weight per unit length, m is the hull mass per unit of length, and $Q_S = \int_0^x (\rho g a - mg) dx$ is a shear force acting on the gull girder in location x.

For the wave condition, the wave profile should be accounted for when calculating the area of the immersed section A.

For the ship in waves, it is helpful to separate out the bending moment into two components - still water and wave-bending moments:

$$M = M_S + M_W \qquad (26)$$

The still-water moment depends on mass and buoyancy distributions, while the wave-bending moment depends only on the geometry of the ship and waves.

Semi-empirical formulas for the calculation of still-water and wave-bending moments are given in ship design codes - for example, in the *Rules for Classification for Ships* by DNV GL in Pt. 3 Ch. 4 Sec. 2 and Sec. 3 (2018 a).

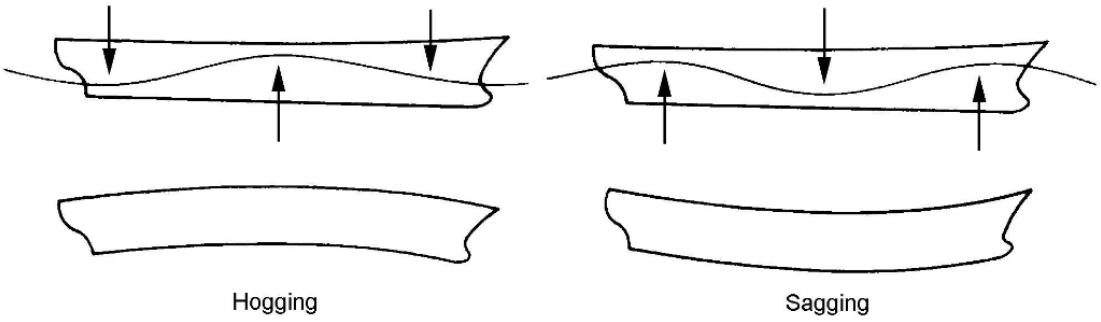

Figure 10. Hull girder bending in hogging and sagging conditions (Fagerberg, 2003).

During Finite Element Method (FEM) based pillar load analysis, loads for hogging and sagging conditions (Figure 10) are calculated in two steps.

First, responses due to hull girder deflections are calculated for hogging and sagging cases. The analysis is conducted on the FE-model without masses. During that step, the FE-model is constrained in three points, the principle is shown in Figure 11.

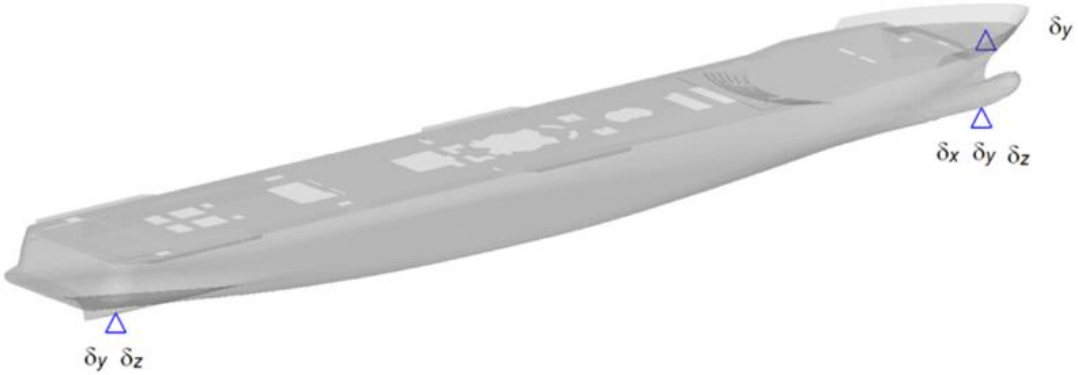

Figure 11. Schematic representation of boundary conditions used during the calculation of pillar forces due to global deflections in hogging and sagging conditions (Lloyd's Register, 2017).

Loads representing the bending-moment distributions (Figure 12) are applied to the submerged part of the web-frame elements as nodal line loads in a global FE-model.

The loads per web-frame are obtained as a second derivative of maximum hogging or sagging vertical bending-moment distribution functions.

The maximum vertical-bending moment curves are obtained by combining permissible still-water moment envelope limit- and vertical wave-bending moment curves for hogging or sagging, as applicable (DNV GL, 2016).

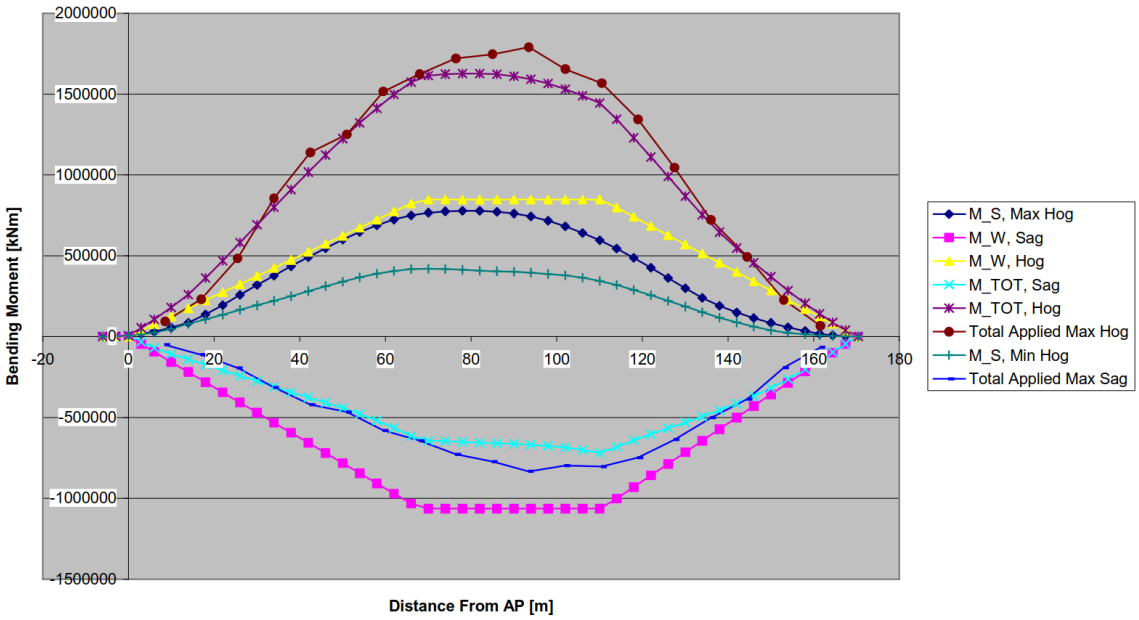

Figure 12. Typical still-water and wave-moment limit curves (DNV GL, 2016).

In the second step, when calculating the response due to deck loads and steel weight, transverse bulkheads are fixed in vertical direction and still-water hydrostatic pressure is applied to the wet part of the hull. Axial vertical accelerations as well as steel structure self-weights are taken into account in loads that are applied to deck plate elements in a global FE-model as distributed nodal loads.

When pillar load components due to global deflections and due to deck loads with steel weight, are calculated in accordance with the procedure described above, they are combined. The total pillar loads are thus obtained.

2.6.2 Calculation of pillar loads for racking condition

When calculating the response in the racking condition, transverse envelope acceleration distribution and vertical gravitational accelerations are applied as body loads in the global FE-model. With the body loads feature, instead of applying loads to the individual entities, they are applied to the whole model. Deck loads, including those due to heavy equipment, are included in the FE-model. The self-weight of steel structures is taken into account through material density.

The model is balanced with a distributed sea pressure in heeled condition applied to the submerged part of the hull (Figure 13). The inertia relief technique is used to deal with the residual counterbalance between the implemented accelerations and pressure field.

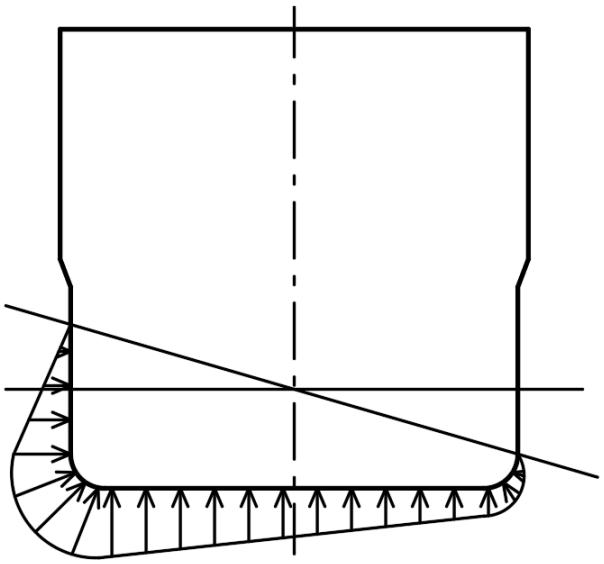

Figure 13. Schematic representation of the transverse distribution of hydrostatic sea pressure in racking condition.

2.6.3 Calculation of pillar loads for docking load case

In docking condition, the forces from the supporting docking blocks are transferred though double bottom girders, floors, and brackets to the bulkheads and pillars above the tank top.

Pillar loads are obtained by docking analysis, which is carried out using the global FE-model.

Docking blocks are modelled with spring elements.

Deck loads and equipment weights are included in the FE-model. The steel self-weight is implemented though material density. Gravitational acceleration is applied to the model as body load.

3 CURRENT PREVALENT ANALYTICAL METHODS

3.1 The Closed-Form Method for column buckling capacity estimation

Based on multiple interviews with hull structural designers, it was determined that the current prevalent capacity checking practice of bulkhead's T-shaped columns is based on the Closed Form Method[4] for axially compressed pillars in accordance with Class Guideline DNVGL-CG-0128 Buckling, Section 4 (further CFM) (DNV GL, 2018b).

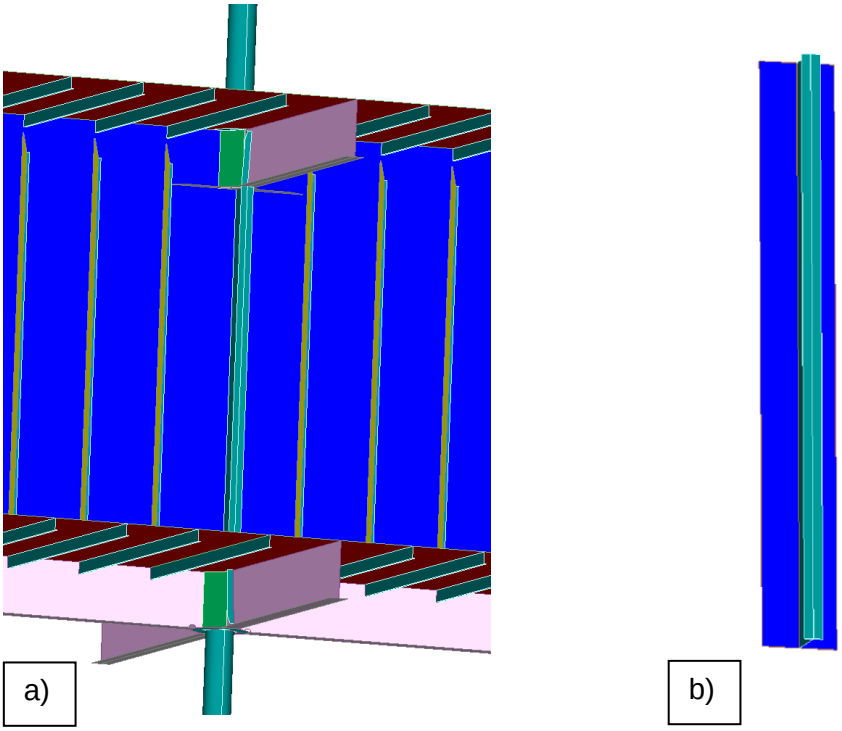

Figure 14. Bulkhead structure under consideration:
a) the T-column in real structure
b) the idealized structure of a T-cloumn with effective flange

In accordance with the method, an idealized structure of the T-shaped column with the effective part of the bulkhead plating (Figure 14b) is subjected to capacity checking in accordance with the procedure described below:

[4] Closed Form Method: The expression is said to be a closed-form if it can be expressed analytically in terms of a finite number of certain generally-accepted functions. In this thesis, a method based on semi-empirical formulations as described in Section 3.1 is referred to as CFM.

First, geometrical characteristics of the cross section are calculated as follows:

Net St. Venant torsional constant, cm^4:

$$I_{sv} = \frac{1}{3}(b_{f1} \cdot t_{f1}^3 + b_{f3} \cdot t_{f3}^3 + d_{wt} \cdot t_w^3) \cdot 10^{-4} \quad (27)$$

where:

b_{f1} is the effective flange width, mm (see Figure 15)

t_{f1} is the effective flange thickness, mm

The vertical position of the shear center relative to the cross sectional centroid, cm:

$$z_0 = z_s - \frac{(b_{f3} \cdot d_{wt} \cdot t_{f3} + 0.5 \cdot d_{wt}^2 \cdot t_w) \cdot 10^{-1}}{d_{wt} \cdot t_w + b_{f1} \cdot t_{f1} + b_{f3} \cdot t_{f3}} \quad (28)$$

where:

d_{wt} is the height of the T − column web, mm

t_w is the thickness of the T − column web, mm

b_{f3} is the width of the T − column flange, mm

t_{f3} is thickness of the T − column flange, mm

The warping constant, cm^6:

$$c_{warp} = \left(I_{f1} \cdot z_s^2 + I_{f3}(\frac{d_{wt}}{10} - z_s)^2\right) \quad (29)$$

where I_{f1} and I_{f3} are moments of inertia of the flanges: $I_{f1} = \frac{b_{f1}^3 \cdot t_{f1}}{12} \cdot 10^{-4}$;

$I_{f3} = \frac{b_{f3}^3 \cdot t_{f3}}{12} \cdot 10^{-4}$; $\quad z_s = \frac{I_{f3} \cdot d_{wt}}{I_{f1} + I_{f3}} \cdot 10^{-1}$

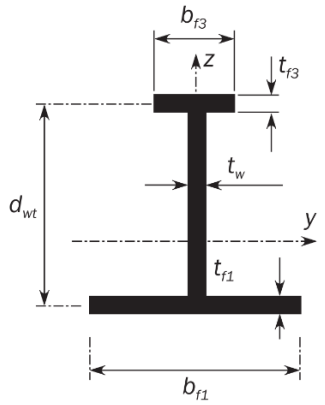

Figure 15. Geometrical characteristics of the T-column with effective flange.

Next, the elastic buckling stresses for the following modes are calculated:

- elastic flexural column buckling
- elastic torsional buckling
- elastic flexural-torsional buckling

Elastic flexural buckling stress:

$$\sigma_{EC} = \pi^2 \cdot E \cdot f_{end} \cdot \frac{I}{A \cdot l_{pill}^2} 10^{-4} \quad (30)$$

where $-$Young's modulus, $\frac{N}{mm^2}$;

f_{end} is the end constraint factor for the flexural buckling (see Figure 16)

I is the net moment of inertia arond the weakest axis of the cross section, cm^4

A is the net cross sectional area of the member, cm^2

l_{pill} is the unsupported length of the column, m

Buckled shape of member		
f_{end}	4.0	1.0

Figure 16. End constraint factors (4.0 – fixed, 1.0 – pinned) (DNV GL, 2018 b)

Elastic torsional buckling stress:

$$\sigma_{ET} = \frac{GI_{SV}}{I_{pol}} + \frac{\pi^2 \cdot f_{end} \cdot E \cdot c_{warp}}{I_{pol} \cdot l_{pill}^2} \cdot 10^{-4} \quad (31)$$

where shear modulus $G = \frac{E}{2}(1+\nu)$, $\frac{N}{mm^2}$; ν is Poisson's ratio; the net polar moment of inertia about the shear center of the cross section $I_{pol} = I_y + I_z + A \cdot (y_0^2 + z_0^2)$, cm4; I_y, I_z are the net moments of inertia against y and z axes; y_0 is a transverse position of

the shear center relative to the cross sectional centroid, cm; z_0 is the vertical position of the shear center relative to the cross sectional centroid, cm.

Elastic flexural-torsional buckling stress:

$$\sigma_{ETF} = \frac{1}{2 \cdot \zeta} \cdot \left[(\sigma_{EC} + \sigma_{ET}) - \sqrt{(\sigma_{EC} + \sigma_{ET})^2 - 4 \cdot \zeta \cdot \sigma_{EC} \cdot \sigma_{ET}} \right] \quad (32)$$

where ζ coefficient is taken as $\zeta = 1 - \frac{(y_0^2 + z_0^2) \cdot A}{I_{pol}}$; y_0 is a transverse position of the shear center relative to the cross-sectional centroid, cm; z_0 is the vertical position of shear center relative to the cross-sectional centroid, cm.

The minimum elastic buckling stress is obtained by comparing the buckling stresses of different buckling modes:

$$\sigma_E = min\{\sigma_{EC}, \sigma_{ET}, \sigma_{ETF}\} \quad (33)$$

The average axial compressive stress in the member is N/mm^2:

$$\sigma_{av} = \frac{F_{pill}}{A} \cdot 10 \quad (34)$$

where F_{pill} is a maximum compressive axial load applied on a column, kN.

The minimum critical buckling stress is obtained by applying plasticity correction to the minimum elastic buckling stress:

for $\sigma_E \leq 0.5 R_{eH}$: $\sigma_{cr} = \sigma_E$ (35)

for $\sigma_E > 0.5 R_{eH}$: $\sigma_{cr} = (1 - \frac{R_{eH}}{4 \cdot \sigma_E}) \cdot R_{eH}$

The buckling utilization factor is calculated according to the formula:

$$\eta = \frac{\sigma_{av}}{\sigma_{cr}} \quad (36)$$

The buckling utilization factor should not exceed the limit value set by the acceptance criteria. The limit values of η for pillars set by DNV GL are between 0.65 and 0.75, depending on the applied design load scenario (DNV GL, 2018a., Pt. 3, Ch.8, Sec.1 [3.4]).

3.2 Methods for evaluating the effective breadth of bulkhead plating

3.2.1 Current approach of 40 x t / 50 x t

Based on the interviews with structural engineers, it was determined that usually simplified method for effective flange width is used for compression columns, being:

$$b_e = 40 \cdot t \tag{37}$$

where t is a thickness of the bulkhead plating. The same formula for an effective flange calculation was also used in a 2002 version of the DNV "Buckling of Pillars" calculator (version 8.50.1234, April 2002). The same formula of 40xt is also proposed in the article "Buckling of transverse bulkheads" (2018). A similar formula, $b_e = 50 \cdot t$, was also mentioned as being used by some designers.

The 40 x t / 50 x t approach probably originated in the effective width concept proposed by Von Karman. He suggested that the minimum effective width b_{em} should be taken as the width of the plate for which the edge stress σ_E is equal to the plate yield stress σ_0. For a simply supported web, the formula takes the following form (Faulkner, 1975):

$$b_{em} = \pi t \sqrt{\frac{\mathrm{E}}{3(1-\nu^2)\sigma_0}} \tag{38}$$

for normal strength steel, the form turns into:

$$b_{em} = \pi t \sqrt{\frac{2.06 \cdot 10^{11}}{3(1-0{,}3^2) \cdot 235 \cdot 10^6}} \approx 56 \cdot t \tag{39}$$

and for the most common high-strength steel with yield strength of 355 MPa is:

$$b_{em} = \pi t \sqrt{\frac{2.06 \cdot 10^{11}}{3(1-0{,}3^2) \cdot 355 \cdot 10^6}} \approx 46 \cdot t \tag{40}$$

3.2.2 Alternative approaches

3.2.2.1 Effective width through plate slenderness parameter

The effective width of plating has been studied by many authors, including Von Karman, Marguerre, Bleich, Frankland, Conley et. al, Clarkson, Koiter, Gerard, Winter, Becker, and others. Different formulations have been proposed. Two fundamentally different approaches to evaluating effective flange width can be distinguished (Bruchman et al., 2000). First, there is the effective breadth approach, which is related to the phenomenon of shear lag. This has been studied, among others, by Clarkson (1965). Another is the effective width approach through plate slenderness parameter, developed and described by Faulkner (1975) with contributions by other authors, including Evans (1975).

The effective flange width for columns of stiffened panels through the plate slenderness parameter was proposed by Faulkner (Bruchman et al, 2000; Amdahl, 2005):

$$\frac{b_e}{b} = \begin{Bmatrix} c_0 + \frac{c_1}{\beta} + \frac{c_2}{\beta^2} & for\ \beta \geq 1 \\ 1 \cdot \beta & for\ \beta \leq 1 \end{Bmatrix} \quad (41)$$

Where β is a plate slenderness parameter:

$$\beta = \frac{b}{t}\sqrt{\frac{\sigma_y}{E}} \quad (42)$$

Where b is the width of the plate element over which uniform compression is applied, usually equal to the stiffener spacing; c_0, c_1, c_2 are the empirical constants derived from experimental data to account for the initial distortions. The values vary by different authors and depend on the magnitudes of the initial distortions. For moderate-high distortions, the values proposed by Faulkner are: $c_0 = 0$, $c_1 = 2$, $c_1 = -1$.
It will be noted that the values of $c_1 = 2$ and $c_1 = -1$ do not account for residual stresses. To take residual stresses into account, the residual stress reduction factor R_r is introduced (Bruchman et al., 2000; Amdahl, 2005):

$$R_r = 1 - \frac{\sigma_r}{\sigma_y}\frac{E_t}{E} = 1 - \frac{2\eta}{\frac{b}{t} - 2\eta}\frac{2(\beta - 1)}{\beta};\ 1 < \beta < 2.5 \quad (43)$$

where E_t is a tangent modulus of the plate.

The value of η varies depending on the magnitude of the residual stress. Faulkner suggested values for η between 3 and 4.5 for ships (Amdahl, 2005).

The effective flange width with reduction due to both initial deflections and residual stress is obtained by multiplying Eq. (41) with Eq. (43):

$$\frac{b_e}{b} = \left\{c_0 + \frac{c_1}{\beta} + \frac{c_2}{\beta^2}\right\} R_r \qquad (44)$$

For design purposes, according to Amdahl (2005), the following values of empirical constants c_1, c_2 might be used to account for both reasonable initial deformations and residual stresses:

$$\frac{b_e}{b} = \begin{Bmatrix} \frac{1{,}8}{\beta} - \frac{0{,}8}{\beta^2} & for\ \beta \geq 1 \\ 1 \cdot \beta & for\ \beta \leq 1 \end{Bmatrix} \qquad (45)$$

The effective flange widths were calculated for different plate thicknesses in order to compare those figures achieved by the method presented above with those commonly used by hull designers for evaluating the effective plate width of T-columns below the pillars (Table 3).

Table 3. Comparison of the effective flange width calculated with the simplified 40 x t formula with effective flange width through plate slenderness parameter for different values of empirical constants of c1 and c2.

	Effective plate width, mm (rounded to tenths)			
Bulkhead plate thickness, mm σ_y = 235MPa stif. spacing s = 0.6 m	**40xt**	**Faulkner c1 = 2, c2 = 1**	**Faulkner, with residual stress reduction c1 = 1.8, c2 = 0.8**	**RINA Pt B, Ch 7, Sec. 2 4.1.1 c1 = 2.25, c2 = 1.25**
6	240	300	280	330
8	320	380	350	420
10	400	440	420	480
15	600	560	540	590

Compared with Faulkner's approach, a moderate underestimation of the effective width by the 40xt method was observed for thin plates and a moderate overestimation was observed for thick bulkhead plates.

The approach proposed by Faulkner is widely accepted for stiffened plates loaded with distributed uniform line loads and is implemented in different shipbuilding codes with slightly varying values for empirical constants c1 and c2 - for example, in Rina (2017). However, the applicability of the formula as it is for the column in considered typical bulkhead structure below the pillar might be questionable, as, in that case, the stiffness difference between the T-column and bulkhead stiffeners is remarkable, and some correction might be necessary to account for the type of loading (point load) and eccentricity.

3.2.2.2 Effective width through elastic shear lag

In Eurocodes EN 1993-1-5, the shear lag is taken into account through the flange effective width that is defined so as to have the same total normal force in the gross flange subjected to the real transverse stress distribution as in the effective flange subjected to a uniform stress equal to the maximum stress of the real transverse distribution (Beg et al, 2011):

$$\int_0^b \sigma_x(y) t_f d_y = b_e t_f \sigma_{xmax} \tag{46}$$

and

$$b_e = \beta b_0 \tag{47}$$

where β is an efficiency factor.

For formulas for calculating the eficiency factor, β refer to Eurocode 3 EN1993-1-5:2006 (E) §3.2.1 (not presented in the present report).

The formulas for effective width through elastic shear lag, as given in Eurocode 3 EN1993-1-5:2006 (E) §3.2.1, are suitable for beams subjected to bending rather than for a column under compressive point load.

3.2.2.3 Effective width as a function of member length or spacing

Sometimes the effective width of the attached plating for a structural member is taken as equal to spacing $b_e = s$ or as a function of the member length (e.g., $b_e = 0{,}2 \cdot l$). Then it should be ascertained that local buckling would not occur in the plate (Rina, 2017, Ch.4, Sec.3 [4.2] and Ch.7, Sec.2 [4.1]).

3.3 Discussion on the simplifications of current methods

The method described in Section 3.1, when applied to checking the buckling capacity of bulkhead structures under pillar loads, is generally considered to be conservative. It should be recognized that the method is simplified as it does not take into account several factors existing in real structure.

The capacity estimation of the structure is performed by calculating the column with the effective flange and the surrounding structure not being taken into account.

The eccentricity in the application of the pillar load in respect to the centroid of the T-column section, which is inherent to the structure, is usually neglected. As is seen from Figure 17, the eccentricity is due to the structural arrangement of members and grows with the increase of the T-column web height.

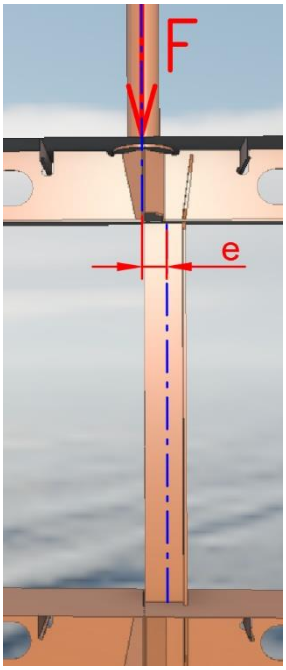

Figure 17. The eccentricity in the load application with respect to the column centroid.

As described in Section 3.1, CFM compares the buckling stresses of those for flexural, torsional, and torsional-flexural modes and considers the lowest of them as being critical. The moment of inertia of the column by default is taken against the weakest axis. In CFM, the long edges of attached plate are considered to be free.

In a real structure without openings, the long edges of the effective flange are not free due to the continuous stiffened bulkhead plate that provides some level of restraint against torsional buckling and against flexural buckling in the direction of the bulkhead plate. That restraint may lead the column to fail in different modes than is predicted by CFM.

The effects of restraint at the edges of the effective plate against movement in the plane and against rotation have been studied, among others, by Marquerre (1937), Cox (1945), and Ratcliffe (1968), showing that the restraints may have a considerable influence.

4 RESEARCH METHODOLOGY

4.1 Selection of the numerical simulation technique

As the present research deals with buckling, for reasons described in Chapter 2, Geometrically and Materially Nonlinear Analysis with Imperfections (GMNIA) was selected as a main analysis technique.

GMNIA is currently one of the most advanced and, arguably, one of the most accurate structural analysis approaches (ABS, 2021; Prabu et al., 2012). Among the known solution techniques, non-linear FEM is certainly the most favored method for dealing with the various buckling and post-buckling behaviors of stiffened plate structures. FEM is especially effective for gaining an understanding of important local effects (X-Y Ni et al., 2002-2012).

Linear Buckling Analyses were used to obtain elastic buckling mode shapes.

4.2 Selection of the solution scheme and parameters for analyses

4.2.1 Element types

Models for the research were made mostly using the 4-node quadrilateral shell elements CQUAD4 (Figure 18).

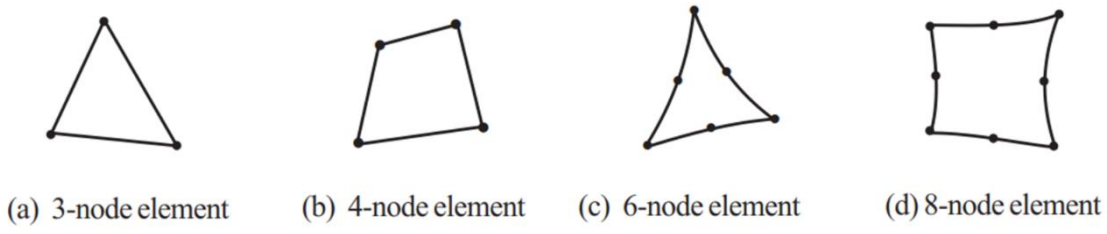

Figure 18. Shell elements in NX Nastran Advanced Nonlinear Solution (SOL601) (Siemens, 2006).

CQUAD4 are 4-node isoparametric bilinear elements and are described by linear shape function in terms of the polynomial terms as (Hellen & Becker, 2013):

$$p_i = (1, \xi, \eta, \xi\eta) = a_1 + a_2\xi + a_3\eta + a_4\xi\eta \tag{48}$$

where p_i is a shape function for node i; (ξ, η) are dimensionless coordinates; and a_i is a function of the nodal geometry for each node on the element.

Shell elements have five degrees of freedom per node: three translational and two rotational (Siemens, 2006). Thus, CQUAD4 has a total of 20 degrees of freedom.

The shape function matrix containing p_i terms is:

$$[N] = \begin{bmatrix} p_1 & 0 & 0 & p_2 & 0 & 0 & & p_i & 0 & 0 \\ 0 & p_1 & 0 & 0 & p_2 & 0 & \dots & 0 & p_i & 0 \\ 0 & 0 & p_1 & 0 & 0 & p_2 & & 0 & 0 & p_i \end{bmatrix}$$

The degrees of freedom at each node i are the displacement components (u_i, v_i), and the shape functions can express the displacements at any point in the element as follows (Hellen & Becker, 2013):

$$u = \sum\nolimits_n p_i\, u_i = p_1u_1 + p_2u_2 + p_3u_3 + p_4u_4 \tag{49}$$

$$v = \sum\nolimits_n p_i\, v_i = p_1v_1 + p_2v_2 + p_3v_3 + p_4v_4 \tag{50}$$

The shell element formulation treats the shell as a three-dimensional continuum with the following two assumptions used in the Timoshenko beam theory and the Reissner-Mindlin plate theory (Siemens, 2006):

- Assumption 1: Material particles that originally lie on a straight line "normal" to the midsurface of the structure remain on that straight line during deformation.
- Assumption 2: The stress in the direction normal to the midsurface of the structure is zero.

Lower-order elements were preferred over high-order elements due to their robustness and computational efficiency. The quadrilateral 4-node elements of appropriate size are considered sufficient for hull structure representation (DNV GL, 2020) and have balanced precision-computational efficiency characteristics. Triangular first-order elements are considered too stiff for the buckling problems, they may under-predict displacement and strain in bending-dominated problems. 8-node quadrilateral elements are more accurate in deformation and strain representation. Despite all the benefits of

8-node elements, those are not computationally as efficient as 4-node elements, which may lead to long calculation times for large models. Moreover, 8-node elements are also distortion-sensitive, which makes it more difficult and time-consuming to prepare the mesh for large models compared to 4-node elements.

Required mesh density depends on selected element types. If low-order elements are used, more elements per half-wave are required than with high-order elements in order to obtain comparable analysis accuracy.

Rigid elements RBE2 were applied at the ends of the pillars. The purpose of the rigid elements was to impose multipoint constraints by one node at each pillar end and to distribute the load.

The Holland profiles[5] (HP) of deck longitudinals (Figure 19) and bulkhead stiffeners were modelled with shell elements as angle-bars of equivalent properties following the recommendations of *Rules for Classification of Ships* Pt. 3 Ch. 3 Sec. 7 (DNV GL, 2018 a).

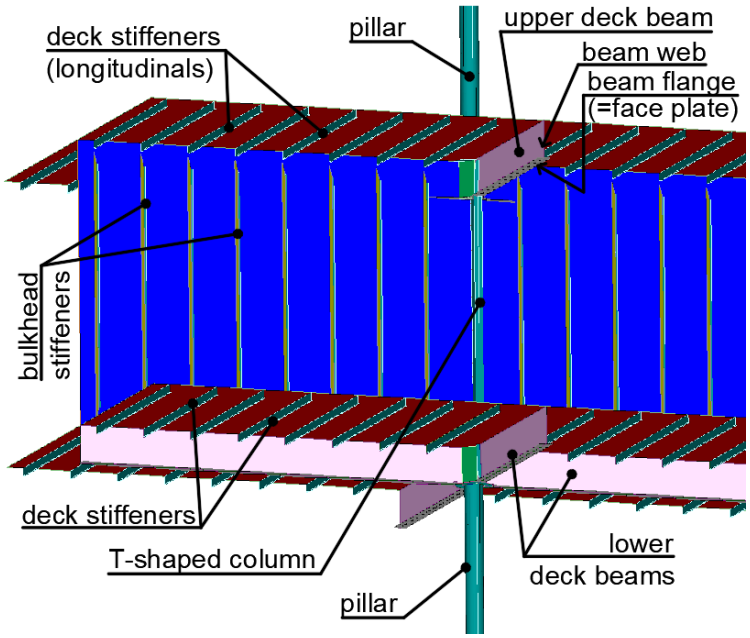

Figure 19. Terms related to the bulkhead structure.

For detailed formulations of elements, refer to Bathe (2014), Element Library Reference *(*Siemens, 2016*),* and NX Nastran 11 Modelling Guide (Siemens, 2006).

4.2.2 Mesh size

The mesh of model elements should be sufficiently detailed in order to capture relevant failure modes. For stability analyses, a minimum of three to six elements per expected half-wave are recommended by DNV-RP-C208 (DNV GL, 2013) and by

[5] Holland Profile or HP bulb flat: A type of a hot-rolled profile with thickening on the edge, widely used in shipbuilding.

DNVGL-CG-0128 (DNV GL, 2018 b). Falzon and Hitchings (2006) recommend a minimum of six quadratic elements per half-wave.

Smooth transitions of mesh density, from the coarser to the finer mesh zones, were maintained, as abrupt transitions cause irregular stiffness changes and may lead to errors of a numerical nature (DNV GL, 2013). More detailed information on applied mesh sizes is given in Section 7.1.1.

4.2.3 Boundary conditions and extent of the models

Generally spoken, the extent of the model and boundary conditions should be such that all relevant failure modes would be able to develop without interference with boundary effects. In this thesis, when making FE-models, recommendations of DNV GL on the model extent were followed (DNV GL, 2018 b).

A minimum of two whole frame spacings plus one-half frame spacing on each side in the longitudinal direction and a minimum of six stiffener spacings in the transverse direction are recommended by DNV GL for stiffened plates (DNV GL, 2018 b, Sec. 6 [5.8]).

Further information on boundary conditions and the extent of FE-models made during the thesis research is given under the relevant sections (7.1.1, 5.1, 5.2).

4.2.4 Material model

Two material models to represent grades with yield limits of 235 MPa and 355 MPa were employed in the research analyses.

Most common material models that are used as input in Finite Element (FE) formulation are based on the “Engineering” stress-strain curves that are calculated based on the initial cross-section of the specimen, “True” stress-strain curves that are calculated based on updated specimen geometry, Green-Lagrange strain-, and the Euler-Almansi strains (Figure 20).

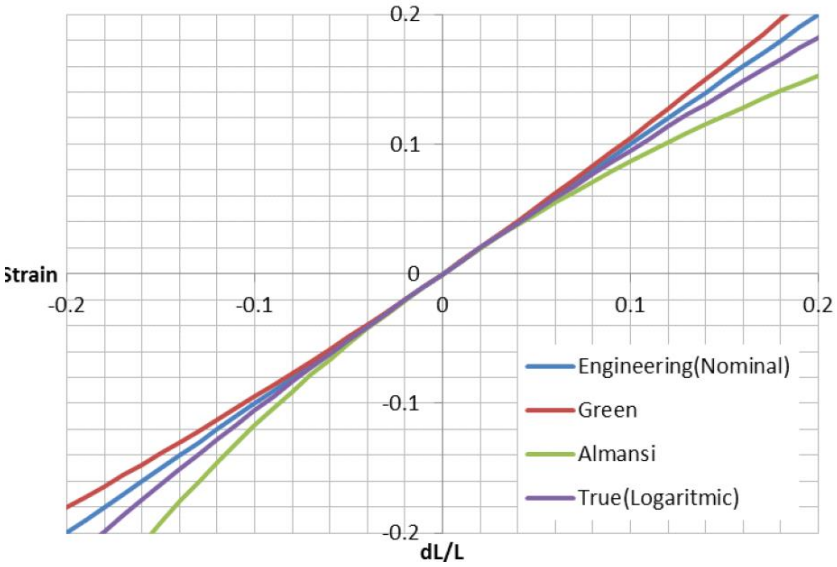

Figure 20. Comparison of strain measures (DNV GL, 2013).

Bilinear elasto-plastic models are also common in materially nonlinear analyses (MNA). An example of a bilinear elasto-plastic model with linear strain hardening is shown in Figure 21.

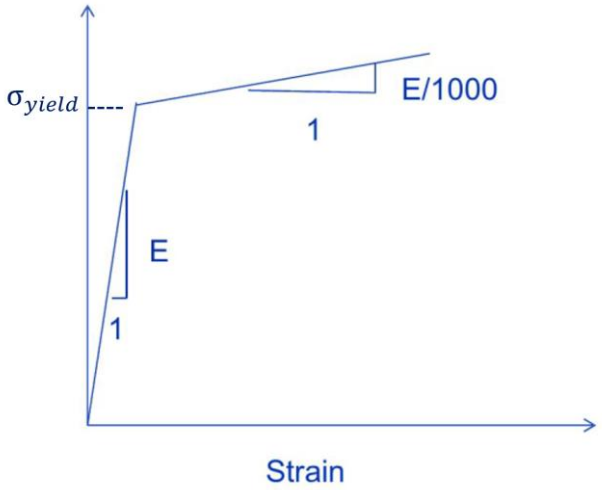

Figure 21. Example of a bilinear material model (DNV GL, 2020).

In present research, plastic-multilinear models based on “engineering” stress-strain curves as shown in Figure 22 and Table 4 were used. The stress-strain curves follow the recommendations of DNVGL-RP-C208 (DNV GL, 2013). Plate thickness effects on stress-strain response were neglected. The isotropic strain hardening rule was applied.

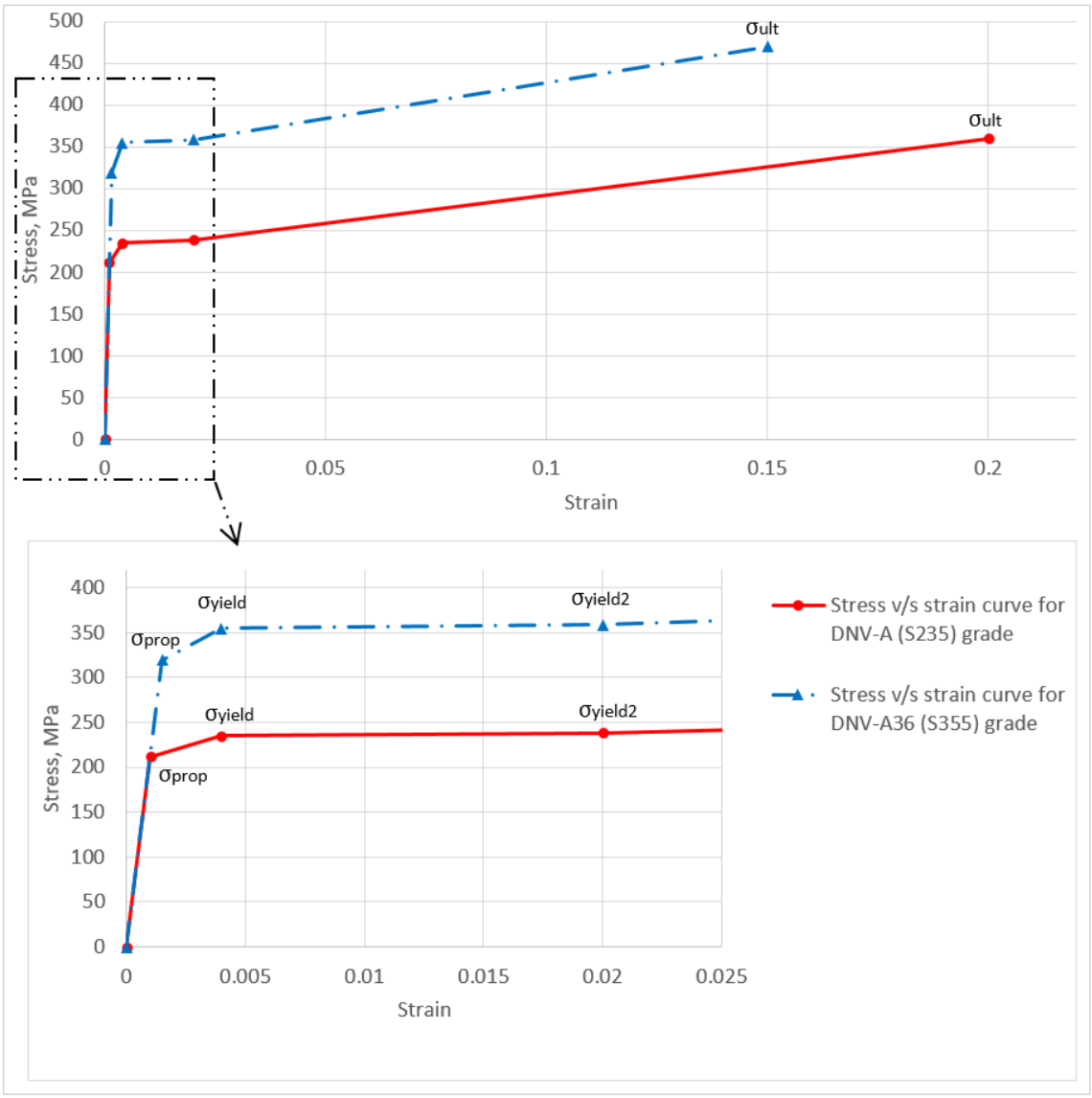

Figure 22. Stress-strain curves used in the research for plastic-multilinear material models.

Table 4. The values of stress and strain at limit points used for material models.

		S235		S335	
		Strain	Stress, MPa	Strain	Stress, MPa
Proportional limit	σ_{prop}	0.001007	211.5	0.00152	319.5
Upper yield point	σ_{yield}	0.004	235	0.004	355
Lower yield point	σ_{yield2}	0.02	238.4	0.02	358.4
Ultimate stress	σ_{ult}	0.2	360	0.15	470

4.2.5 Imperfections

Non-linear analyses in the research were performed on models with geometrical imperfections included. Imperfection sensitivity study with different imperfection shapes was carried out. For further information on imperfection types and amplitudes used in the research, refer to Chapter 6.

4.2.6 Non-linear solution scheme

Non-Linear analyses in the research were carried out using the load-displacement control method (LDC). The current research deals with point loads, which makes the method with displacement control well applicable. The method is more complex when applied to problems with distributed loads (Hellen & Becker, 2013). In large displacement non-linear analyses, conventional load-control methods often fail at regions of high non-linearity because of non-positive definite terms in the stiffness matrix (Ship Structure Committee, 2003). Displacement control methods help to overcome problems associated with snap-through, certain types of geometrical nonlinearities, or material softening, when load-control methods may face convergence problems (Hellen & Becker, 2013). Displacement control methods can be used to solve whole nonlinear equilibrium path until collapse, including post-buckling response (NX Nastran 11, 2006).

In the LDC method, enforced displacement is applied to the specified degree of freedom (DOF), and the level of applied load is adjusted by the program automatically. Load increments are not associated with any user-specified time-function and are increased or decreased at different steps of the equilibrium path in order to reach convergence efficiently in each step. As is seen from Figure 23, with LDC method, initially, when the equilibrium path is linear, relatively large load increments are employed. However, as the critical point is approached and the equilibrium path becomes increasingly nonlinear, load increments become significantly smaller to be able to traverse the collapse point (NX Nastran 11, 2006; Bathe, 2014).

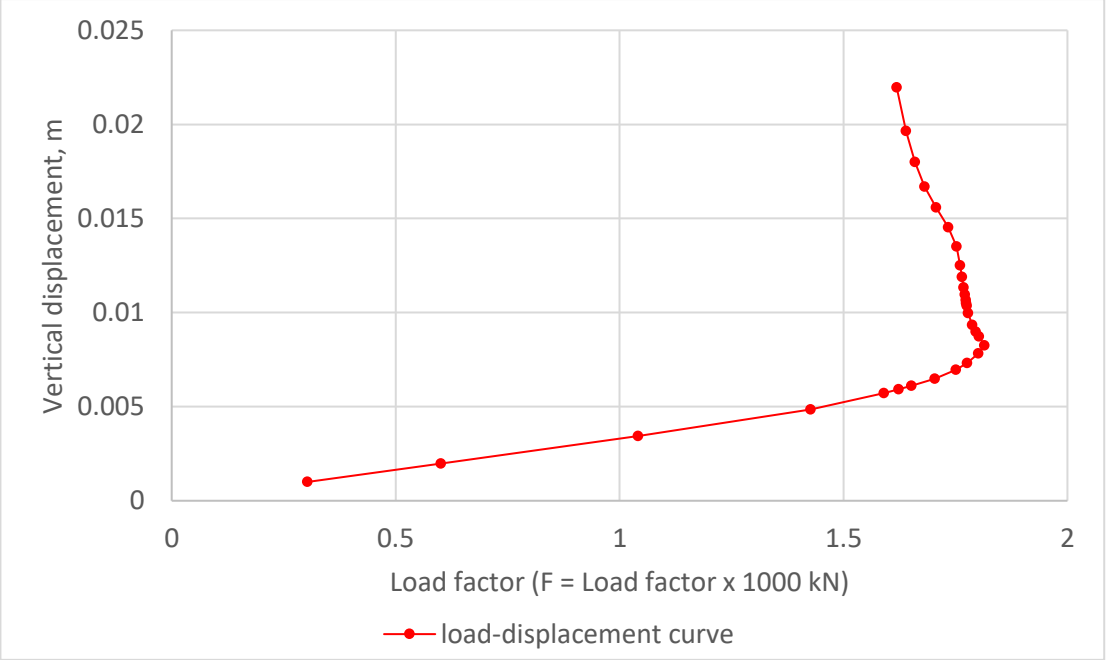

Figure 23. Example of the model's equilibrium path obtained by non-linear FEM analysis.

The general equations employed in the LDC method equilibrium are as follows (Bathe, 2014; NX Nastran 11, 2006):

$$ {}^{t+\Delta t}_{i-1}K_t \cdot {}_i\Delta u = ({}^{t+\Delta t}_{i-1}\lambda + {}_i\Delta\lambda) \cdot f_{ext} - {}^{t+\Delta t}_{i-1}f_{int} \quad (51) $$

$$ {}^{t+\Delta t}_{i}u = {}^{t+\Delta}_{i-1}u + {}_i\Delta u \quad (52) $$

$$ f({}_i\Delta\lambda, {}_i\Delta u) = 0 \quad (53) $$

where ${}^{t+\Delta t}_{i-1}\lambda$ is a load scaling factor at time $t + \Delta t$ at the end of iteration (*i-1*); ${}_i\Delta\lambda$ is an increment in the load scaling factor at iteration (*i*); other units are as denoted in Section 2.3.

The load multiplier for the first step of the LDC analysis ${}^{\Delta t}\lambda$ is calculated based on user-specified initial enforced displacement acting on a given DOF of a specific node. After the first step, the program automatically scales the external load vector so that at any discrete time *t* in iteration *i* the external load vector is ${}^{t}_{i}\Delta\lambda \cdot f_{ext}$ (NX Nastran 11, 2006).

The LDC procedure terminates when one of the following conditions is satisfied (NX Nastran 11, 2006):

- Maximum specified displacement is reached.

- A critical point on the load-displacement path is passed. The condition can be skipped in order to evaluate the post-buckling response.
- The number of converged solution steps is reached.
- The maximum number of subdivisions has been attempted, but convergence was not reached within the set maximum number of iterations.

Analysis with displacement-controlled loading generally converges faster than with force-controlled loading (NX Nastran 11, 2006).

The energy convergence criterion was used for most of analyses during the research.

The direct sparse solver was used for the nonlinear analyses. The direct sparse matrix solver is reliable and robust and is recommended by the NX Nastran 11 modeling guide (Siemens, 2006) for use as a default solver for most of the non-linear problems. For very large problems, when the computer storage resources do not satisfy those required by a direct solution, the iterative multigrid solver could be used. The 3D-iterative solver is best suited for large models with 3-D solid elements (NX Nastran 11, 2006).

The number of steps used in the analyses varied from 20 to 50 with the maximum number of iterations per step from 20 to 100 depending on the analysis complexity and the size of the model.

Restart capabilities were utilized in analyses of some large and stiff models, when the limit point was not reached with initial settings and the analysis was terminated before reaching a desired point. Restart is a feature that allows to fine-tune or change the settings of the terminated analysis and continue the analysis beyond its previous end point. For example, time steps can be tightened, the maximum number of iterations per step can be increased, or line-search and convergence criterion tolerances can be changed in order to reach convergence and pass over a limit point.

Every nonlinear analysis in the research was preceded with linear static and buckling analyses. First purpose of the linear analyses was to check model integrity and if boundary conditions and loads are applied correctly, as well as to also examine the quality of the FE-mesh. The second purpose of the LBA was to obtain linear elastic buckling modes, which were used to introduce eigenmode-shape-based imperfections to the FE-model prior to non-linear buckling analyses (see chapter 6).

Load-displacement curve (Figure 23) represents the relationship between loads and displacements in the model during non-linear analysis. Load-displacement curve

appears in the literature under many different names, for instance as *stability path, displacement response, equilibrium path, load-shortening curve* (Skotny, 2017). The tangent at any point of the load-displacement curve represents the stiffness of the structure at the point of the response history. The load at any point of the response history may be found by multiplying the reference load with the load factor.

5 METHOD VALIDATION STUDY

5.1 Idealized column with idealized boundary conditions

Before running time-consuming non-linear analyses for the main large research models, a method validation study was conducted in order to validate the non-linear approach with selected solution scheme, boundary conditions, and settings.

In the first part of the validation study, 11 models of idealized structures were created, as shown in Figure 24. These modelled T-columns with the effective part of the bulkhead plating correspond those idealized structures that are considered during capacity verifications according to the current prevalent simplified analytical practice (see Figure 14b). Columns 3050 mm high were modelled, which correspond to the typical selected deck-height of 3500 mm, minus 450 mm height of deck beams. 3500 mm is a rather typical deck height in cruise ship´s public spaces. Effective flange widths were calculated by equation (37).

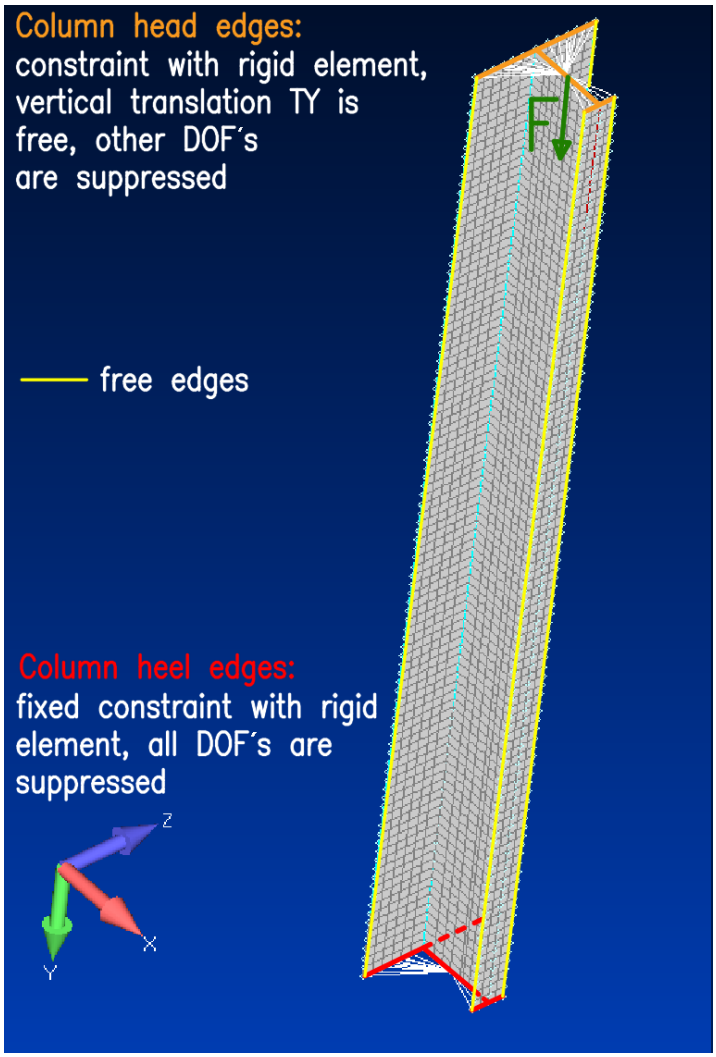

Figure 24. FE model for T-column with effective flange

5.1.1 GMNIA analyses

Materially and Geometrically Non-Linear Finite Element Analyses with Imperfections (GMNIA) were performed in accordance with the procedure presented in Section 4.2.6. The lowest elastic eigenmode-shape based imperfections (Figure 25) were applied with amplitude, as described in Chapter 6. Nine models were created for three common T-column sizes, each with three different effective flanges. In addition, two models for T-columns with a high height-to-width ratio were made.

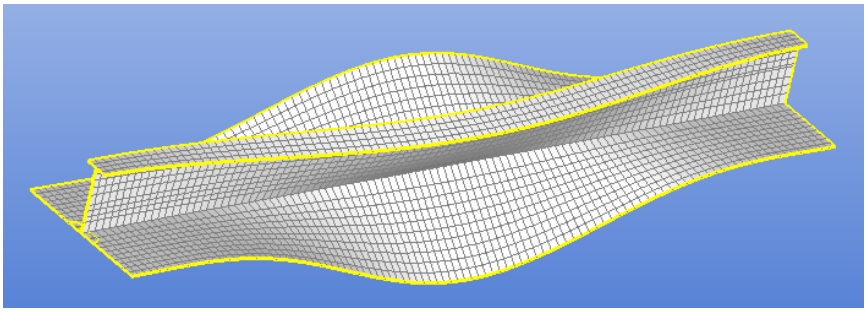

Figure 25. Example of the imperfection shape used in the analyses.

The validation study was performed for models with the following T-column sizes: T-150x8+FB100x10, T-250x8+FB100x10, T-150x10+FB200x20 and T-400x10+FB200x20, representing columns with different web height to face plate width ratios, and following bulkhead thicknesses: 6 mm, 10 mm and 15 mm, representing “thin”, “medium” and “thick” bulkhead plates.

5.1.2 CFM solutions

All the columns to which GMNIA analyses were done in Section 5.1.1 were also calculated by the closed-form semi-empirical method (CFM), in accordance with Class Guideline DNVGL-CG-0128 Buckling, Section 4 (DNV GL, 2018 b). The method is described in Section 3.1. The CFM results are presented in Table 5. The critical buckling load given in the table is an ultimate load as buckling utilization factor $\eta_{Allow} = 1$ was applied. All structures were calculated for both constraint factors 1 (ends pinned) and 4 (ends fixed) (Figure 16).

5.1.3 Results and discussion

Load-displacement curves of GMNIAs for idealized columns are presented in Figures 26 and 27. The displacement is indicated for the node to which load was applied.

The results of the CFM solutions in accordance with DNVGL-CG-0128 Buckling Section 4 are shown in Table 5. Animations of the GMNIA analyses can be found in Appendix A.

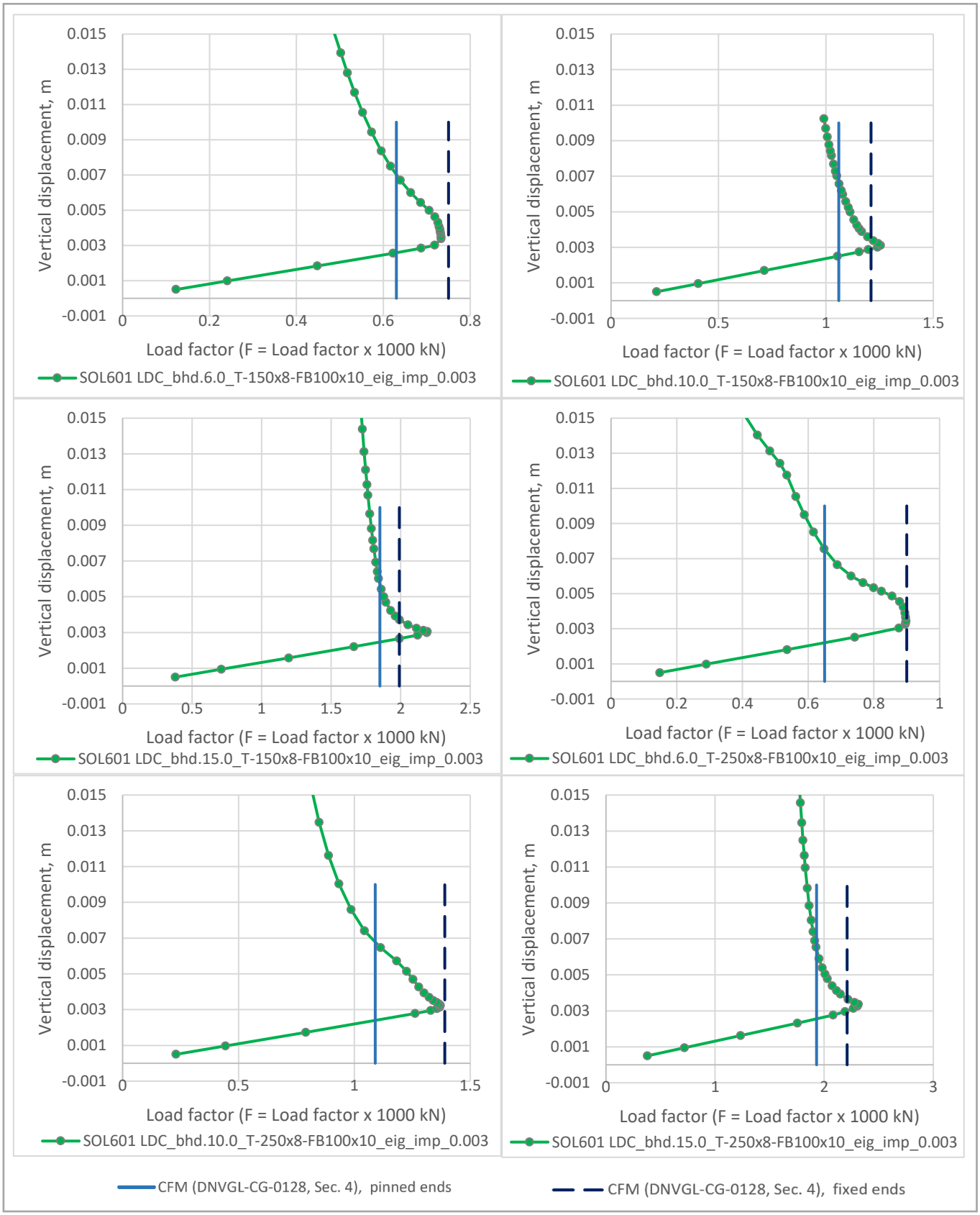

Figure 26. GMNIA load-displacement curves for columns of T-150x8-FB100x10 and T-250x8-FB100x10 with various effective flanges.

(Bhd.xx.x value denotes the effective flange thickness, effective flange width = thickness x 40).

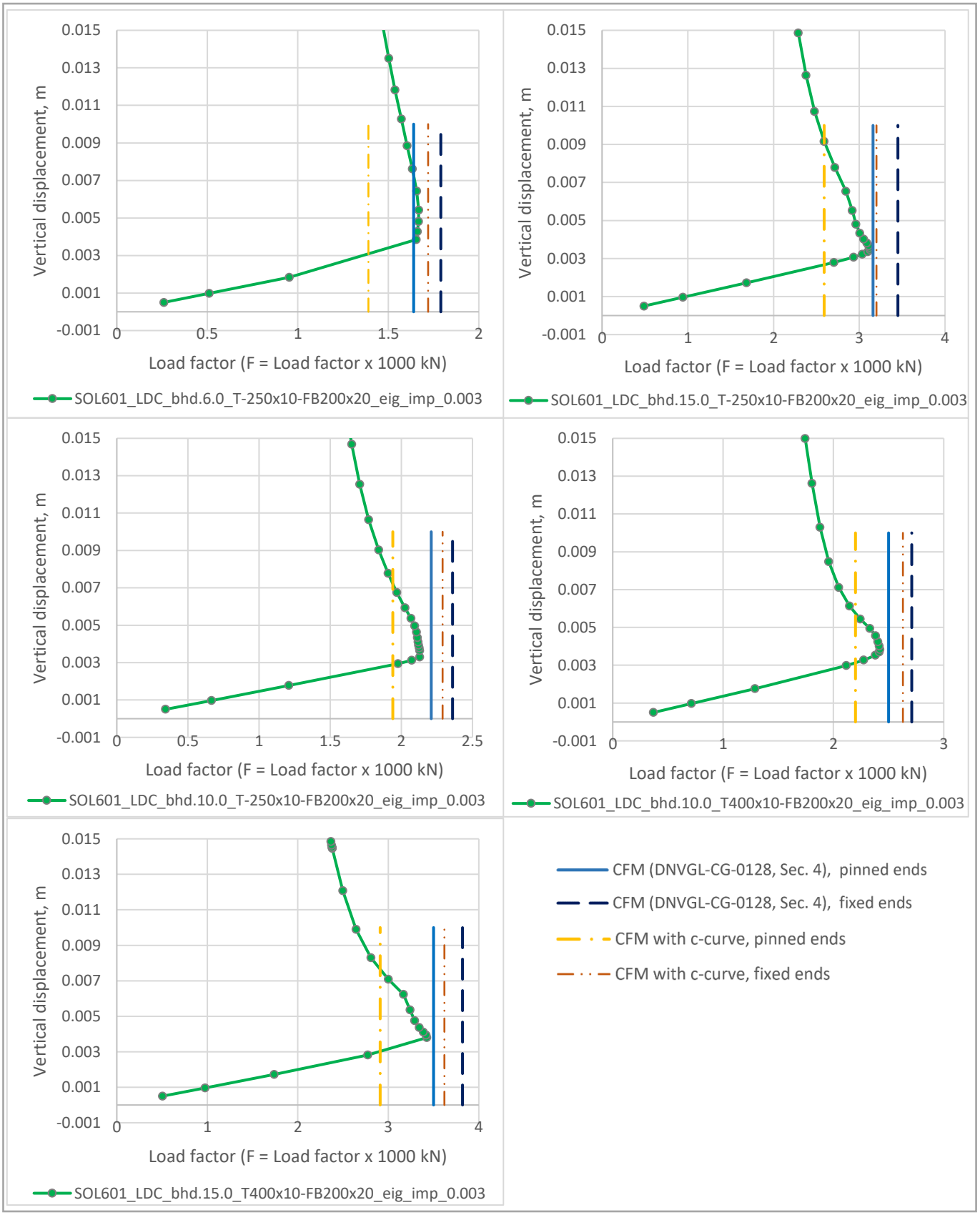

Figure 27. GMNIA load-displacement curves for columns of T-250x10-FB200x20 and T-400x10-FB200x20 with various effective flanges.

(Bhd.xx.x value denotes the effective flange thickness, ef.fl. width = thickness x 40).

Table 5. Buckling load calculation results for idealized structures in accordance with DNVGL-CG-0128 Buckling, Section 4

		Input						Input for torsion				Results				Utilisation			
T-column sise	Effective flange thickness t, mm (width = 40 x t)	I_{net} [cm^4]	A_{pill_net} [cm2]	f_{end}	ℓ_{pill} [m]	F_{pill} [kN]	R_{eH} [MPa]	I_{sv_net} [cm4]	I_{pol_net} [cm4]	c_{warp} [cm6]	ζ	σ_{EC} [MPa]	σ_{ET} [MPa]	σ_{ETF} [MPa]	Pillar no	σ_{av} [MPa]	σ_{cr} [MPa]	η	η_{Allow}
T-150x8-FB100x10	6.0	775	36	1.0	3.050	630	235	7.6	3194.0	16732.7	0.72	473.8	303.6	237.4	1	176.2	176.8	0.996	1.00
T-150x8-FB100x10	6.0	775	36	4.0	3.050	750	235	7.6	3194.0	16732.7	0.72	1895.0	647.0	576.9	1	209.7	211.1	0.994	1.00
T-150x8-FB100x10	10.0	2172	61	1.0	3.050	1,060	235	19.2	8400.6	18461.5	0.90	775.8	229.4	220.9	7	173.2	172.5	1.004	1.00
T-150x8-FB100x10	10.0	2172	61	4.0	3.050	1,210	235	19.2	8400.6	18461.5	0.90	3103.2	373.5	368.7	7	197.7	197.6	1.001	1.00
T-150x8-FB100x10	15.0	2588	111	1.0	3.050	1,850	235	73.4	30159.7	18692.3	0.98	509.5	206.4	204.1	10	166.7	167.4	0.996	1.00
T-150x8-FB100x10	15.0	2588	111	4.0	3.050	1,990	235	73.4	30159.7	18692.3	0.98	2038.1	247.0	246.4	10	179.3	179.0	1.002	1.00
T-250x8-FB100x10	6.0	776	44	1.0	3.050	650	235	9.3	8675.3	46479.6	0.63	387.4	202.3	160.3	1	148.5	148.9	0.998	1.00
T-250x8-FB100x10	6.0	776	44	4.0	3.050	900	235	9.3	8675.3	46479.6	0.63	1549.4	553.6	475.5	3	205.7	206.0	0.999	1.00
T-250x8-FB100x10	10.0	5418	69	1.0	3.050	1,090	235	20.9	15284.4	51282.1	0.79	1711.1	181.8	177.6	7	157.5	157.3	1.002	1.00
T-250x8-FB100x10	10.0	5418	69	4.0	3.050	1,390	235	20.9	15284.4	51282.1	0.79	6844.4	401.8	396.8	9	200.9	200.2	1.003	1.00
T-250x8-FB100x10	15.0	8173	119	1.0	3.050	1,930	235	75.1	37247.4	51923.1	0.95	1501.0	190.2	188.8	10	162.2	161.9	1.002	1.00
T-250x8-FB100x10	15.0	8173	119	4.0	3.050	2,210	235	75.1	37247.4	51923.1	0.95	6004.0	281.6	280.9	12	185.7	185.8	0.999	1.00
T-250x10-FB200x20	6.0	2027	78	1.0	3.050	1,640	235	63.4	10408.8	284510.0	1.00	567.1	1080.0		1	210.0	210.7	0.997	1.00
T-250x10-FB200x20	6.0	2027	78	4.0	3.050	1,790	235	63.4	10408.8	284510.0	1.00	2268.4	2872.1		3	229.2	228.9	1.001	1.00
T-250x10-FB200x20	10.0	6669	104	1.0	3.050	2,210	235	75.0	26089.8	666666.7	0.78	1408.2	786.2	657.7	7	213.5	214.0	0.998	1.00
T-250x10-FB200x20	10.0	6669	104	4.0	3.050	2,360	235	75.0	26089.8	666666.7	0.78	5632.8	2461.7	2161.4	9	228.0	228.6	0.997	1.00
T-250x10-FB200x20	15.0	18818	153	1.0	3.050	3,160	235	129.2	55300.2	794117.6	0.85	2683.7	498.9	483.3	10	206.2	206.4	0.999	1.00
T-250x10-FB200x20	15.0	18818	153	4.0	3.050	3,450	235	129.2	55300.2	794117.6	0.85	10734.8	1440.5	1409.1	12	225.1	225.2	1.000	1.00
T-400x10-FB200x20	10.0	6670	119	1.0	3.050	2,500	235	80.0	60507.7	1706666.7	0.72	1230.2	721.2	577.3	7	211.0	211.1	0.999	1.00
T-400x10-FB200x20	10.0	6670	119	4.0	3.050	2,710	235	80.0	60507.7	1706666.7	0.72	4920.7	2570.6	2118.8	9	228.7	228.5	1.001	1.00
T-400x10-FB200x20	15.0	28336.5	168.3	1.0	3.050	3,500	235.0	134.2	104217.8	2032941.2	0.76	3680.9	528.3	508.6	10	208.0	207.9	1.001	1.00
T-400x10-FB200x20	15.0	28336.5	168.3	4.0	3.050	3,820	235.0	134.2	104217.8	2032941.2	0.76	14723.8	1807.3	1750.3	12	227.0	227.1	1.000	1.00

As is seen from Figures 26 and 27, results on the buckling load of the structure received with GMNIA correlate relatively well with those received with analytical solutions; the deviations within 11% for all studied models when compared to the corresponding results of CFM with the end constraint factor 4, which corresponds to the fixed column ends (Table 6).

Table 6. Comparison of the buckling load prediction by CFM (DNV GL, 2018 b, sec 4) and GMNIA.

		Critical buckling load, kN			Difference CFM/GMNIA, %	
T-column, mm	Effective flange, mm	CFM pinned	CFM fixed	GMNIA	pinned	fixed
T-150x8-FB100x10	240x6	630	750	720	14%	-4%
T-150x8-FB100x10	400x10	1060	1210	1240	17%	2%
T-150x8-FB100x10	600x15	1850	1990	2180	18%	10%
T-250x8-FB100x10	240x6	650	900	890	37%	-1%
T-250x8-FB100x10	400x10	1090	1390	1370	26%	-1%
T-250x8-FB100x10	600x15	1930	2210	2300	19%	4%
T-250x10-FB200x20	240x6	1640	1790	1650	1%	-8%
T-250x10-FB200x20	400x10	2210	2360	2120	-4%	-10%
T-250x10-FB200x20	600x15	3160	3450	3120	-1%	-10%
T-400x10-FB200x20	400x10	2500	2710	2420	-3%	-11%
T-400x10-FB200x20	600x15	3500	3820	3420	-2%	-10%

Generally, the observed correlation between CFM and GMNIA results is considered by the author as good, justifying the usage of CFM for I-shaped columns on the one hand and GMNIA with selected solution scheme for analyses of more complex models in the research, on the other hand.

However, for stiff columns with 20 mm thick flange, moderate systematic over-estimation of loading capacity by CFM compared to GMNIA was observed (Figure 27). When considering possible reasons for this, it was realized that the Johnson-Ostenfeld-formula-based plasticity correction is integrated into the method according to DNVGL-CG-0128.

The Johnson-Ostenfeld formula is an empirical equation derived from column tests conducted in the 1950s. It was developed in order to take into account the effects of plasticity on buckling, but it does not account for initial imperfections (Bai., 2003).

The columns were recalculated according to the same CFM method but with the European non-dimensional buckling curves-based plasticity correction instead of Johnson-Ostenfeld. European column buckling curves in accordance with Eurocodes (see Figure 28) are based on the Ayrton-Perry approach and better account for initial

imperfections (Jönsson & Stan, 2017; The Steel Construction Institute, 2012; Baroudi, 2020). The imperfection factor $\alpha = 0.49$ was applied, which corresponds to the buckling curve c.

The Ayrton-Perry formula for the buckling resistance reduction factor χ, as given in Eurocode 3 (Baroudi, 2020), is as follows:

$$\chi = \frac{1}{\phi + \sqrt{\phi^2 - \bar{\lambda}^2}} \tag{54}$$

where $\phi = \frac{1}{2}\left[1 + \alpha(\bar{\lambda} - 0{,}2) + \bar{\lambda}^2\right]$ and column relative slenderness $\bar{\lambda} = \sqrt{\frac{A\sigma_y}{N_E}}$.

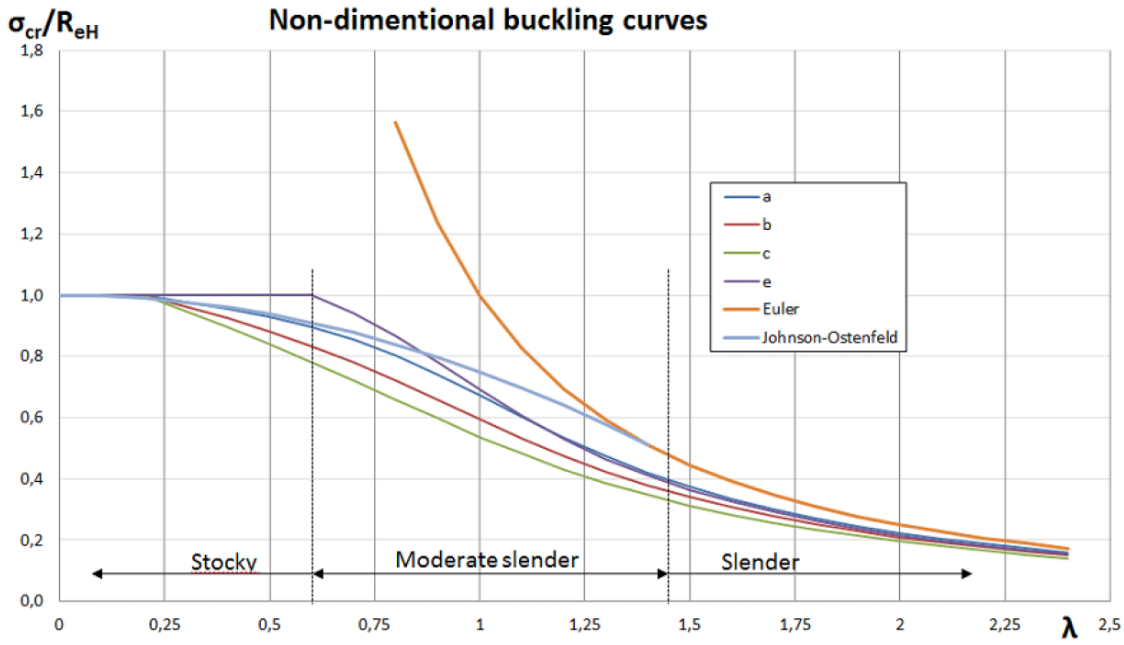

Figure 28. Non-dimensional buckling curves.

The limit load prediction with European non-dimensional buckling curves showed better correlation with GMNIA for stiffer columns shown in Figure 27, GMNIA results being in between of those for fixed and pinned end constraint factors and closer to those with pinned for all recalculated cases (see Table 7 and Figure 27).

Table 7. Comparison of buckling load prediction by CFM with c-curve and GMNIA.

		Critical buckling load, kN			Difference CFM/GMNIA, %	
T-column, mm	**Effective flange, mm**	**CFM pinned**	**CFM fixed**	**GMNIA**	**pinned**	**fixed**
T-250x10-FB200x20	240x6	1390	1720	1650	19%	-4%
T-250x10-FB200x20	400x10	1940	2290	2120	9%	-7%
T-250x10-FB200x20	600x15	2590	3200	3120	20%	-3%
T-400x10-FB200x20	400x10	2200	2630	2420	10%	-8%
T-400x10-FB200x20	600x15	2910	3620	3420	18%	-6%

It must be noted, that buckling curves are based on a large amount of experimental data from various collapse tests and account for such types of imperfections as geometric imperfections of cross-sections, residual stresses, eccentricities, material variability, and others. All these effects remain inaccessible through mathematical modelling only, and thus 100% correlation between the analytical solution and the FE-modelled solution cannot be achieved (Baroudi, 2020).

In order to check the hypothesis, if the observed deviation is caused by the difference in imperfections used in the FE-model during NA and the plasticity correction model in CFM, several models were analyzed with very little imperfection amplitudes. Minimal imperfections (scale factor of 0.001, amplitudes $<<$ 1 mm) were applied simply in order to introduce perturbation to the system and to initiate the buckling. As is seen from Figure 29, a significantly better correlation with CFM results were observed, and this, at least partially, proves the hypothesis.

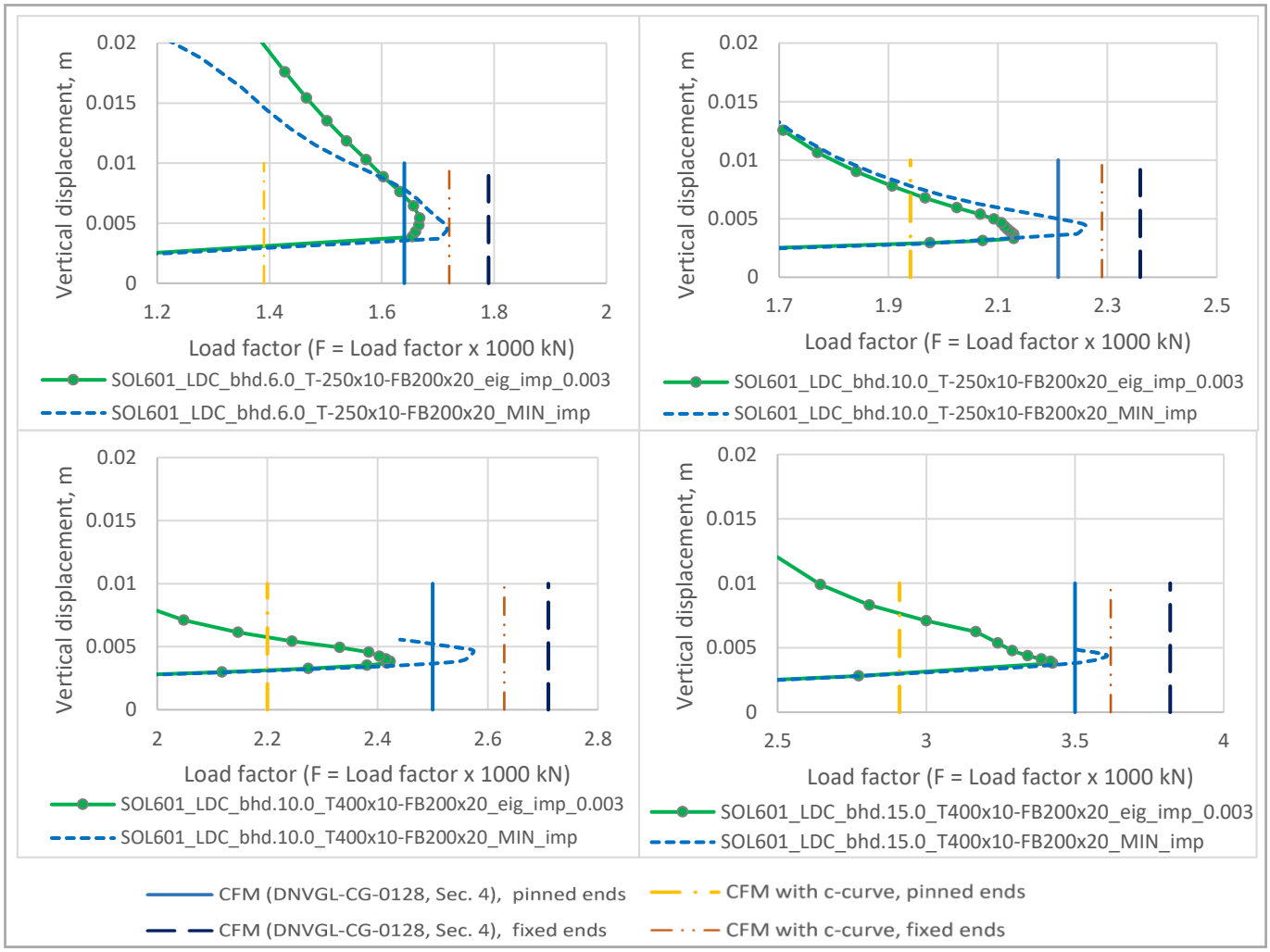

Figure 29. Impact of initial imperfection on the predicted buckling load.

A more thorough study on the reasons for the observed phenomena was not performed within the framework of present thesis research. It remained unclear, therefore, why columns with stiffer flanges showed better correlation with CFM with plasticity correction applied according to the European non-dimensional buckling curves while those with lighter flanges showed better correlation with CFM with the Johnson-Ostenfeld plasticity correction.

While a more detailed study might be required with more analyses on various column sizes in order to receive statistically significant data, it is still undeniable that imperfections are inherent to real structures (Ellobody et al, 2013; Efstein et al, 2016, Baroudi, 2020); thus, the application of plasticity correction models that account for a reasonable level of initial imperfections, such as the European-Buckling curves, seems to be a rational approach.

5.2 Idealized column with more realistic boundary conditions

5.2.1 GMNIA analyses

In the second part of the validation study, in addition to idealized structures of the same T-columns with effective flanges as in the first part, decks, pillars, and typical pillar-to-deck connections were also included in the FE models. This was done in order to better represent conditions existing in a real ship structure, including eccentric positioning of pillars with respect to the T-columns, and to simulate more realistic boundary conditions. The example of the model with applied boundary conditions is shown in Figure 30. The extent of the model and mesh parameters are identical to those as described in Section 7.1.1.

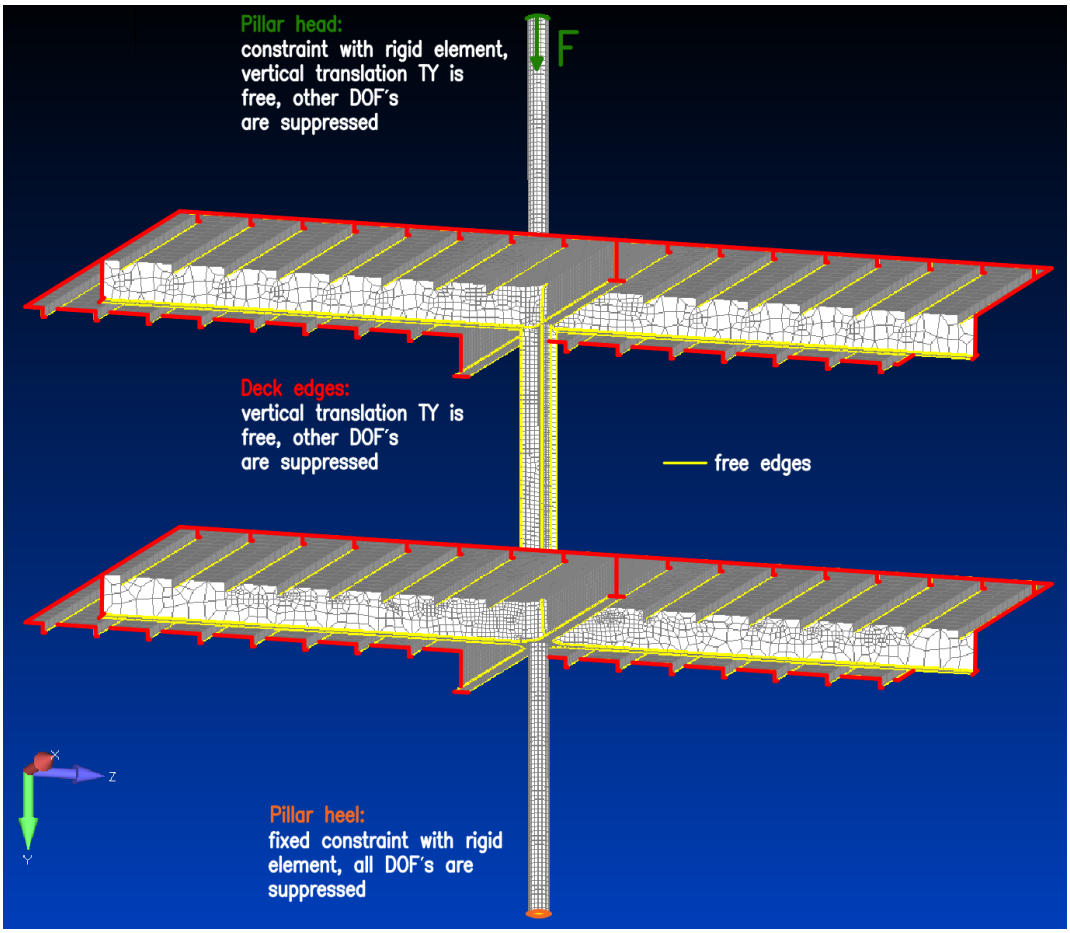

Figure 30. Boundary conditions for FE models of idealized columns with the effective part of the bulkhead plating with decks and pillars included.

5.2.2 Results and discussion

Results of the analyses for models with decks and pillars included are presented in Figures 31 and 32. For animations of the analyses see Appendix A.

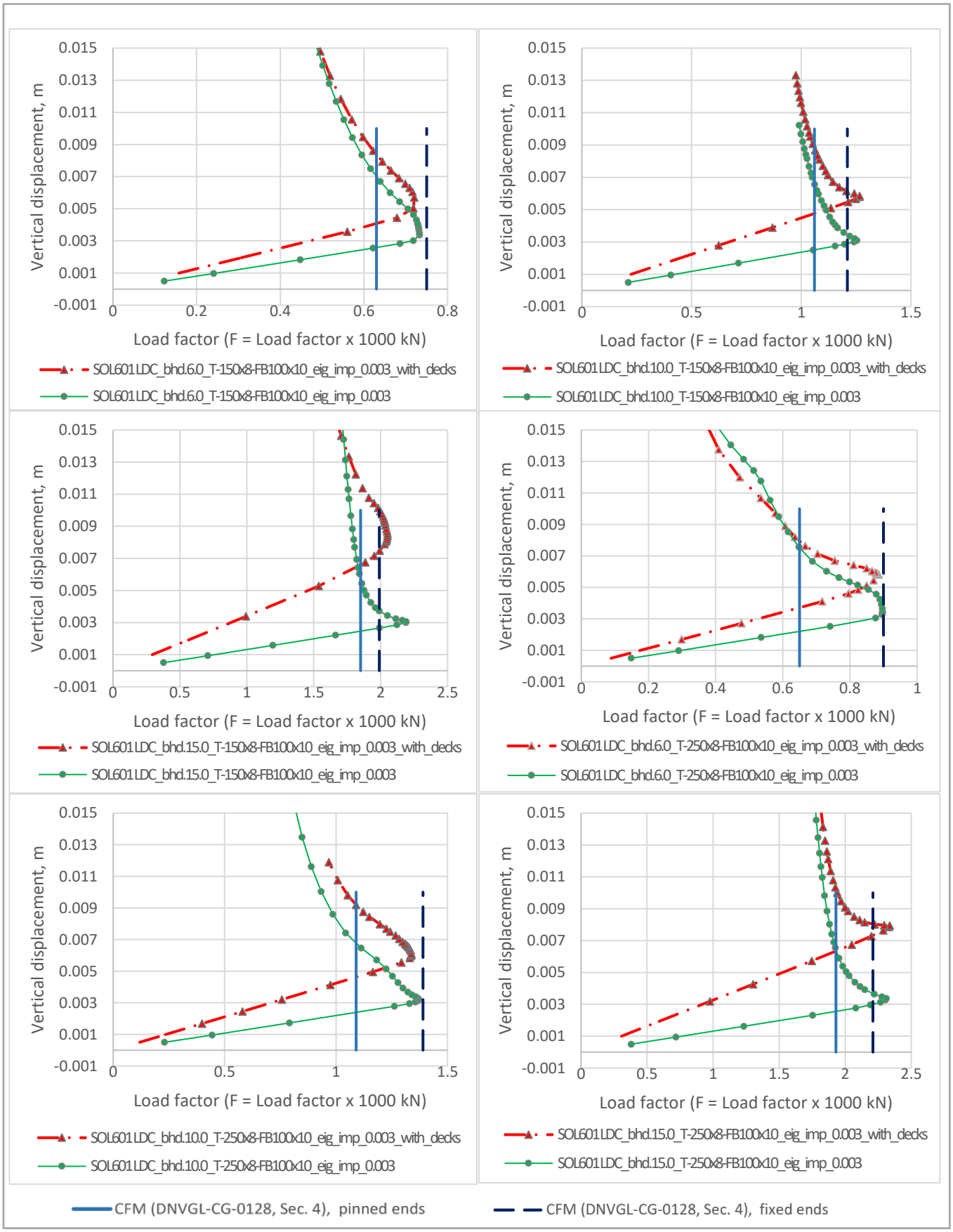

Figure 31. GMNIA load-displacement curves for columns of T-150x8-FB100x10 and T-250x8-FB100x10 with various effective flanges for structures modelled with decks and pillars.

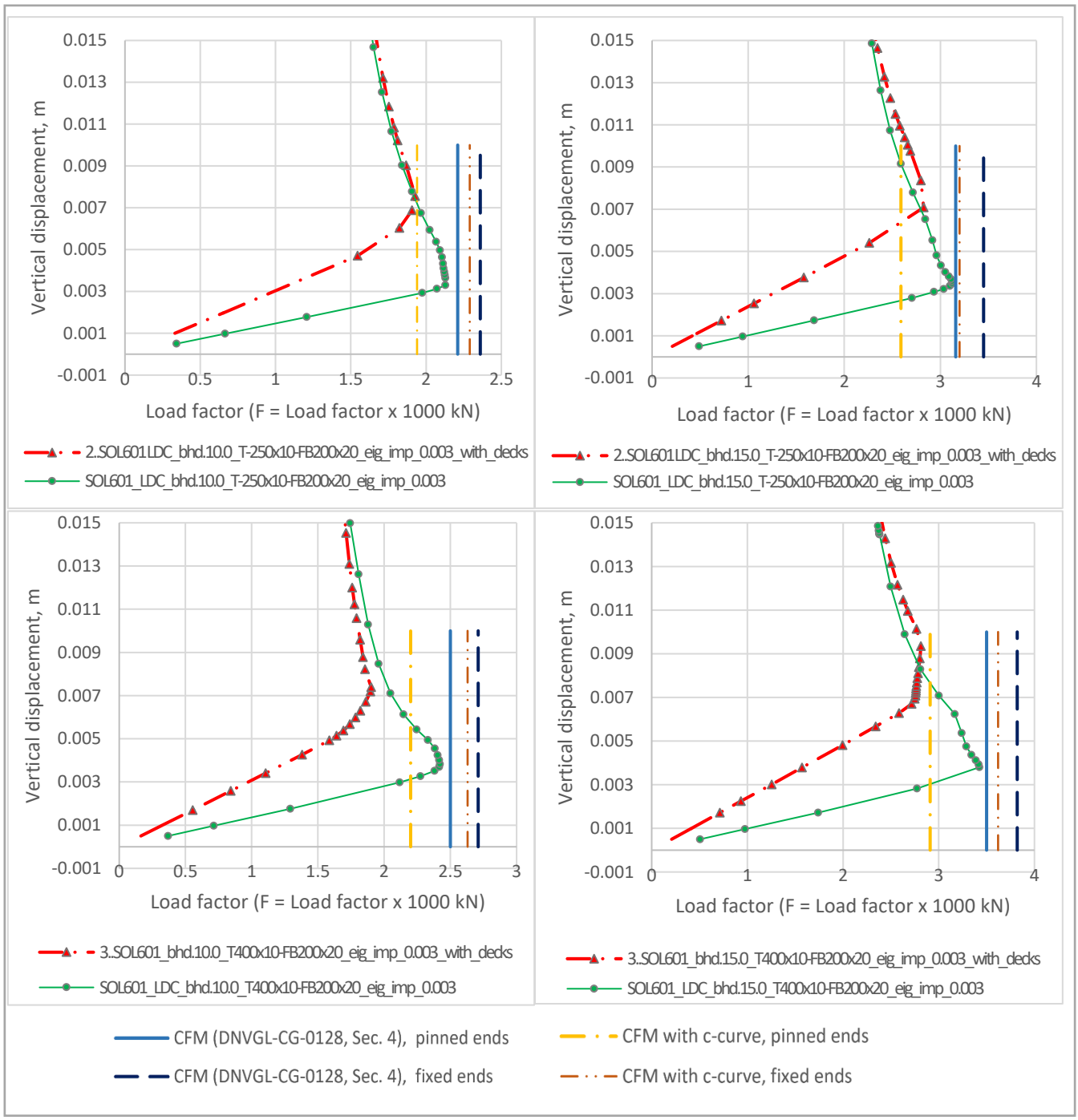

Figure 32. GMNIA load-displacement curves for columns of T-250x10-FB200x20 and T-400x10-FB200x20 with various effective flanges for structures modelled with decks and pillars.

Results of GMNIA analyses for models of *idealized columns with decks and pillars included* were compared with the results of analyses for *idealized columns with idealized boundary conditions*.

First, the results for the columns shown in Figure 31 will be compared. Differences in the load-displacement curve angles can be observed, which is due to the changed total stiffness of the models because of the included pillars. However, the buckling loads remained almost identical for both boundary condition cases. It could be stated that boundary conditions existing in ship structures have a minor impact on the capacity of that columns compared with idealized ones.

When reviewing results for heavier columns, which are shown in Figure 32, it can be noticed that columns with heavier flanges and especially those with higher webs in models with decks and pillars buckle at lower loads than the same columns in models with idealized boundary conditions.

Moreover, it was noted that while buckling modes for the former ones (Table 8) are almost identical for both boundary condition cases, for the latter ones (Table 9), the buckling modes differ. It is clearly visible from the stress distribution patterns that stress is distributed more-or-less evenly across column cross sections for columns with idealized boundary conditions; however, for models with the same columns with decks and pillars included, the stress is concentrated in the bulkhead plate/column web region. The column flange effectiveness decreases due to the eccentricity of the pillar's position with respect to the column cross section; this resulted in plate-induced flexural buckling modes for columns with decks and pillars included shown in Table 9 and decreased loading capacities, while the same columns with idealized boundary conditions buckled in lateral-torsional modes.

In summary, it can be stated that for idealized columns listed in Figure 31 and Table 8, the impact of more realistic boundary conditions compared with idealized ones remained minor, while for those with heavier flanges and higher webs (Figure 32 and Table 9), the impact becomes increasingly noticeable as the eccentricity in the pillar's position with respect to the column cross section grows.

Table 8. Comparison of buckling modes for cases studied in Sec. 5.1 and Sec. 5.2, columns withT-150x8-FB100x10 and T-250x8-FB100x10 (continues on the next page.)

Column si:	**Case 1, idealized column** (Sec. 5.1 analyses)		**Case 2, model with decks and pillars** (Sec. 5.2 analyses)		**Observed buckling mode**
	buckling shape at critical point	post-buckled shape	buckling shape, at critical point	post-buckled shape	
T-150x8-FB100x10 + Fl.240x6	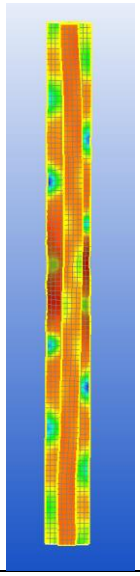	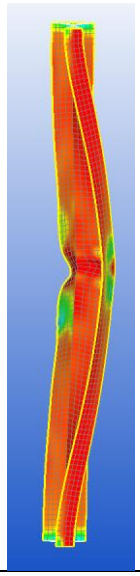	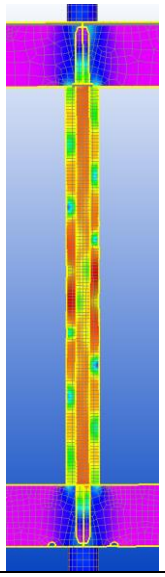	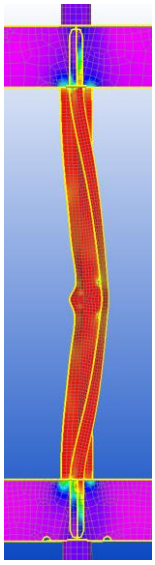	Case 1: Flexural-torsional buckling Case 2: Flexural-torsional buckling
T-150x8-FB100x10 + Fl.400x10	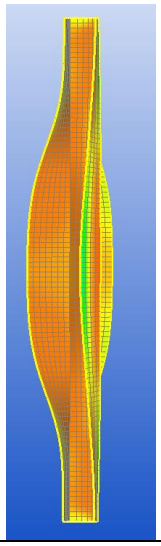	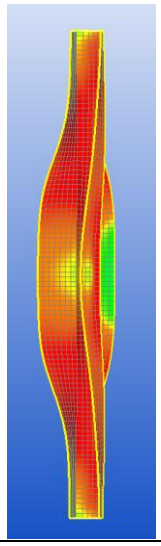	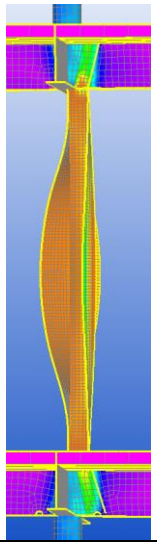	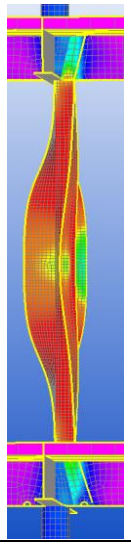	Case 1: Flexural-torsional buckling Case 2: Flexural-torsional buckling
T-150x8-FB100x10 + Fl.600x15	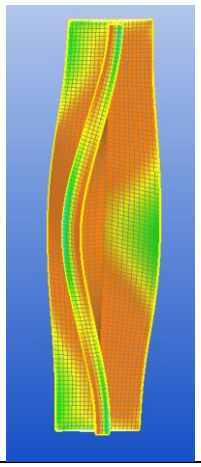	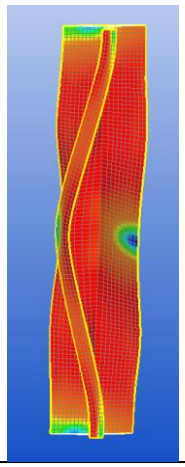	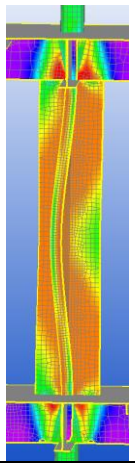	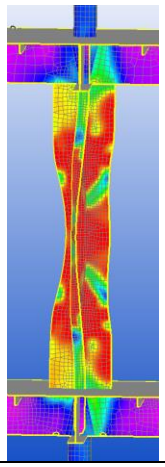	Case 1: Flexural-torsional buckling Case 2: Flexural-torsional buckling

Table 8. Comparison of buckling modes for cases studied in Sec. 5.1 and Sec. 5.2 for columns with T-150x8-FB100x10 and T-250x8-FB100x10 (continued).

T-250x8-FB100x10 + Fl.240x6	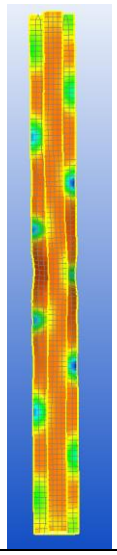	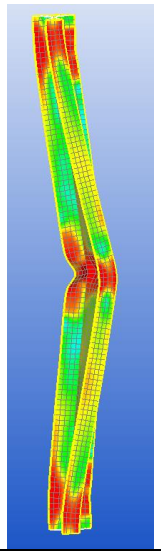	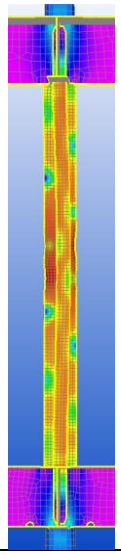	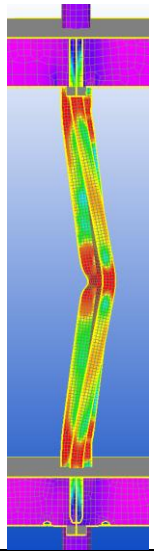	Case 1: Flexural-torsional buckling Case 2: Plate-induced overall buckling
T-250x8-FB100x10 + Fl.400x10	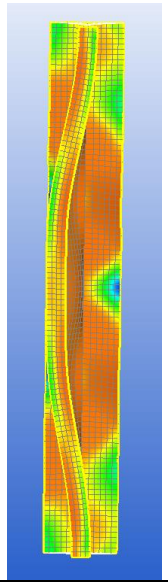	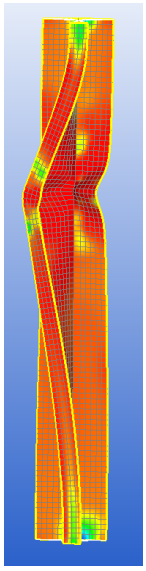	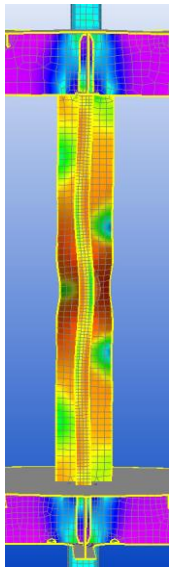	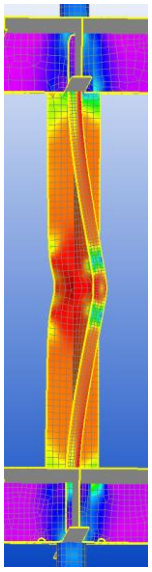	Case 1: Flexural-torsional buckling Case 2: Flexural-torsional buckling
T-250x8-FB100x10 + Fl.600x15	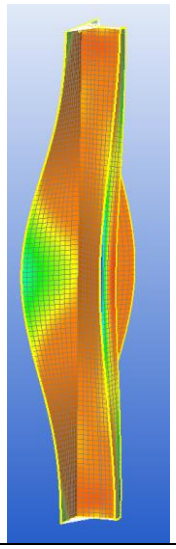	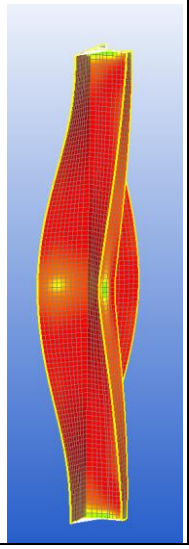	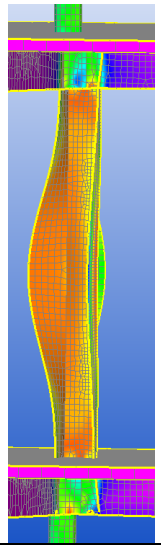	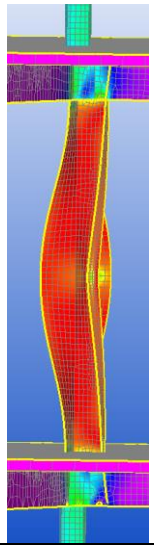	Case 1: Flexural-torsional buckling Case 2: Flexural-torsional buckling

Table 9. Comparison of buckling modes for cases studied in Sec. 5.1 and Sec. 5.2 for columns with T-250x10-FB200x20 and T-400x10-FB200x20 (continues on the next page).

Column size	**Case 1, idealized column (**5.1**)**		**Case 2, model with decks and pillars** (5.2)		**Observed buckling mode**
	buckling shape at critical point	post-buckled shape	buckling shape, at critical point	post-buckled shape	
T-250x10-FB200x20 + Fl.400x10	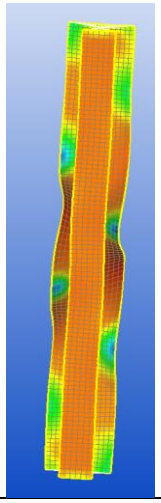	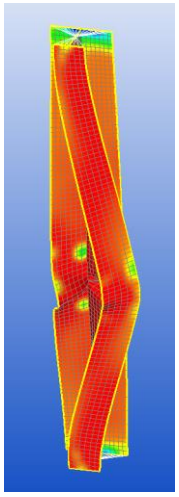	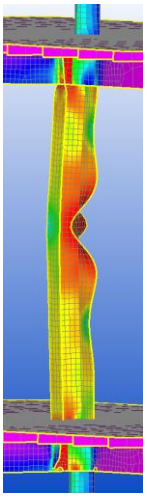	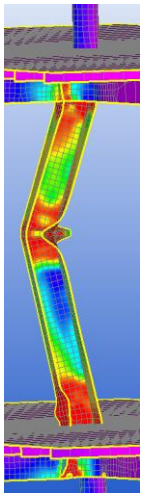	Case 1: Flexural-torsional buckling Case 2: Plate-induced flexural buckling
T-250x10-FB200x20 + Fl.600x15	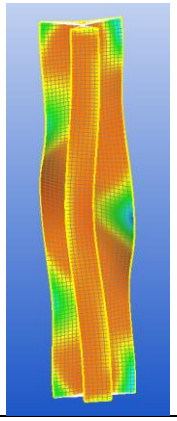	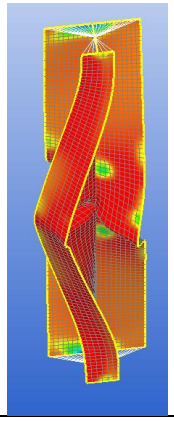	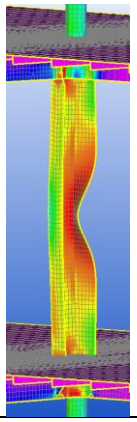	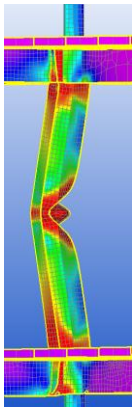	Case 1: Flexural-torsional buckling Case 2: Plate-induced flexural buckling
T-400x10-FB200x20 + Fl.400x10	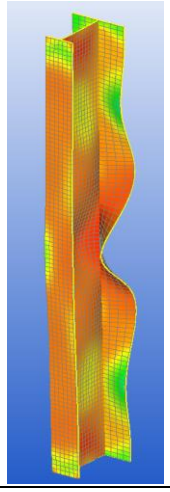	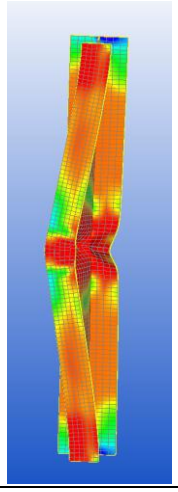	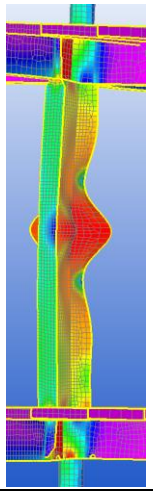	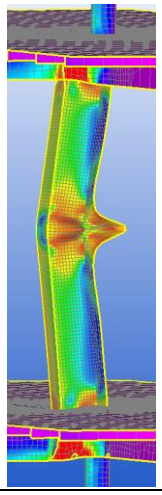	Case 1: Flexural-torsional buckling Case 2: Plate-induced flexural buckling

Table 9. Comparison of buckling modes for cases studied in Sec. 5.1 and Sec. 5.2 for columns with T-250x10-FB200x20 and T-400x10-FB200x20 (continued).

T-400x10-FB200x20 + Fl.600x15	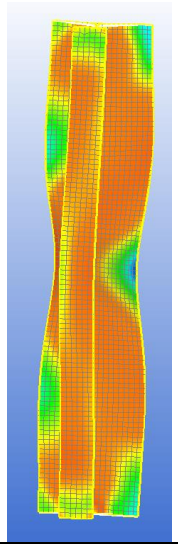	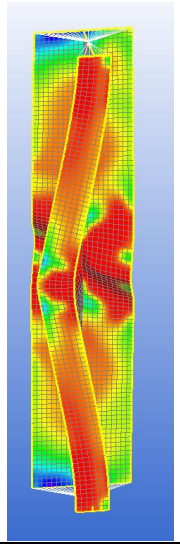	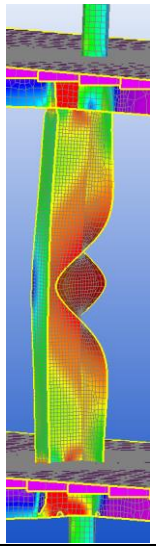	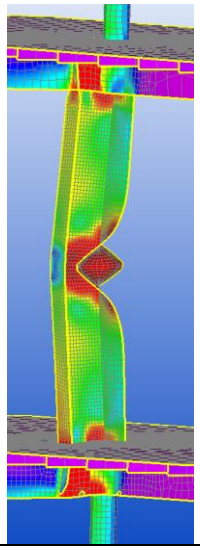	Case 1: Flexural-torsional buckling Case 2: Plate-induced flexural buckling

6 IMPERFECTION STUDY

As was stated in Section 2.5, imperfections not only have an impact on the ultimate capacity of the compressed structures, but are also important for the correct execution of numerical simulations, particularly in buckling problems.

In order to check the imperfection sensitivity of the studied structures and select proper imperfection shapes and amplitudes for research analyses, the imperfection study was performed.

6.1 Ways to model initial imperfections

There are two different approaches to modeling initial imperfections.

- One approach to including the effects of the initial geometrical imperfections in the analysis is to model them directly.
- Another approach is to add in to the model equivalent fictitious forces that simulate the imperfections (CEN, 2006; Saha & Culpepper, 2014).

The first approach was used in the analyses conducted during the thesis research.

6.2 Description of models and applied imperfection types

An imperfection sensitivity study was performed on one selected structural configuration for multiple anticipated imperfection types.

The typical bulkhead structure in the way of a pillar without openings with a T-column size of T-150x8-FL-100x10, which is one of the most typical default sizes[6] of T-columns for vertically stiffened bulkheads, was selected for the imperfection study. The structural configuration is the same as shown in Figure 40 in Chapter 7. The initial geometric imperfections were modelled directly. Five models of the same structure with different types of initial geometrical distortions were made for the imperfection study.

[6] By “default size” the size before strengthening is meant

Initial geometric imperfections can be classified into two main categories: local and overall, or global (Ellobody et al., 2013). Models with the following global imperfections were made: four models with bow imperfections and one model with a twist imperfection.

In order to represent bow imperfections, initial distortions were applied to structural members as follows:

- Out-of-straightness in the plane of web was applied to the T-column, bulkhead plate, and stiffeners (camber deflection) (Figure 33, a);
- Out-of-straightness in the plane of flange was applied to the T-column and bulkhead stiffeners (Figure 33, b).

In the model with a twist imperfection, distortion was applied to the T-column (Figure 33, c).

The impact of local imperfections was checked by applying initial distortion which shape corresponds to the lowest critical elastic buckling mode (Figure 33, d). The imperfection covers both local and global stability aspects. Linear buckling modes (eigenvectors) were received with linear buckling FE-analyses and were factored so as to obtain a meshed model with geometrical distortions that correspond to the imperfection amplitude values indicated in Section 6.3.

The basic idea behind the eigenmode-shape-based approach is that the imperfections exercise the most adverse effect on the structure when they have the shape of the lowest elastic critical buckling mode (Brodnianskya et al., 2014; Lindgaard et al., 2010; DNV GL, 2018 b).

The eigenmode-shape-based method, also referred to as the Equivalent Unique Global and Local Imperfection (EUGLI), is described in Eurocode 3 EN1993-1-1:2005 Section 5.3.2(11). The formula for calculating the imperfection amplitude as given in Eurocode 3 depends on the characteristic moment resistance, characteristic normal force resistance, non-dimensional slenderness, critical elastic buckling force, bending moment, and a number of other parameters. The basis of the method was developed by Chladný.

During the present research, a simplified approach to determining the eigenmode-shape-based imperfection amplitude was applied. The amplitude value was taken according to the DNV GL Recommended Practice DNV-RP-C208 5.4.3 Table 5-7 (DNV GL, 2013) and is given in Section 6.3.

Each of the above-mentioned models with global and eigenmode-shape-based imperfections were analyzed for both “thin” and “medium-thick” bulkhead plates, 6 mm and 10 mm, respectively. Boundary conditions, mesh size, and solution scheme were as described in Section 7.1.

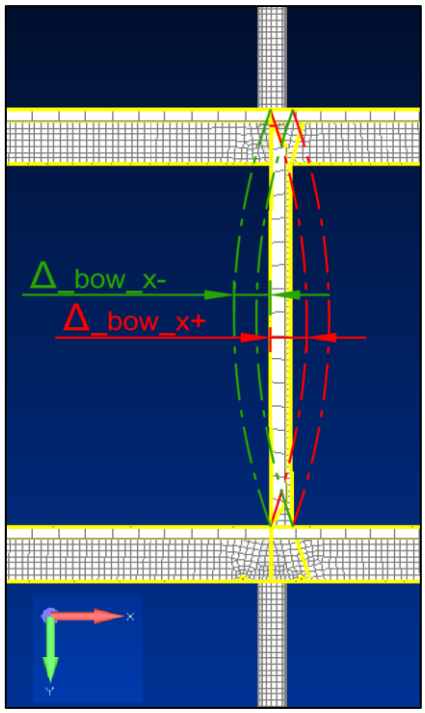

a). Bow imperfections in the plane of the column web.

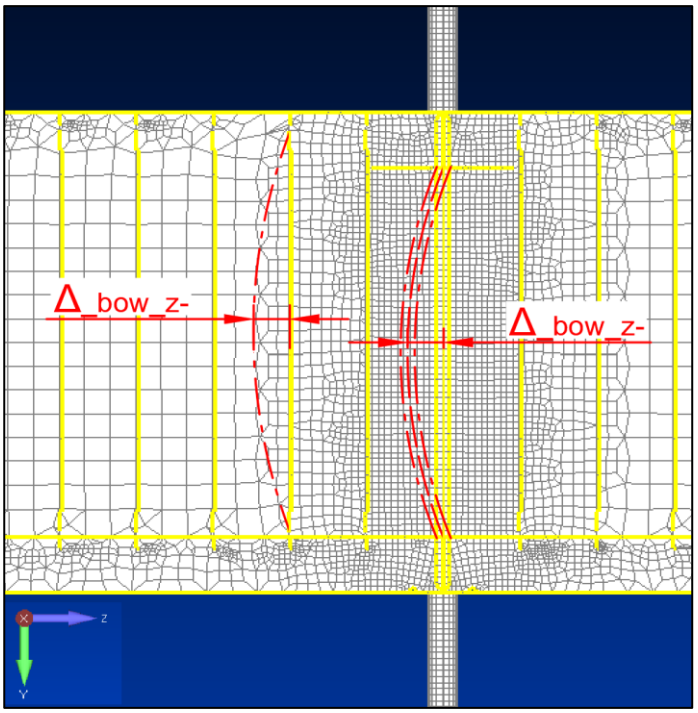

b). Bow imperfections in the plane of the column flange.

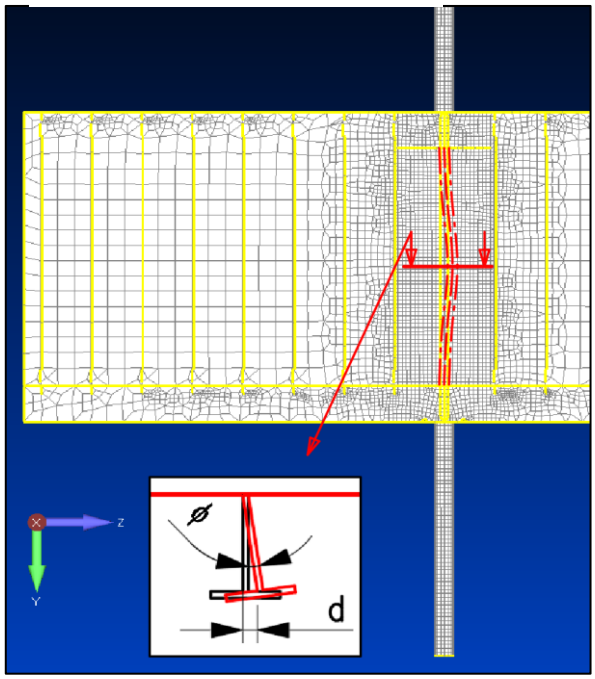

c). Twist imperfection.

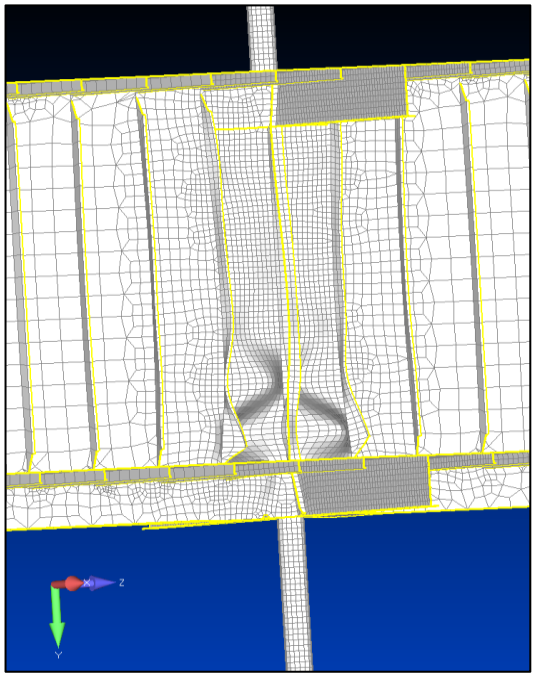

d). Lowest elastic eigenmode-shape-based imperfection.

Figure 33. Imperfection types applied to the studied structure.

Residual stresses were neglected, following the recommendation of the Class Guideline for Buckling (DNV GL, 2018 b). The guideline states that it is not necessary to include residual stresses in the FE-plate and shell models if the main focus is the ultimate strength and not the highly localized behavior associated with the welds.

6.3 Imperfection magnitudes

During the present research, the approach to selecting the imperfection amplitudes was to account for manufacturing tolerances set by the standards for ship structures. The assumption is that deviations in ship structures would normally not exceed the limit values of those set in manufacturing and quality standards. When selecting imperfection amplitude values for the study (Table 10), the following manufacturing standards and publications were reviewed:

- Shipbuilding and Repair Quality Standard (IACS, 2013).
- Survey of Structural Tolerances in the United States Commercial Shipbuilding Industry (Basar et al, 1978).
- DNV-RP-C208 Recommended Practice: Determination of Structural Capacity by Non-linear FE Analysis Methods (DNV GL, 2013).
- Dimensional Tolerances in Hull Structures (Meyer Turku, 2016).
- Dimensional Control Plan in Turku Shipyard in the NB1400 Project (Meyer Turku, 2019)

Table 10. Manufacturing tolerances and selection of imperfection amplitudes (continues on the next page)

		IACS, 2013	**Basar et al, 1978**	**Meyer Turku, 2019**	**DNV GL, 2013**	**Applied imperfection amplitude** (deck height – 3.5m deck beam height 0.45 m)
Distortion of a built-up member in the plane of the web	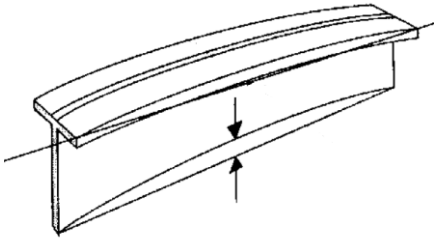	per 10 m length: standard: ±10mm limit: ±25 mm		6 mm	L/400	±8.75 mm
Distortion of a built-up member in the plane of the flange	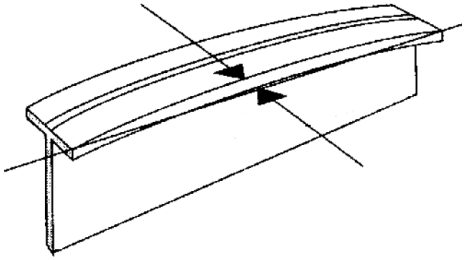	per 10 m length: standard: ±10mm limit: ±25 mm	for lengths from 30″ up to 125″: $d \leq \frac{1}{4} + \frac{\mathrm{L}}{500}$, inches	6 mm	L/300 for strict tolerances and low residual stresses; L/200 for moderate tolerances and residual stresses	±8 mm and ±15 mm
Stiffener out of straightness in plane of web	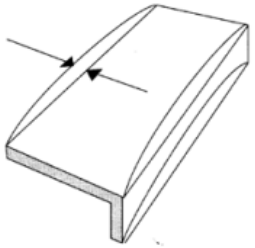	per 10 m length: standard: ±10mm limit: ±25 mm		6 mm	L/400	±8.75 mm

Table 10. Manufacturing tolerances and selection of imperfection amplitudes (continued)

Stiffener out of straightness in the plane of the flange	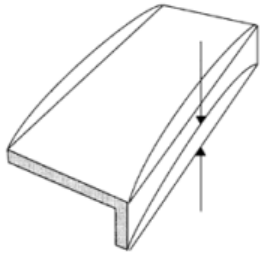	per 10 m length: standard: ±10mm limit: ±25 mm	for lengths from 30″ up to 125″: $d \leq \frac{1}{4} + \frac{\mathrm{L}}{500}$, inches	6 mm	L/300 for strict tolerances and low residual stresses; L/200 for moderate tolerances and residual stresses	±9 mm and ±18 mm
permissible warping	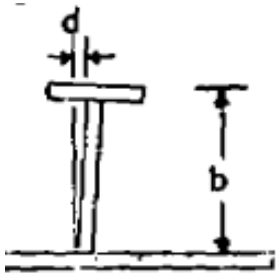		b=8″ => d≤3/8″ b=20″ => d≤3/4″ b=40″ => d≤1″ intermediate values are interpolated			d = 7,5 mm α ≈ 3°
plate between stiffeners	lowest elastic buckling eigenmode				spacing / 200	3 mm

It will be noted that the “hungry horse” mode imperfection (Figure 34), which is typical to stiffened panels, was not applied to the structure studied here. The “hungry horse” plate deformation shape usually has a strengthening effect against the load directed in the plane of the stiffener’s main axes (Amdahl, 2005); thus, not taking the “hungry horse” imperfection into account might be considered to be a conservative approach.

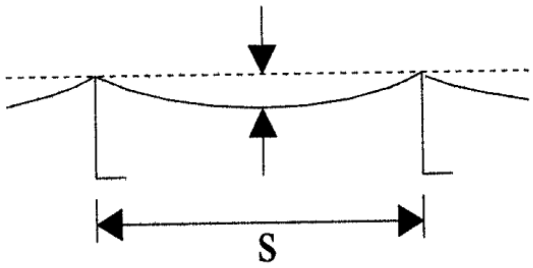

Figure 34. "Hungry horse" imperfection.

A considerable amount of research on imperfection magnitudes in real ship hull structures has been undertaken by different authors, including Soares, Kmiecik, and Estefen (Estefen et al., 2016; Witkowska & Soares, 2015). A full-scale study on imperfection magnitudes in real ship structures was conducted by Faulkner (1975), during which nearly 300 plate distortion measurements were taken in dry docks from the hulls of multiple ships. Average plate distortions were in the range of $0.3 \cdot t$ to $0.11 \cdot t$ and $0.005 \cdot s$ to $0.0024 \cdot s$, depending on the ship, with maximum deflections reaching 3x these values. These distortion magnitudes, measured in real ship structures, correlate well with the imperfection amplitudes used in this thesis research. For example, the 3 mm amplitude that was used for eigenmode based imperfections for plates, corresponds to those of $0.005 \cdot s$ for the stiffener spacing of $s = 600$ mm and $0,3 \cdot t$ for $t = 10$ mm thick plate.

6.4 Results and discussion

The load-displacement curves, obtained during analyses of the structure with different initial distortions, are shown in Figure 36 for 6 mm thick and in Figure 38 for 10 mm thick bulkhead plates.

For the 6 mm thick bulkhead, the lowest capacity showed the model with bow imperfection in the plane of the web in the -x direction (bow_X- imperfection model). This was expected, as in all of the models the global buckling shape eventually turned into

the flexural one in the -x direction (column induced). The imperfection applied in the direction opposite the primary global buckling shape (bow_X+ imperfection model) resulted in a small strengthening of the model, showing a 0.8% higher capacity than the model without imperfections. Despite notable differences in the observed localized buckling shapes of models with different imperfection types (Figure 37), the impact of applied imperfections on the ultimate capacity of the structure remained minor. The difference was 1.3% between the model with the lowest capacity (bow X- imperfection) and the model without imperfections, and 2.2% between models with the lowest (bow X- imperfection) and the maximum (bow X+ imperfection) capacities.

The structure with 10 mm thick bulkhead showed low imperfection sensitivity with capacity differences being less than 1%. Low imperfection sensitivity of the structure is in line with the theory described in Section 2.5 as structure failure is induced by material yielding (see Figure 35).

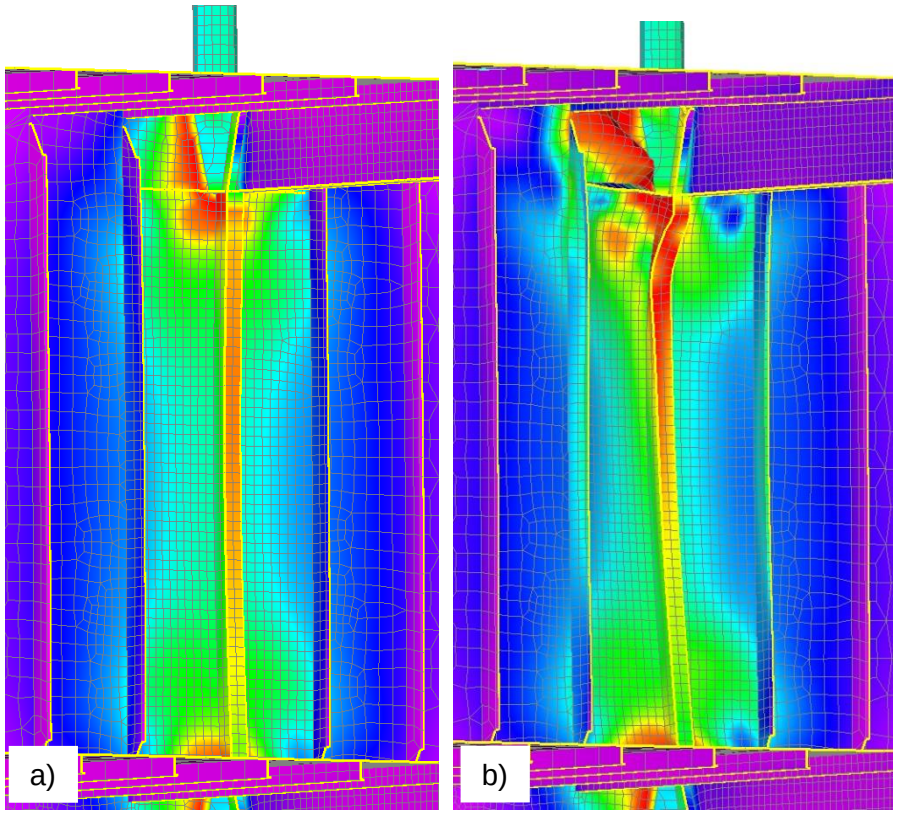

Figure 35. Failure mechanism of structure with T-150x8-FB100x10, bulkhead 10.0 mm, deck beam webs 10.0 mm 355 Mpa

a) Yield limit reached at load 1.73 kN.
b) Structure buckled after material softening (1.74 kN step is shown).

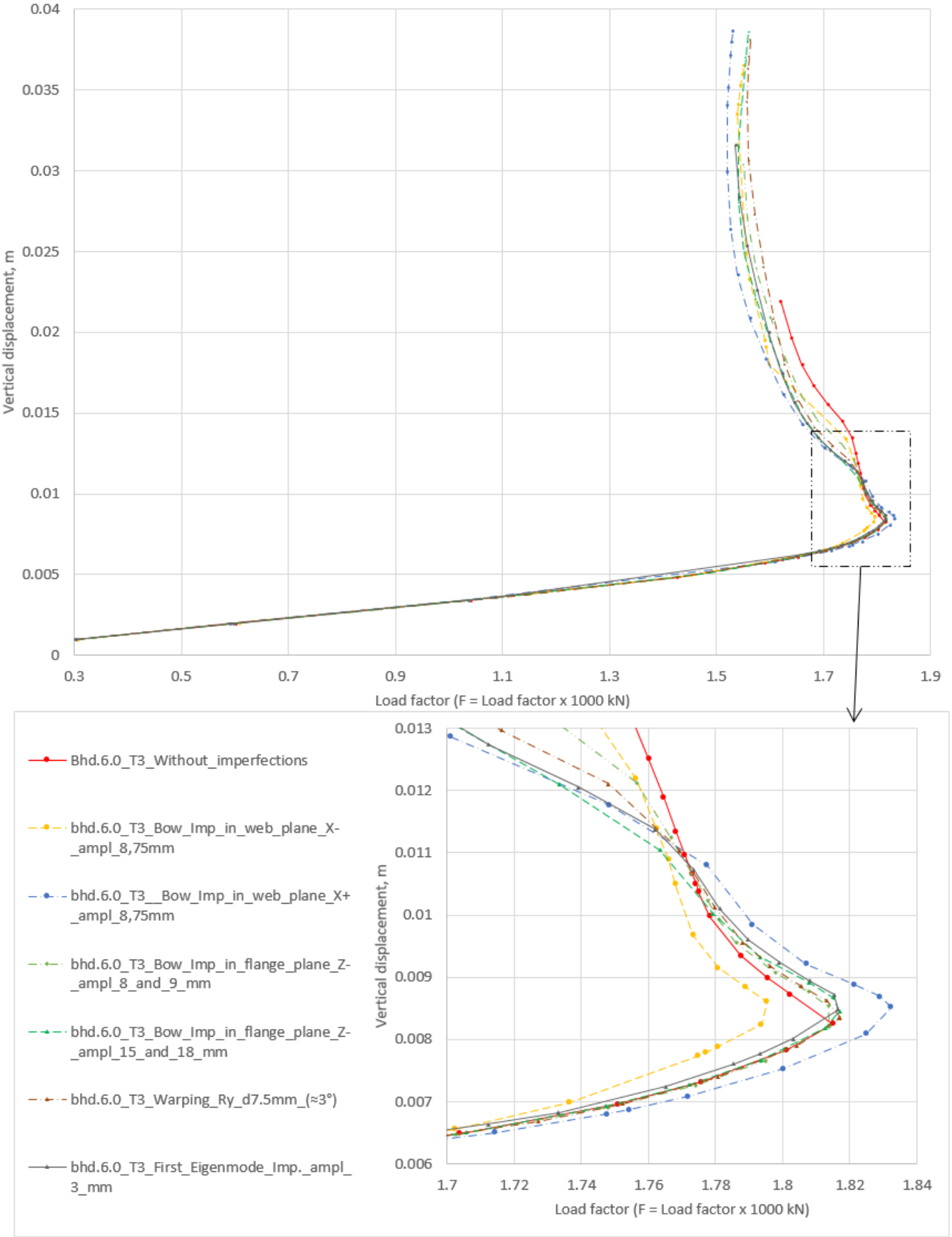

Figure 36. The load-displacement curves for different imperfection types for structures with T-150x8-FB100x10 and bulkhead plate thickness of 6 mm.

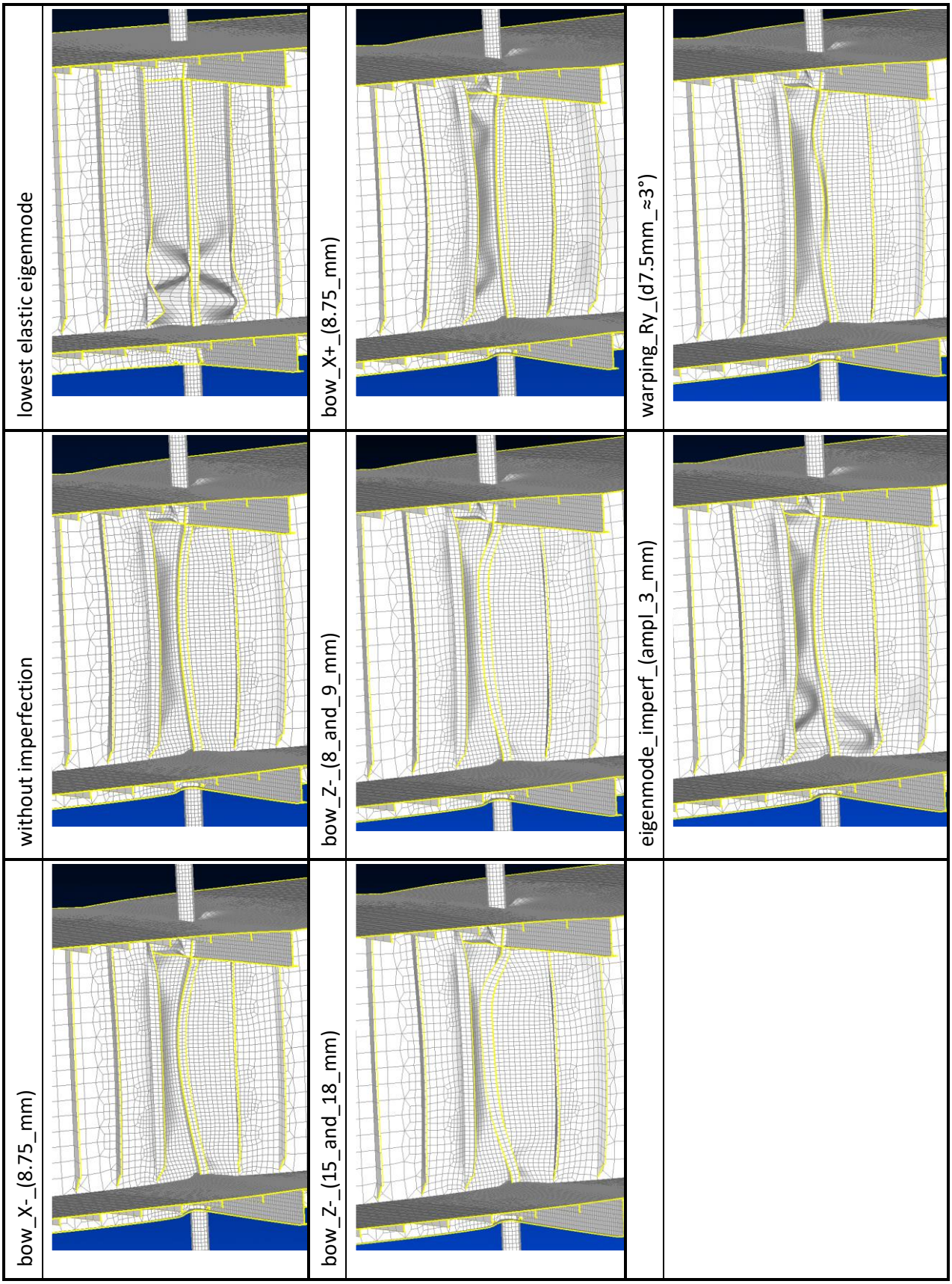

Figure 37. Deformation shapes at limit points of GMNIA analyses for structure with bulkhead thickness of 6 mm and T-column of T-150x8-FB100x10 for different types of initial imperfections. Deformation scaled 50x.

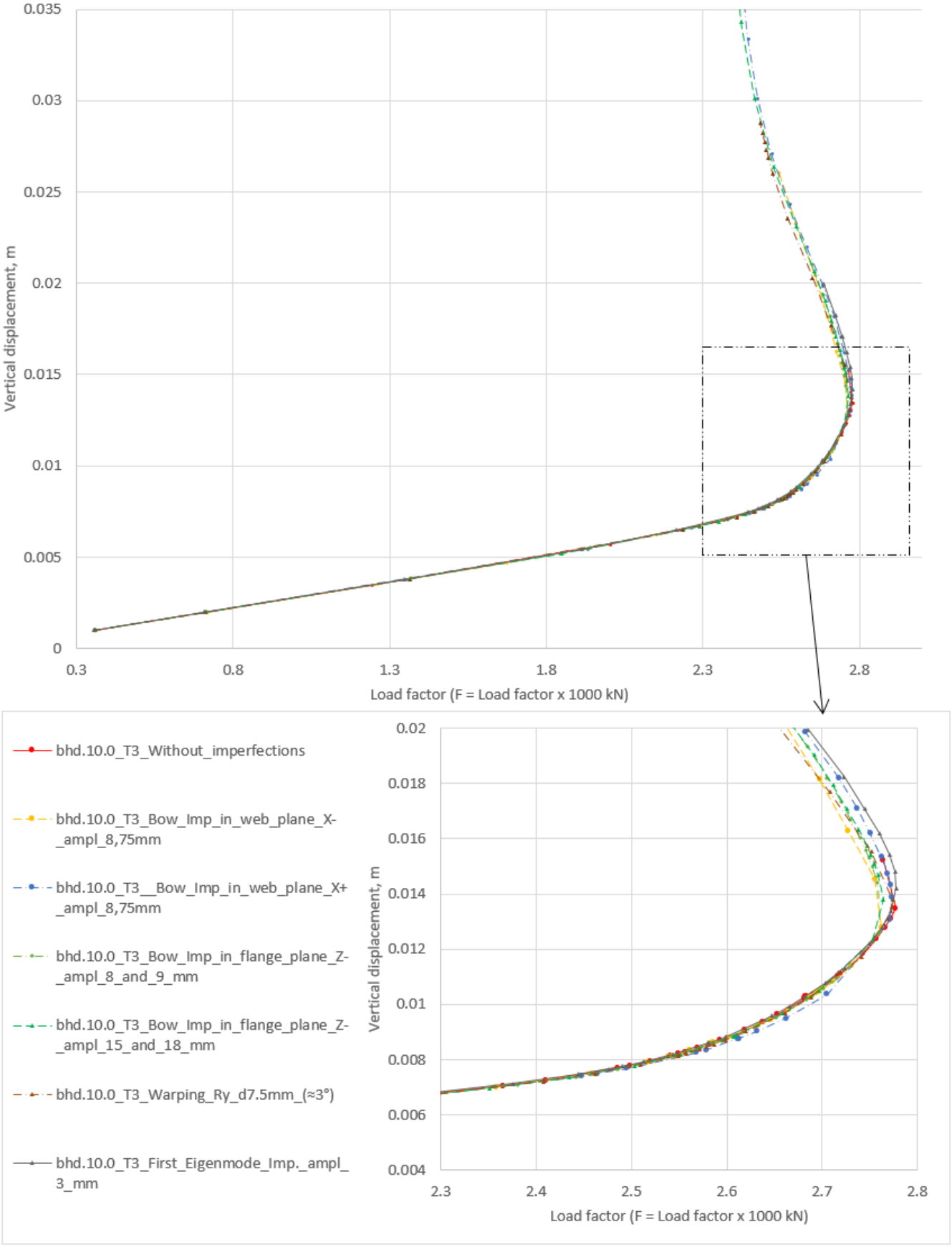

Figure 38. Load-displacement curves for different imperfection types, structures with T-150x8-FB100x10 and bulkhead plate thickness of 10 mm.

Whilst imperfection study in the thesis was conducted on bulkheads made of material with yield strength of 235 MPa, two analysis made on model where all elements were changed to the material with yield strength of 355 MPa also showed a low imperfection impact on the total capacity (Figure 39). However, more comprehensive study on imperfection sensitivity of the bulkheads made of high strength steel might be beneficial. Higher imperfection sensitivity for the high strength steel bulkheads is expected, as the buckling-problems may become dominant.

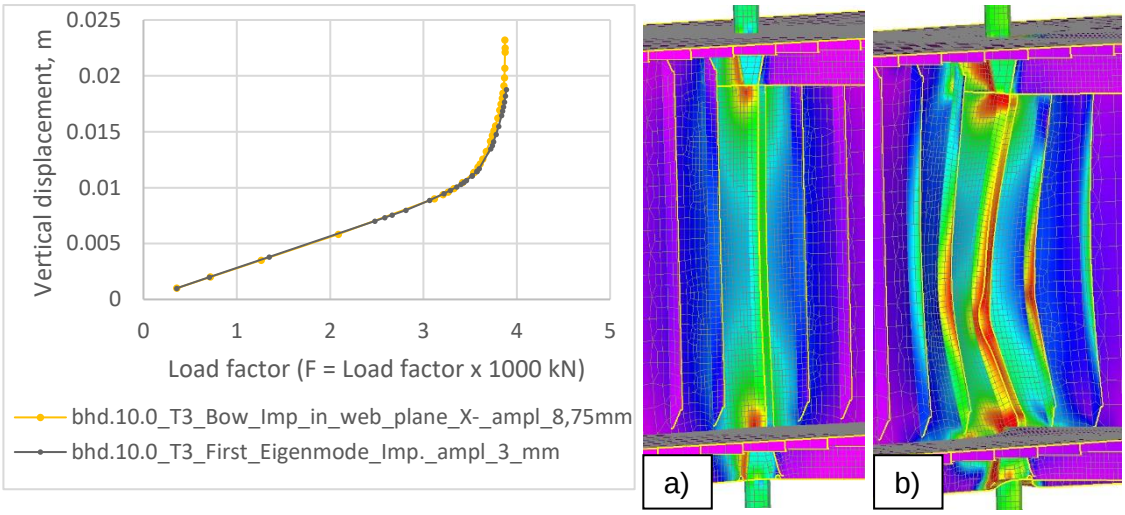

Figure 39. Imperfection sensitivity analyses on model with all the elements' material being the high-strength steel with yield strength of 355MPa. T-150x8-FB100x10 and bulkhead plate thickness of 10 mm.

a) Deformed shape and VonMises stress distribution at the point of occurrence of the first yield. Step at 3.1 kN loading (model with X- bow imperfection shown).

b) Deformed shape and VonMises stress distribution at limit point. Step at 3.87 kN loading.

It could be concluded that studied structures showed relatively low imperfection sensitivity, with load capacity differences for various imperfection types being insignificant for the questions set in the research. Differences in local modes were observed; however, global final deformation patterns, failure modes, and ultimate capacities were similar for all applied imperfection types.

7 STUDY OF TYPICAL BULKHEAD STRUCTURE WITH T-SHAPED COLUMN

7.1 Structure without openings

7.1.1 Description of models

In order to represent realistic typical structures existing in ships, FE-models as shown in Figure 40 were constructed. The model extent in the longitudinal direction is one web frame[7] spacing on each side of the column, which corresponds to the three frame spacings. (A minimum of 2.5 frames of spacing per side is recommended by DNV GL (2018 b).) The model extent in the transverse direction is eight stiffener spacings on both sides of the column. (A minimum of six stiffener spacings per side is recommended by DNV GL (2018 b).) The modeled deck height is 3500 mm, which is rather typical for cruise ship public spaces, and the height of the deck beams is 450 mm. Deck beams were modeled with flanges of FB150x15. For reasons described in Section 7.1.4.1, models with different deck beam web thicknesses were analyzed.

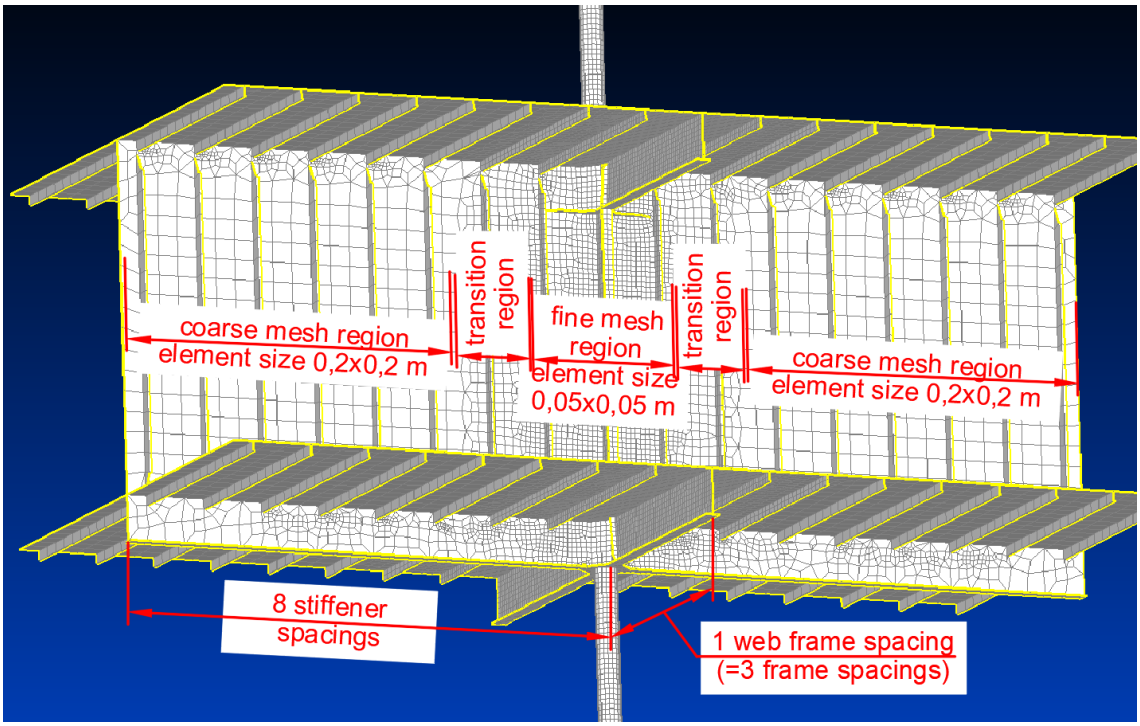

Figure 40. Extent of the model and mesh size.

[7] Web frame: In ship construction - the frame of heavy scantling.

The bulkhead's and deck's HP-stiffeners were modeled with shell elements as angle-bars of equivalent properties (see Section 4.2.1). Angle bars equivalent to HP-120x6 for the bulkhead and HP-100x5 for the decks were used.

The region close to the T-column, where overall and local buckling are expected to take place, was fine meshed with 0.05x0.05 m shell elements. To increase computational efficiency, stiffened deck plate and bulkhead plate sides were meshed with 0.2x0.2 m elements with a smooth transition between regions of different mesh density. Rigid elements were applied to the pillar's ends. More detailed information on principles for selection of element types for the research models is given in Section 4.2.1.

Plated elements as well as profiles were modeled with material with a yield stress of 235 MPa if not otherwise stated. Pillars and their connections were modeled with material with a yield stress of 355 MPa, which is a commonly used material for pillars and their connection elements. Non-linear material models, as described in Section 4.2.4, were employed. Boundary conditions were applied, as shown in Figure 41.

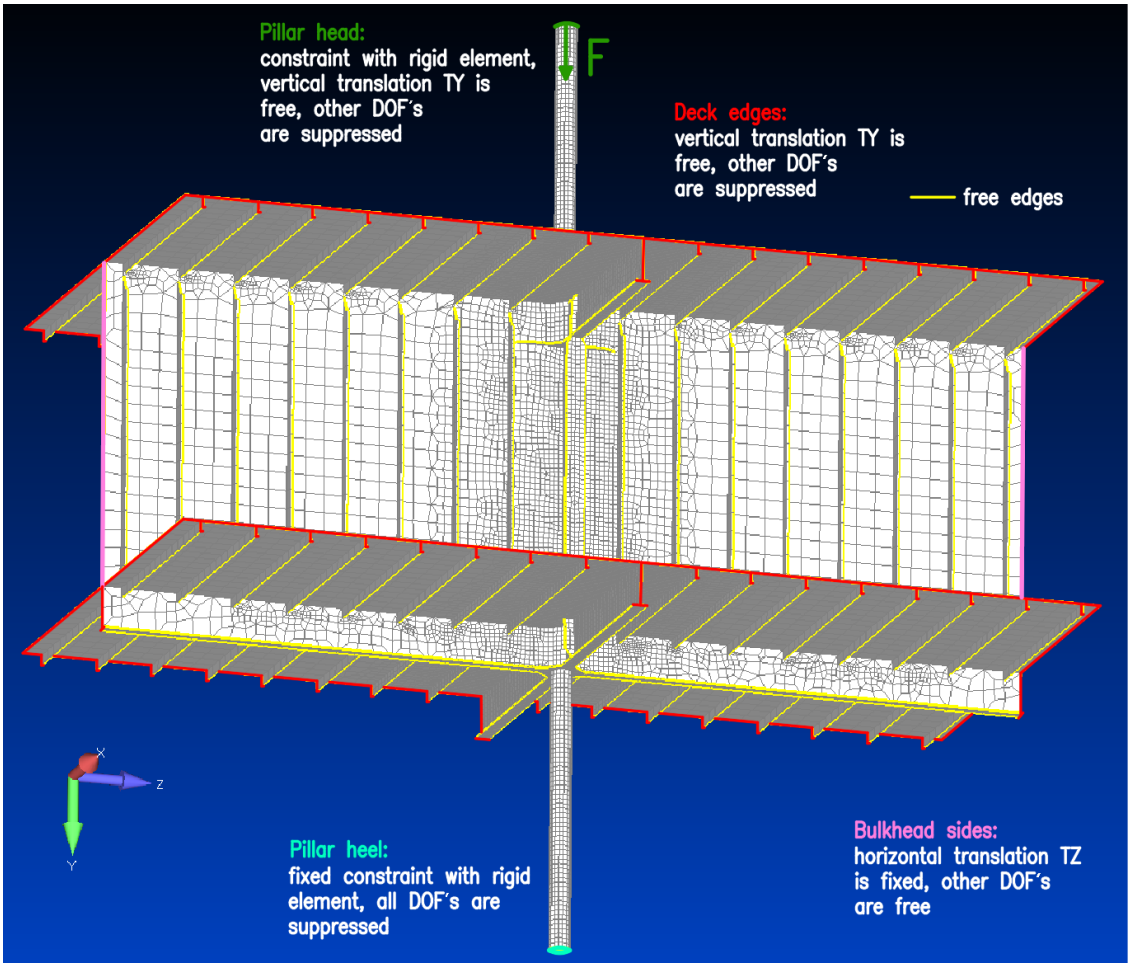

Figure 41. The FE model of a typical bulkhead in the way of a pillar with applied boundary conditions. (The model for T-400x10-FB200x20 is shown.)

Models were made for six different sizes of T-shaped columns (see Section 7.1.3), and each was analyzed with both “thin” and “medium” bulkhead plate thicknesses, 6 mm and 10 mm, respectively.

7.1.2 Mesh sensitivity study

Before proceeding with further numerical analysis, a brief mesh sensitivity study was conducted to determine if the selected mesh refinement level is appropriate. In addition to the model with the mesh as described in Section 7.1.1, two models with alternative mesh sizes were made (Figure 42):

- A whole model meshed with 0.05x0.05 m elements.
- A model with a 2x finer mesh in the T-column region compared with that in Section 7.1.1.

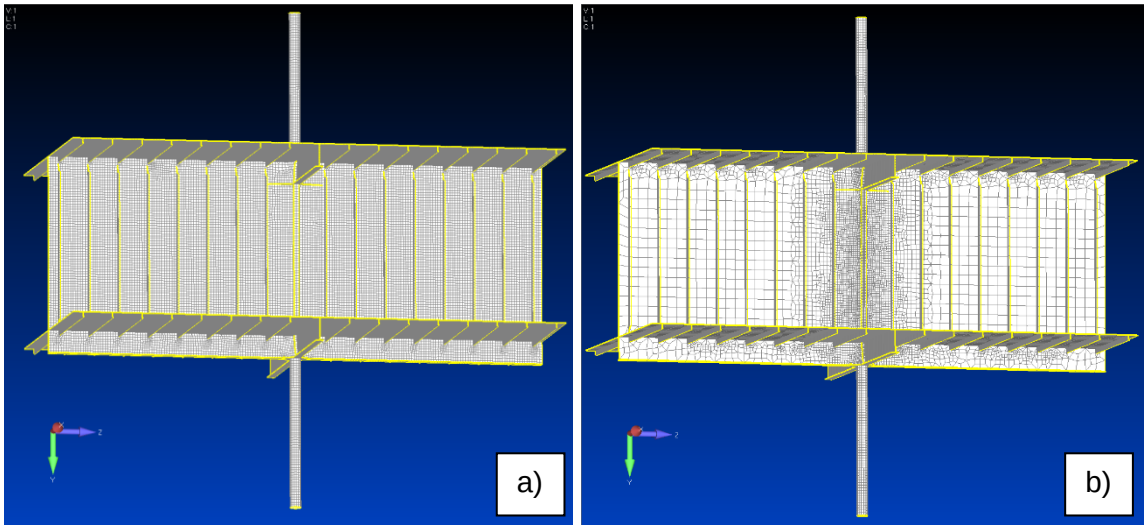

Figure 42. Models for mesh sensitivity study:
a) A whole model meshed with 0.05x0.05 m elements.
b) A model with a 2x finer mesh in the T-column region compared with the model in Sec. 7.1.1.

GMNIA analyses with settings identical to those in Section 7.1.3 were conducted. Any notable difference, except in the post-buckling response, was not observed; the pre-buckling response being almost identical and the limit points being were at 1.814 MN for the initial model, 1.807 MN for the 0.05x0.05 model, and 1.813 MN for the model with a 2x finer mesh in the T-column region (Figure 43). A slight tangential angle difference in the load-shortening curve was observed for the whole model meshed with 0.05x0.05 m fine mesh. The minor tangential angle difference is due to the stiffness of the bulkhead plate mesh, as larger elements have a stiffening effect compared to the finer mesh.

Based on the mesh sensitivity study results, selected mesh size is considered adequate.

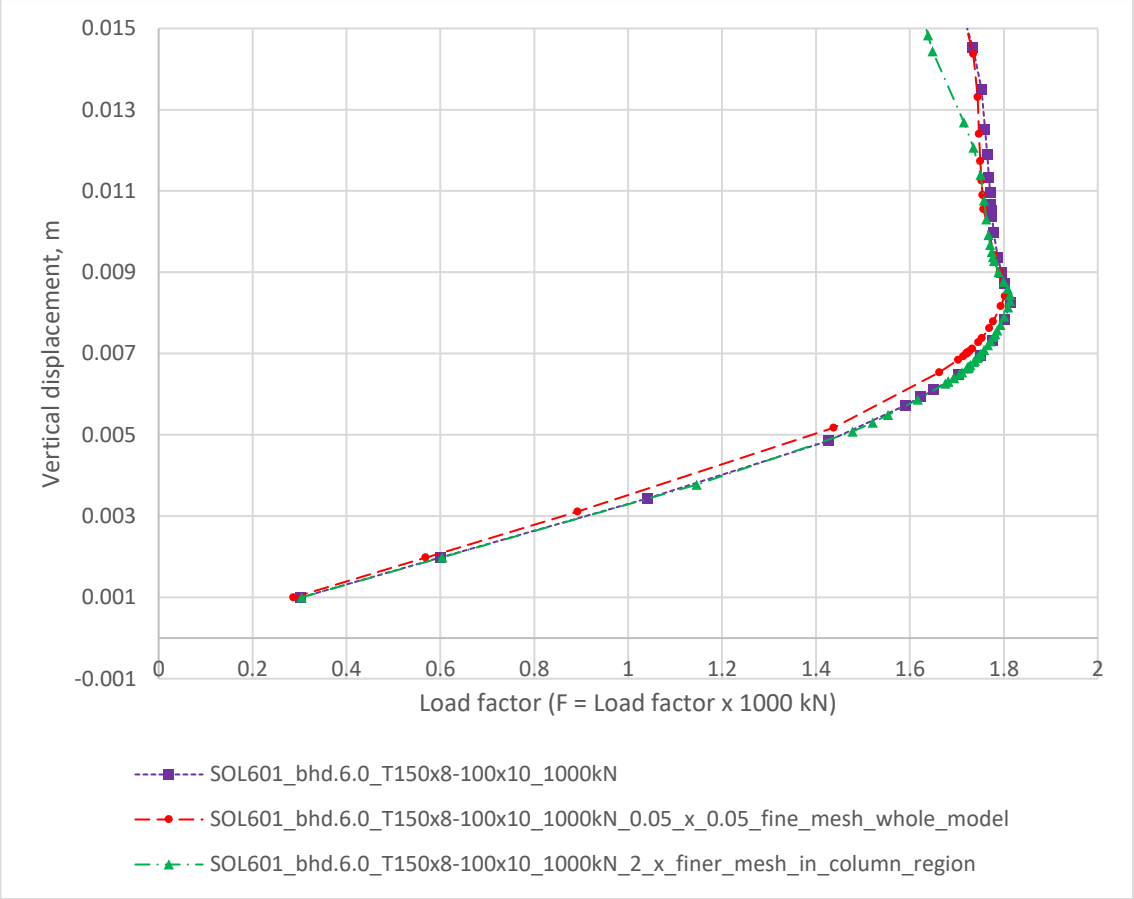

Figure 43. The load-displacement curves of mesh sensitivity analyses.

7.1.3 FE analyses and results

GMNIA analyses on models for typical intact bulkhead structures with T-shaped columns described in Section 7.1.1 were performed with displacement control in accordance with the procedure presented in Section 4.2.6.

Analyses for 6 mm thick bulkheads were performed with the deck beam's web thicknesses of 7.0 mm, 235 MPa, which is a typical minimum deck beam thickness in the ship hull design projects and, along with 8.0 mm, it is the most common deck beam web thickness in the reviewed ship hull models. The resulting load-displacement curves for 6 mm thick bulkheads are shown in Figure 44. Vertical lines represent the ultimate buckling loads calculated with simplified CFM as described in Section 3.1.

In practical designs, it is advised to check the bulkhead plate buckling capacity, in particularly for thin bulkhead plates, with an analytical method, for example according to the DNVGL-CG-0128 Sec.3 [2.2] (DNV GL, 2018 b) or with semi-analytical method, like Panel Ultimate Limit State (PULS) (DNV GL, 2018 b).

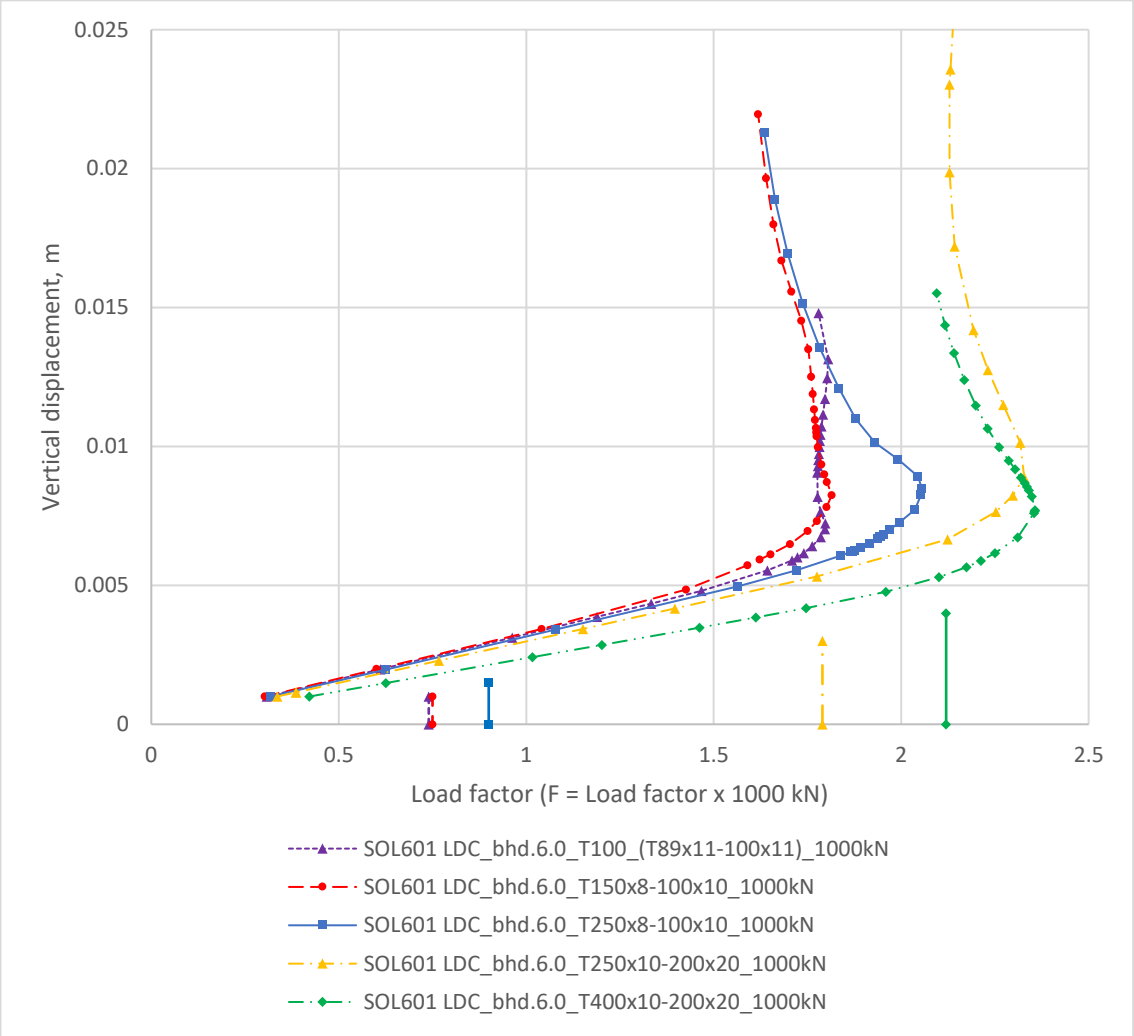

Figure 44. The load-displacement curves for the bulkhead structure with different sizes of the T-shaped columns with bulkhead plate thickness of 6.0 mm.

When performing analyses for 10 mm thick bulkheads, it was observed that with the standard minimum deck beam web thickness of 7.0 mm, the webs fail before the capacity of the bulkhead structure is reached (see Section 7.1.4.1). In order to receive results on the behavior of the bulkhead structure and eliminate a disturbance due to weak webs, the deck beam webs were strengthened to 10.0 mm thick, and their material was changed to that with a yield strength of 355 MPa. The resulting load-displacement curves are shown in Figure 45. Vertical lines represent ultimate buckling loads calculated with CFM, as described in Section 3.1. It will be noted that the ultimate capacities calculated by CFM and shown in Figures 44 and 45 are given for reference only and might be not directly comparable with GMNIA limit loads as idealized columns may represent different failure modes than the continuous bulkhead structure.

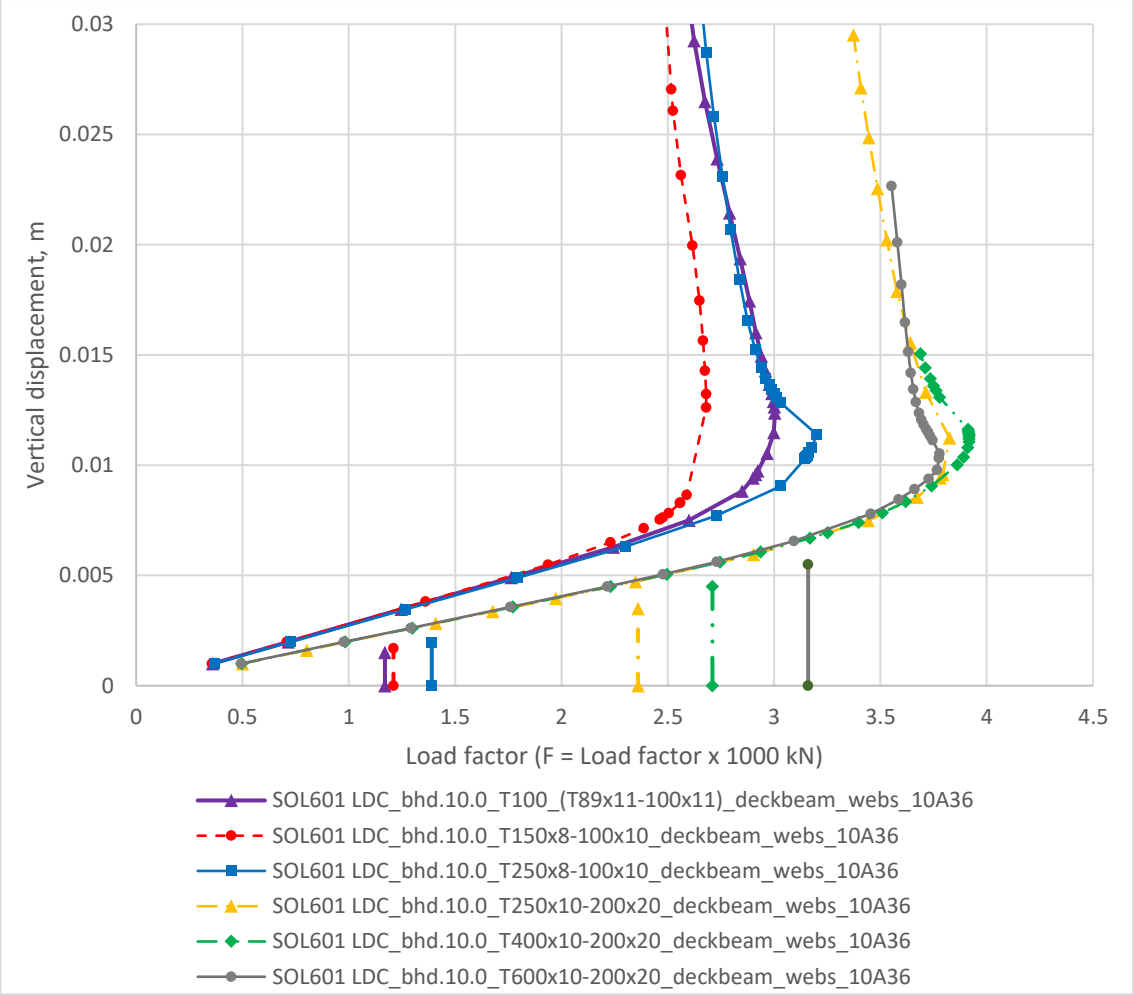

Figure 45. Load-displacement curves for the bulkhead structures with different sizes of the T-shaped column with bulkhead plate thickness = 10.0 mm.

Table 11. Occurrence of first yield. Bulkhead plate thickness = 10.0 mm, 235 Mpa, deck beam webs = 10.0 mm, 355 Mpa.

Indication for place of first-yield occurrence:
Bulkhead: the bulkhead plate in the region adjacent to the upper pillar connection.
Column Web: the vertical column web in the region close to the upper pillar connection.
Column cross-section: the overall cross-section of the vertical column.

	GMNIA		Linear Static Analysis	
Column size	**First yield, F [MN]**	**place of yield occurrence**	**First yield, F [MN]**	**place of yield occurrence**
T-100 EN10055 (T89x11-FB100x11)	≈2.7	*bulkhead, column cross-section*	≈2.1	*Bulkhead*
T-150x8-FB100x10	≈2.4	*bulkhead, column web*	≈1.9	*Bulkhead*
T-250x8-FB100x10	≈3.0	*Bulkhead, column web*	≈2.2	*Bulkhead*
T-250x10-FB200x20	≈3.2	*Bulkhead*	≈2.5	*Bulkhead*
T-400x10-FB200x20	≈3.2	*Bulkhead*	≈2.5	*Bulkhead*
T-600x10-FB200x20	≈3.2	*Bulkhead*	≈2.5	*Bulkhead*

The points of first yielding occurrence are indicated in Table 11. The force values for first yield occurrence are given based on both non-linear and linear static analyses. The values of the forces are higher in NA analyses mostly due to the non-linear stress redistribution. Due to non-linear material behavior, especially after the stress in elements reaches a proportionality limit, the material “softens” due to the stiffness reduction that implies an extensive load-shedding to adjacent elements. Thus, stress is redistributed to the larger area, resulting in lower peak-stress values in the non-linear analysis compared to the linear elastic. The material behavior at the stress values between the proportionality limit and the yield limit are still considered to be elastic while being non-linear.

Stress redistribution observed during nonlinear analyses better corresponds to the behavior of real material, while relying on linear analysis stress values when setting the force limits based on the occurrence of first yielding, might be considered to be a conservative approach. Correction techniques exist, such as the Neuber or Glinka method, that enable to estimate the magnitude of a realistic non-linear stress based on a linear elastic analysis in regions of local stress concentrations.

It will be noted, that, in practical designs, it must be ensured, for example with the analytical method according to DNVGL-CG-0128 Sec.3 [2.2] (DNV GL, 2018 b), that local plate buckling would not take place before the occurrence of the first yield indicated in Tables 11 and 12.

7.1.4 Findings and discussion

7.1.4.1 Failure of the lower deck beam webs

During the analyses on typical bulkhead structures as described in Sections 7.1.1 and 7.1.3, it was found that in many cases the weakest part of the structure is not the T-column with the effective part of the bulkhead plating, which is subjected to capacity verification during the standard procedure. Due to the nature of standard pillar-to-bulkhead connection (Figure 46), the force from the pillar approaching from below is distributed to the bulkhead structure through the deck beam webs, mostly by shear.

Figure 46. The pillar to the deck beam’s webs connection in production.

In order to represent the impact of weak deck beam webs on the total capacity of the structure, comparative analyses were performed for structures with both thicknesses of deck beam webs: 7.0 mm grade A and 10.0 mm grade A36. The results are shown in Figure 47 and Table 12. Animations of the analyses can be found in Appendix A.

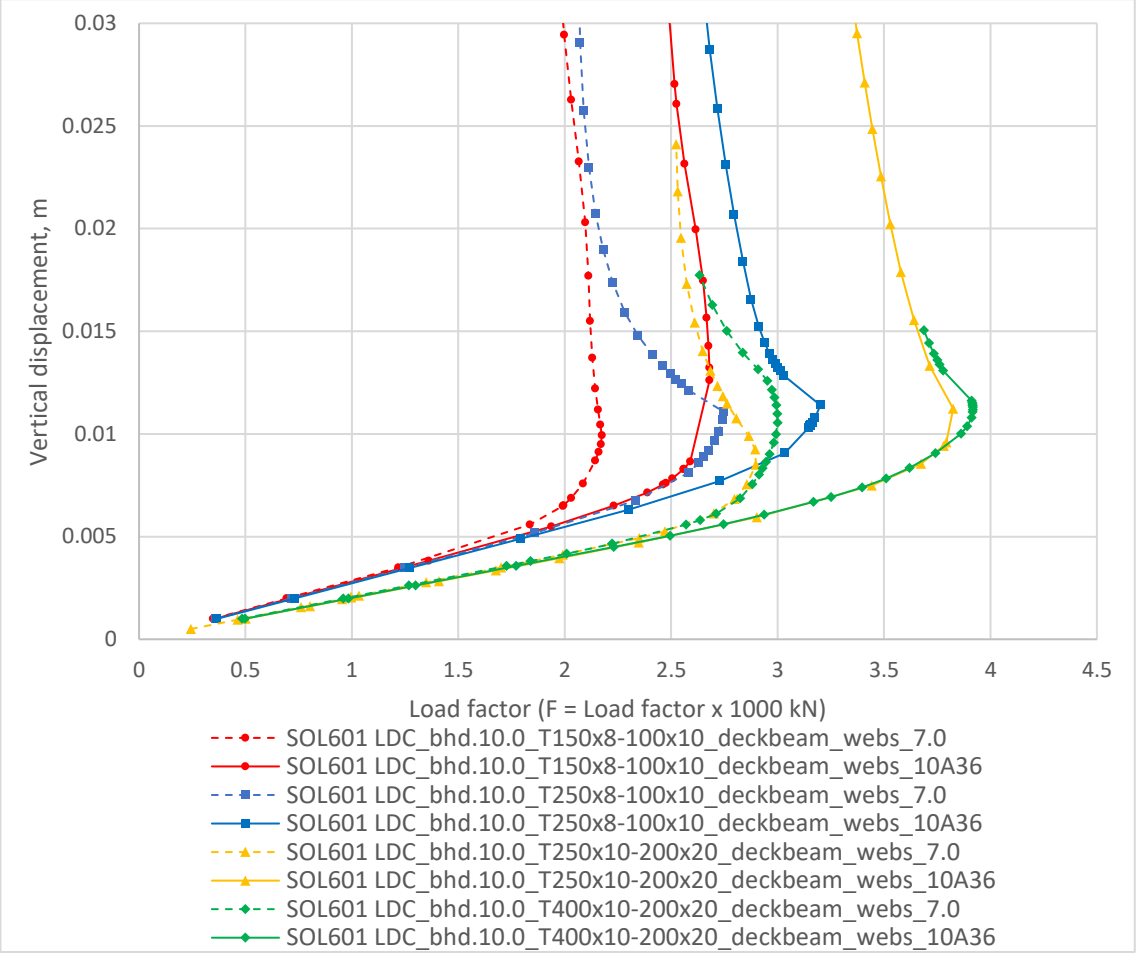

Figure 47. A comparison of the equilibrium paths of GMNIA for structures with deck beam web thicknesses of 7.0 and 10.0A36.

Table 12. Occurrence of first yield. Bulkhead thickness = 10.0 mm, 235 Mpa, deck beam webs = 7.0 mm, 235 MPa.

Indication for place of first-yield occurrence: *Web*: The web of the lower deck beam co-directional with bulkhead.				
	GMNIA		**Linear Static Analysis**	
Column size	**First yield, F [MN]**	**Place of first yield occurrence**	**First yield, F [MN]**	**Place of first yield occurrence**
T-150x8-FB100x10	≈1.8	*Web*	≈1.5	*Web*
T-250x8-FB100x10	≈2.3	*Web*	≈1.7	*Web*
T-250x10-FB200x20	≈2.6	*Web*	≈1.9	*Web*
T-400x10-FB200x20	≈2.6	*Web*	≈1.9	*Web*

As is seen from Figures 48 and 49, while for structures with strengthened deck beam webs, failure occurs in the bulkhead structure between two decks, for structures with

regular non-strengthened webs, the failure is induced by the high shear stress in the webs. For structures with columns of T180x8-100x10 and T250x8-100x10 it showed about 500 kN or 20% lower capacities; and for structures with T250x10-200x20 and T400x10-200x20 showed about 1000 kN or 30% lower total capacities (Figure 47). The yield stress of the modeled bulkhead's material and T-columns was 235 MPa in the analyses, if the bulkheads were made with high strength steel, the difference in capacities would be even higher.

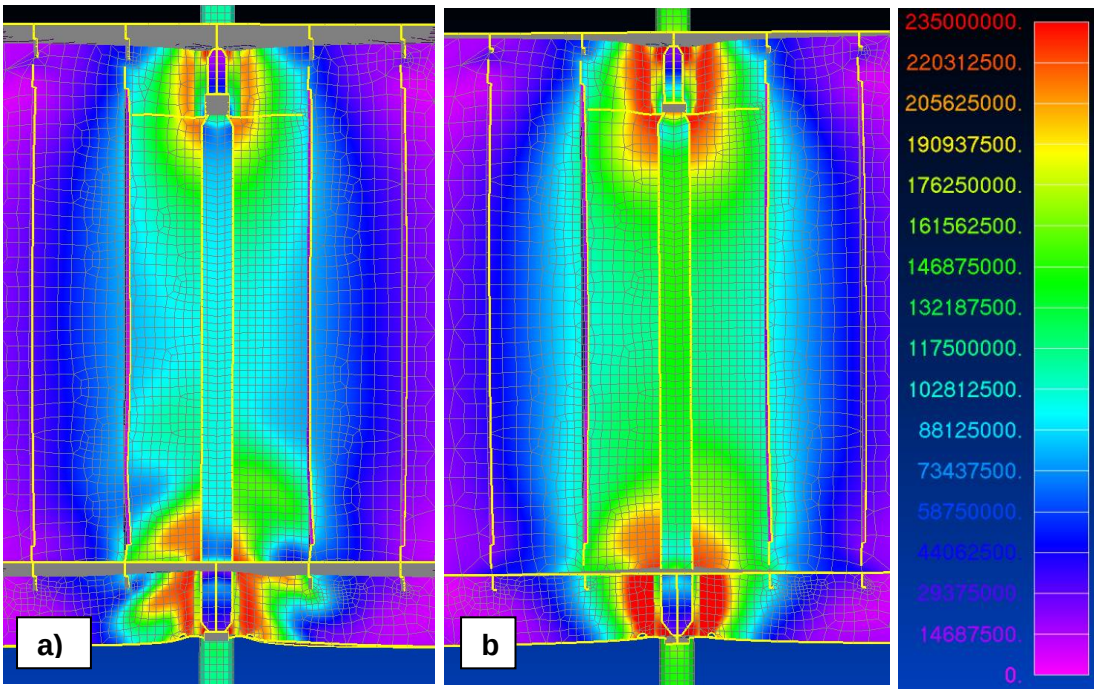

Figure 48. First-yield occurrence points of GMNIA on structure with T250x10-200x20, bhd. 10.0 mm. Von Mises stress.

a) - deck beam webs 7.0A, stress in the lower deck beam webs exceeded the elastic limit at step with a load factor = 2,7 (2700 kN).

b) - deck beam webs 10.0A36, stress in bulkhead plate in the region of the upper pillar connection exceeded the elastic limit at the step with the load factor = 3,4 (3400 kN).

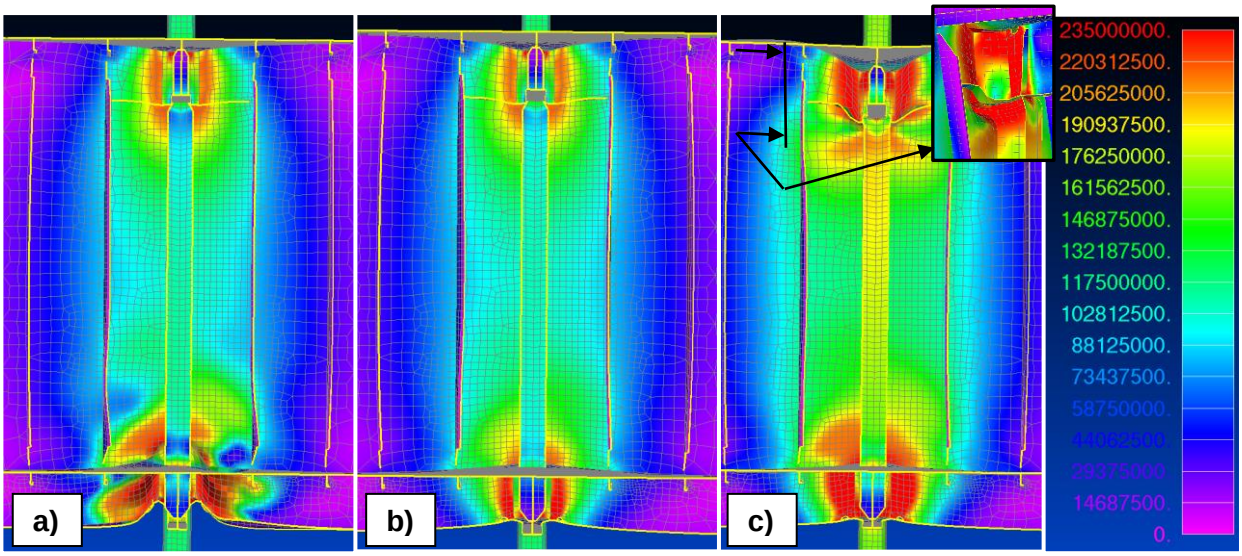

Figure 49. Limit points of GMNIA with T250x10-200x20, bhd. 10.0 mm. Von Mises stress.
a) deck beam webs 7.0A, step at the load factor = 2.9, the deck beam webs buckled.
b) deck beam webs 10.0A36, step at the load factor = 2.9, the reserve capacity exists.
c) deck beam webs 10.0A36, step at the load factor = 3.8, the bulkhead plates and T-column webs buckled.

Based on this finding, the author recommends including the deck beam web stress level and web-plate buckling capacity checking in a bulkhead's capacity against the pillar forces verification procedure, along with checking the buckling capacity of the T-columns.

The feasible approach to consider in future projects might also be applying of the high strength steel with a yield strength of 355 MPa instead of the mild steel for all deck beam webs that are intersecting with the pillar lines, in particular, for those of lower decks. This would increase the shearing capacity of the connections by about 50% without increasing the weight.

The problem with weak deck beam webs in a way of pillar connection is relevant for both loading cases: compression and tension.

7.1.4.2 Failure in the bulkhead plate - deck beam web region adjacent to the upper pillar connection

It was observed from analyses with strengthened lower deck beam webs that, for heavy columns, the failure is not induced by overall column buckling or by plastic deformation in column cross-section, but rather with failure, mostly due to shear, in the region adjacent to the upper pillar connection (Figure 48 b, Figure 49 c, Figure 50). The region is located above the upper deck beam flange, and checking such a structure against column buckling capacity might be not sufficient.

Based on that finding, a checking mechanism, which will ensure that plastic deformation or plate buckling in the region of the upper pillar connection to the bulkhead would not occur, needs to be included in the capacity verification procedure.

7.1.4.3 Impact of the eccentric position of pillar

As is seen from load-displacement curves for columns of T250x10-200x20, T400x10-200x20, and T600x10-200x20 (Figure 44 and Figure 45), due to the eccentric positioning of the pillar with respect to the column centroid, starting from a certain point, increasing the T-column web height does not produce any gain in total capacity for the structure against the pillar load, as the effectiveness of the T-column flange decreases due to shear lag and the resulting non-uniform stress distribution in the cross-section of the column. As shown in Figure 50, the flange of the column with lower web (c) is more effective than those with higher webs (a and b). Furthermore, starting from a certain point, increasing the column web height would lead to decrease in the capacity of the structure against the pillar load, which might otherwise be expected if the eccentricity is not taken into account. The phenomenon is clearly visible from the load-displacement curves for the T-columns with high webs, as shown in Figure 45.

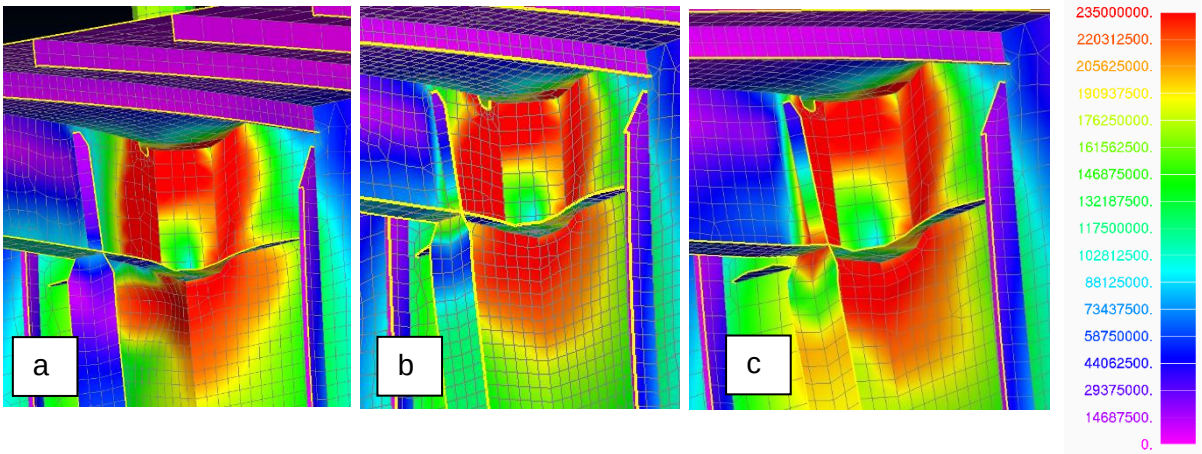

Figure 50. Effectiveness of the T-column flange. Non-linear analyses for: a) T600x10-200x20, b) T400x10-200x20, c) T250x10-200x20, at step with a load factor of 3.7 (F=3700 kN). Stress distribution. Von Mises stress.

7.1.4.4 Alternative approach based on the standardized solutions verified with direct calculations

It was shown that on the one hand the current analytical approach tends to be over-conservative as it insufficiently takes into account actual capacity of the intact stiffened

bulkhead structure. On the other hand, with the analytical method it might be difficult to account for all possible local failure modes, including those that occur due to the inherent eccentricity. The approach described below could prove to be more practical.

The current approach:

- In the initial stage of the hull design project, typical default sizes for the bulkhead's vertical T-columns are defined. Usually, default sizes are applied to large regions, with one or two sizes covering multiple decks. At this stage, usually no difference is made between the bulkhead's T-columns positioned in the way of pillars and those not in pillar lines. The variety of different T-column sizes is small at this stage. It is estimated that three to four typical column sizes would cover more than 90% of the places.
- Pillar analysis is conducted utilizing the global FE-model (as described in Section 2.6).
- Structures where the pillar is positioned above or below the bulkhead are checked on a one-by-one basis with analytical methods against the pillar loads and are strengthened, if required.

An alternative approach:

- This approach is intended to determine the ultimate limit capacities for bulkhead structures with selected standard sizes of T-columns by direct strength calculations (FE analysis) or with a combination of direct and analytical methods. Analyses should be done for different selected common bulkhead thicknesses and for the upper bounds of selected deck height ranges. It is estimated that two ranges with deck heights up to about 2800 mm and up to about 3600 mm would cover most of the cases in cruise ship designs, as the first one is typical for cabin-decks and the second is typical for public spaces.
- Apply the safety factor to the limit capacities to obtain the safe design capacities for the standardized column sizes and bulkhead plate thicknesses. The safety margin should be large enough to cover possible inaccuracies in the direct calculation method, inaccuracies in pillar load calculations, possible structure weakening factors such as a reasonable amount of openings that might be added to the structure in later phases of the project.

- After global pillar analysis, as described in Section 2.6, is conducted, filter out all places where the pillar load is lower than the design capacity.
- Apply standard solutions with higher capacities to those places where the default capacity is not sufficient.
- For structures with large openings, either standardized opening strengthening solutions should be developed that would guarantee that ultimate capacity of the structure with openings is not lower than the set design capacity for certain T-column size. Another approach would be to use a reduced design capacities for structures weakened with openings.
- Special cases should be checked on a one-by-one basis, as should also be done with the traditional approach. For lines with extremely high loads, the solution described in Section 7.1.4.5 might be applied.

Advantages of the alternative approach:

- More effective designs, as the actual capacity of the bulkhead structure is better taken into account.
- Both column buckling as well as local yielding effects would be reliably taken into account when setting the limit design capacities.
- The approach would serve the goal of standardization. For efficiency reasons, the approach should be cross-project in nature. Standardized solutions verified once should be transferred into future projects.

7.1.4.5 Replacement of the T-column with closed section pillar

Besides the solution with T-column, another solution with closed section pillar in the middle of bulkhead is known (Figure 51). The solution with the T-column on top of the bulkhead plate is considered economically effective as long continuous bulkhead panels might be produced on automated panel lines. The solution with closed section pillar is structurally very efficient against axial load as the pillar equivalent to that approaching the bulkhead is used and local effects due to shear would not occur as the force is transferred by compression. Whereas the current research does not aim to speculate about which solution is economically more efficient, either with the T-column or with a closed-section pillar, author recommends the solution with closed section pillar or equivalent solution to be used in pillar lines that experience extremely high loads. The purpose is to transfer the load by compression and to eliminate the possibility of local material failure and buckling in plated elements due to high shear stress.

Figure 51. Solution with the circular pillar in the middle of the bulkhead.

7.2 Impact of openings

The bulkhead structures of a cruise vessel include many large openings, especially in superstructure, such as door and free passage openings, windows, and balcony openings. Different opening arrangements were observed while reviewing existing ship hull models (Figure 52).

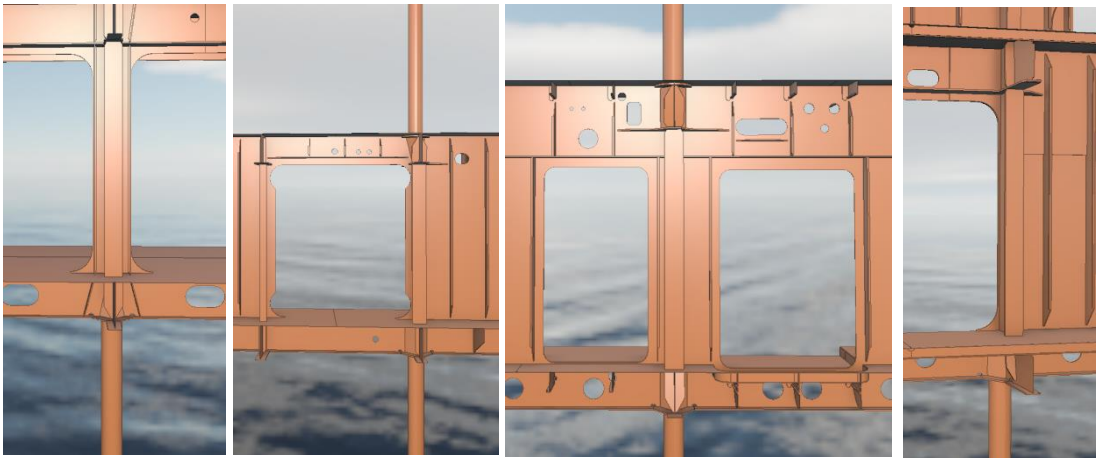

Figure 52. Examples of bulkhead openings in cruise ship hulls, positioned close to the pillar-line.

The aim of this part of the research was to estimate the impact of bulkhead openings positioned in the vicinity of the T-column on the behavior of the structure compared to the intact one and to identify favorable and non-favorable opening arrangements. FE-models for the following opening arrangements were made (see Figure 53):

a) Two openings positioned on both sides of the T-column, width of the bulkhead plate flange 400 mm, edges stiffened with flat bars 2 x FB100x10.
b) Same as 1, edges not stiffened.
c) Opening one side, positioned close to the T-column.

Models with these opening arrangements were constructed for three different column sizes: T-150x8-FB100x10, T-250x8-FB100x10, and T-250x10-FB200x20. A total of nine FE-models with openings were made. All models were analyzed by GMNIA with bulkhead thicknesses of 10.0 mm. The model with T-150x8-FB100x10 was analyzed with both bulkhead thickness: 6.0 mm and 10.0 mm. The deck beam webs were set to 10.0 mm 355MPa in order to eliminate the disturbance due to the weak webs. All analyses were performed with the lowest eigenmode-shape-based imperfections (see Sections 6.2 and 6.3). The resulting load-shortening curves with deformed shapes and stress distributions at limit points, as well as post-buckling shapes, are presented in Figures 54, 55, 56, and 57. For analysis animations, refer to Appendix A.

The structures with two openings without stiffeners showed a low performance for all cases, resulting in limit capacities 45% to 50% or 1000 kN to 1600 kN lower than those without openings.

The structures with two openings with stiffeners (FB100x10) and with one opening positioned close to the column both showed 30% to 40% lower limit capacities than the intact structure for all analyzed cases.

As is seen in Figures 54, 55, 56, and 57, the openings lead to different failure modes than have the corresponding intact structures. For example, while intact structures with columns of T-250x8-FB-100x10 and T-250x10-FB-200x20 experience localized failure due to high shear stress in the region of the pillar connection, the corresponding structures with two openings with stiffened edges fail with column flexural or flexural-torsional buckling.

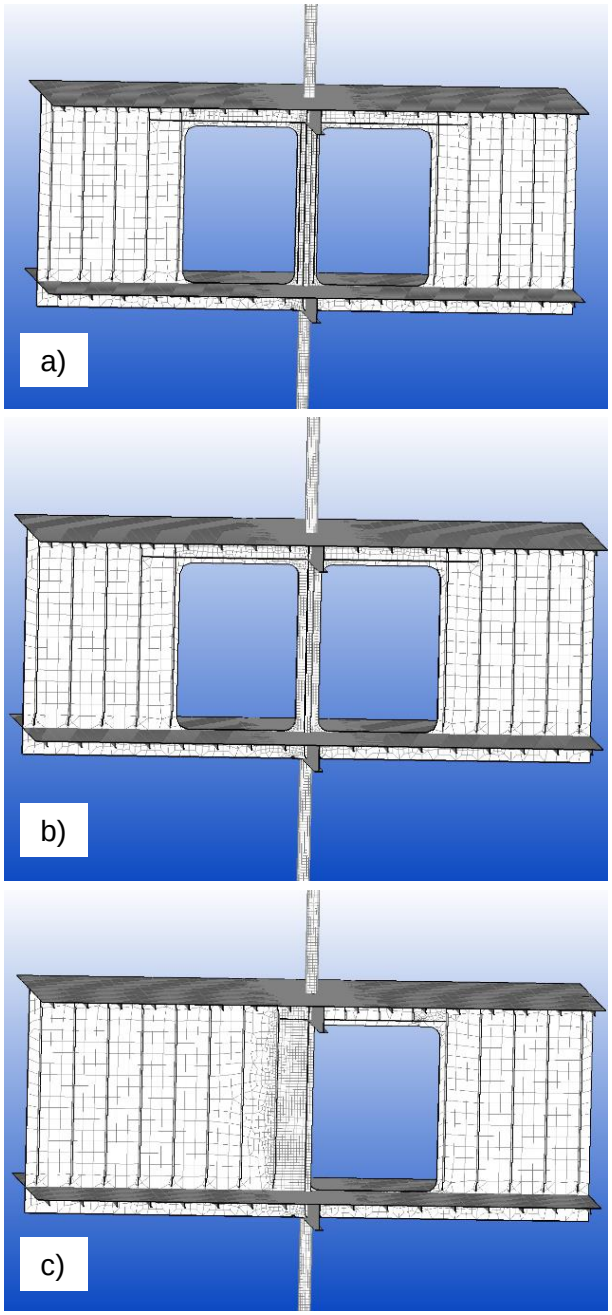

Figure 53. FE-models with openings:
a) two openings, stiffened
b) two openings, no stiffeners
c) one opening, positioned close to the column root

Opening positioned one side of the column results in uneven stiffness at each side and to stress concentration at the intact side so that yield limit is reached at significantly lower load than with the symmetrical structure. This must be accounted when analytically evaluating the shearing capacity of the region adjacent to the pillar connection. The phenomena is visible at stress distribution patterns on Figures 54 - 57.

Given the framework of this thesis, more detailed investigation into the most effective ways of strengthening for all the studied cases was not conducted; however, it must be noted that effective strengthening strategies must be failure-mode-dependent. The research showed that it might be difficult to predict failure modes in complex structures relying only on analytical simplified solutions.

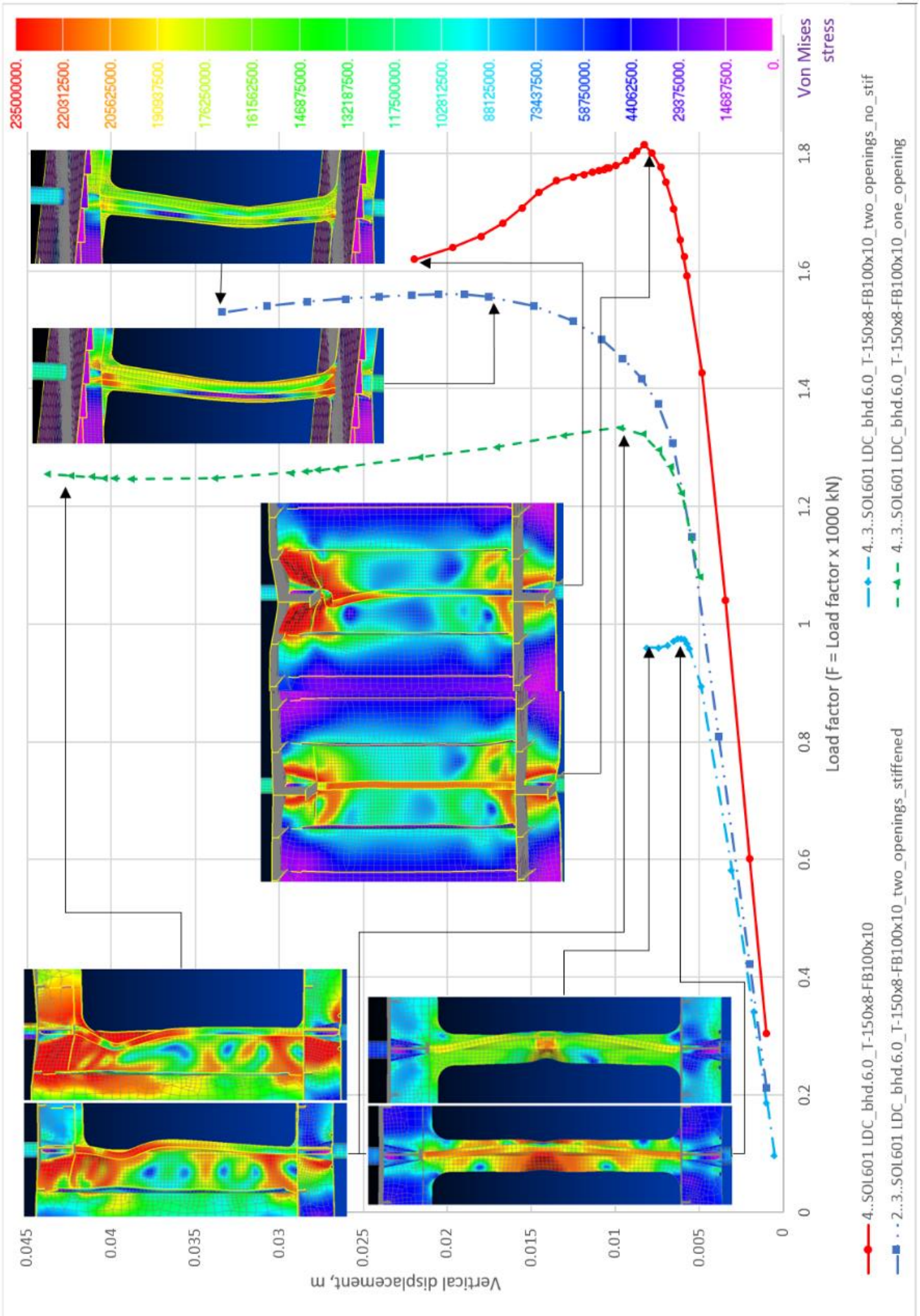

Figure 54. The load-displacement curves with buckling and post-buckling shapes for T-150x8-FB100x10, bulkhead 6.0 mm for different opening arrangements.

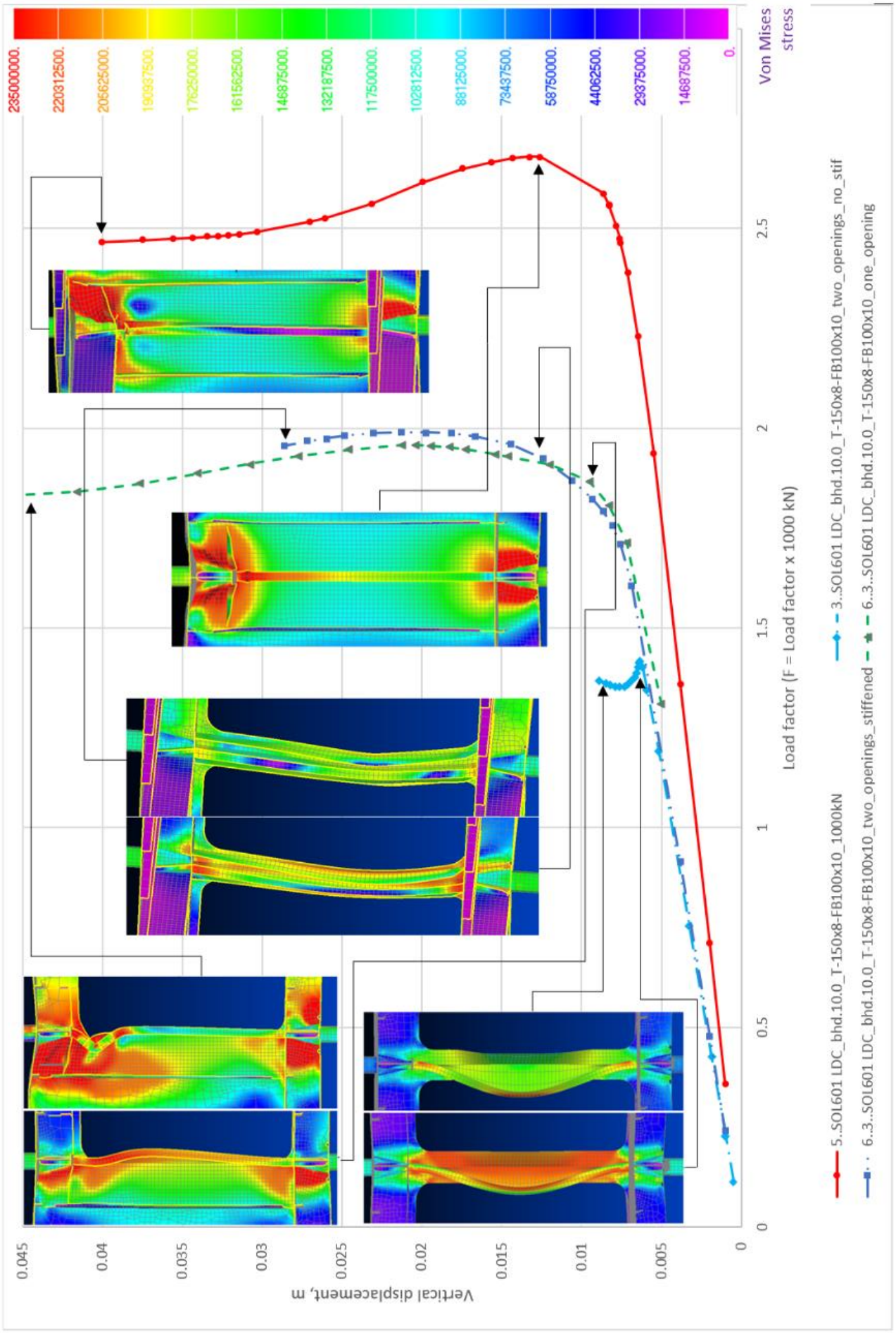

Figure 55. The load-displacement curves with buckling and post-buckling shapes for T-150x8-FB100x10, bulkhead 10.0 mm for different opening arrangements.

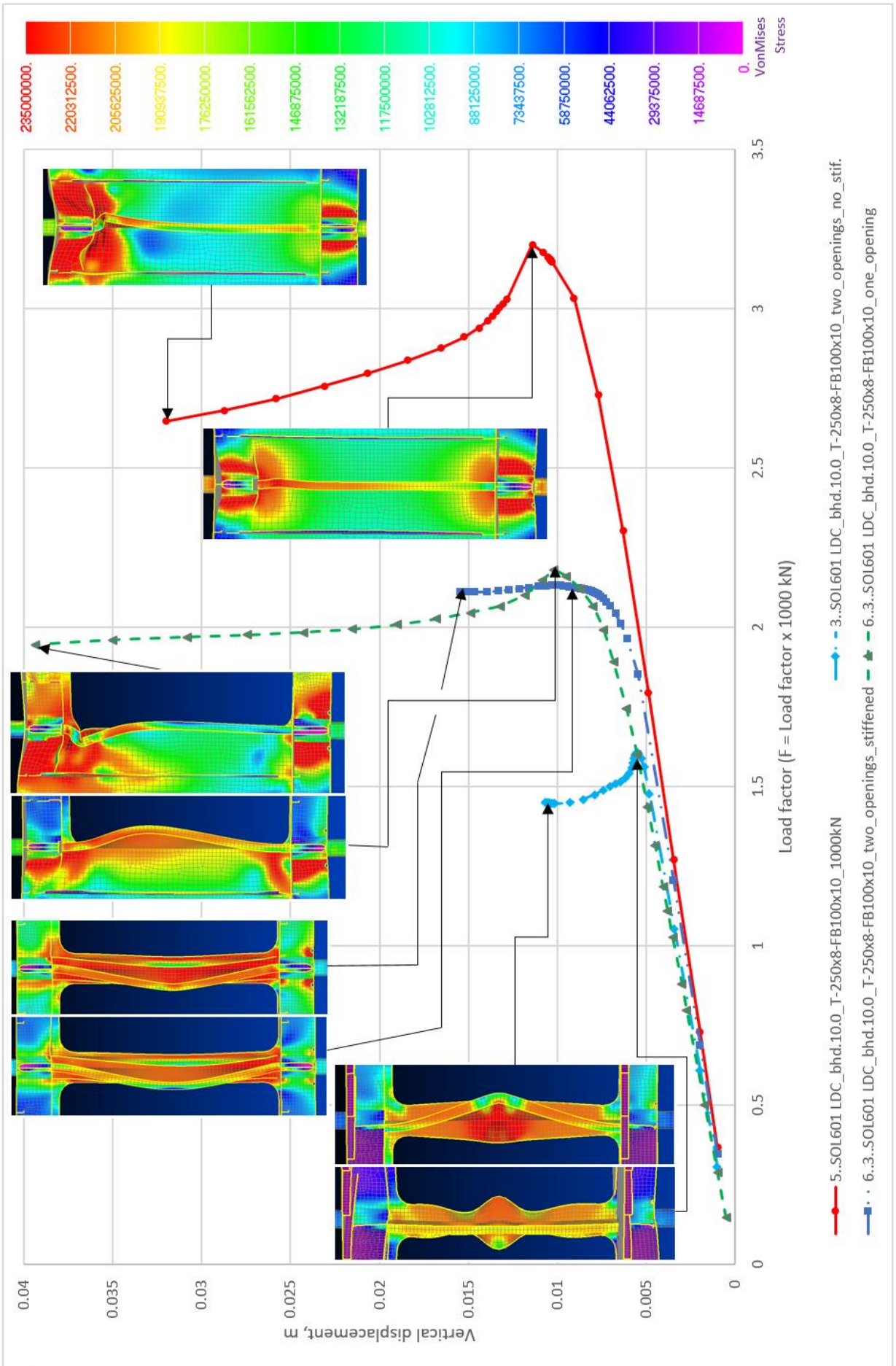

Figure 56. The load-displacement curves with buckling and post-buckling shapes for T-250x8-FB100x10, bulkhead 10.0 mm for different opening arrangements.

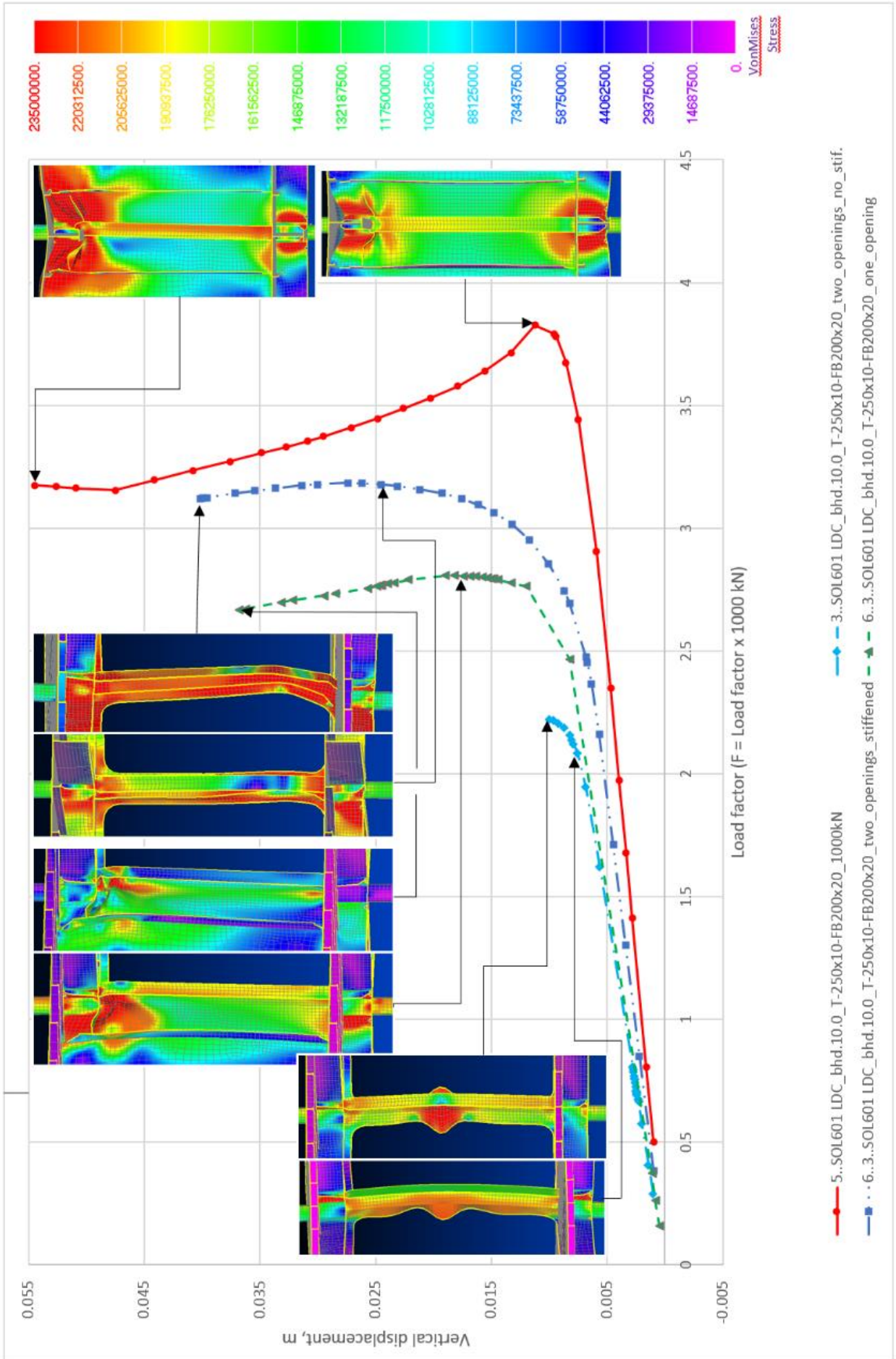

Figure 57. The load-displacement curves with buckling and post-buckling shapes for T-250x10- FB200x20, bulkhead 10.0 mm for different opening arrangements.

8 INTERSECTION OF TWO BULKHEADS

8.1 Description of model

Bulkhead intersection in the way of pillar is a common type of structure in ship hulls. To check the behavior of the structure under compressive loads, one FE model was made with pillars below and above (Figure 58). The standard pillar connections were included in the model.

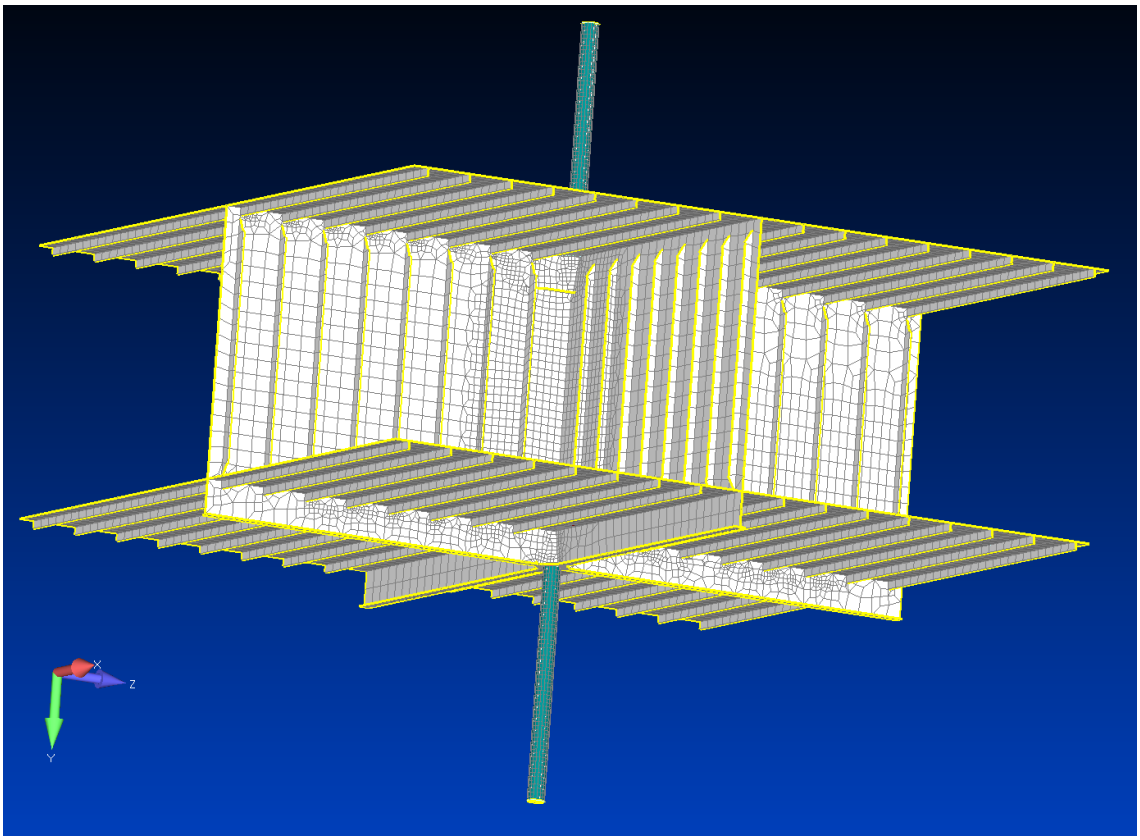

Figure 58. The FE model for the typical structure of the intersection of two bulkheads in the way of pillars.

8.2 FE analyses and results

GMNIA analyses were performed with different parameters, as follows. First, three analyses were performed for intersections of bulkheads with plate thicknesses of 6/6[8], 8/8, and 10/10 mm with a typical minimum deck beam web thickness of 7.0 mm,

[8] X/X symbol denotes the thicknesses of bulkhead plates. For example, 6/6 means that both intersecting bulkheads had the plate thicknesses of 6.0 mm in the analysis.

235 Mpa. During the analyses, it was observed that for 8/8 and 10/10 bulkhead thickness cases, the plastic deformation in deck beam webs took place far before the limit capacity of the bulkhead intersection itself was reached (see Figure 59 (a), and Table 13).

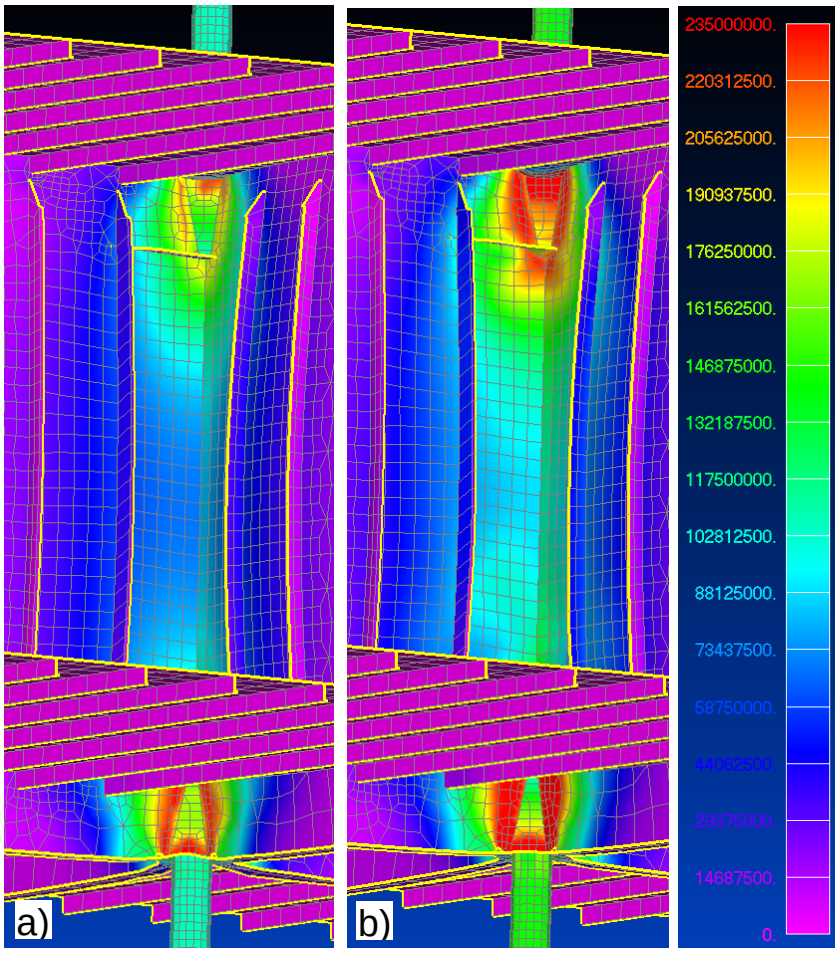

Figure 59. 10/10 bulkhead intersection GMNIA. Deformed shape and stress distribution at points of reaching the elastic limit. Von Mises Stress.

a) - deck beam webs 7.0A, step at the load factor = 2.94. Elastic limit reached in the deck beam webs.

b) - deck beam webs 10.0A, step at load factor = 3.93. Elastic limit reached in the bulkhead plate.

In order to identify the maximum capacity of bulkhead intersections between decks, deck beam webs were strengthened to 10.0 mm 355 Mpa, and GMNIA analyses were performed for the same bulkhead thicknesses as in the first case. In that case, failure occurs in the bulkhead plates instead of the deck beam webs for the 8/8 and 10/10 bulkhead intersections (see Figure 59, b). As is seen from the load-displacement curves (Figure 60), the structures have a reserve capacity after occurrence of the first yielding; but, as plastic deformations (except marginal and very localized ones) are not

usually allowed (DNVGL-CG-0128b, Sec. 2.1), the point where the first plastic deformation occurs might be considered as a critical one.

Table 13. Bulkhead intersection analyses. Occurrence of the first yield.

Indication for place of first yield occurrence: *Webs*: the deck beam webs adjacent to the lower pillar connection. *Bulkheads:* the bulkhead plates adjacent to the upper pillar connection.				
	GMNIA		**Linear Static Analysis**	
Bulkhead intersection	**First yield, F [MN]**	**place of yield occurrence**	**First yield, F [MN]**	**place of yield occurrence**
8/8; deck beam webs 7.0A	≈2.7	*webs*	≈2.0	*webs*
10/10; deck beam webs 7.0A	≈2.8	*webs*	≈2.1	*webs*
8/8; deck beam webs 10.0A36	≈3.1	*Bulkheads*	≈2.4	*Bulkheads*
10/10; deck beam webs 10.0A36	≈3.7	*Bulkheads*	≈2.9	*Bulkheads*

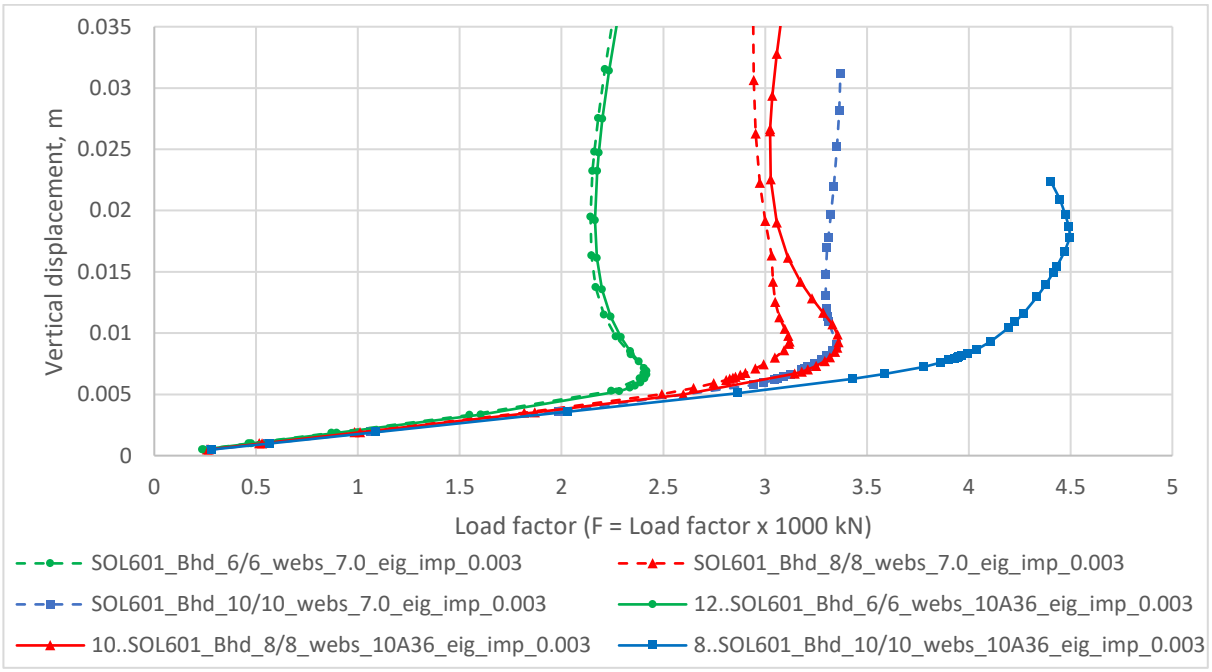

Figure 60. The load-displacement curves of GMNIA for bulkhead intersections.

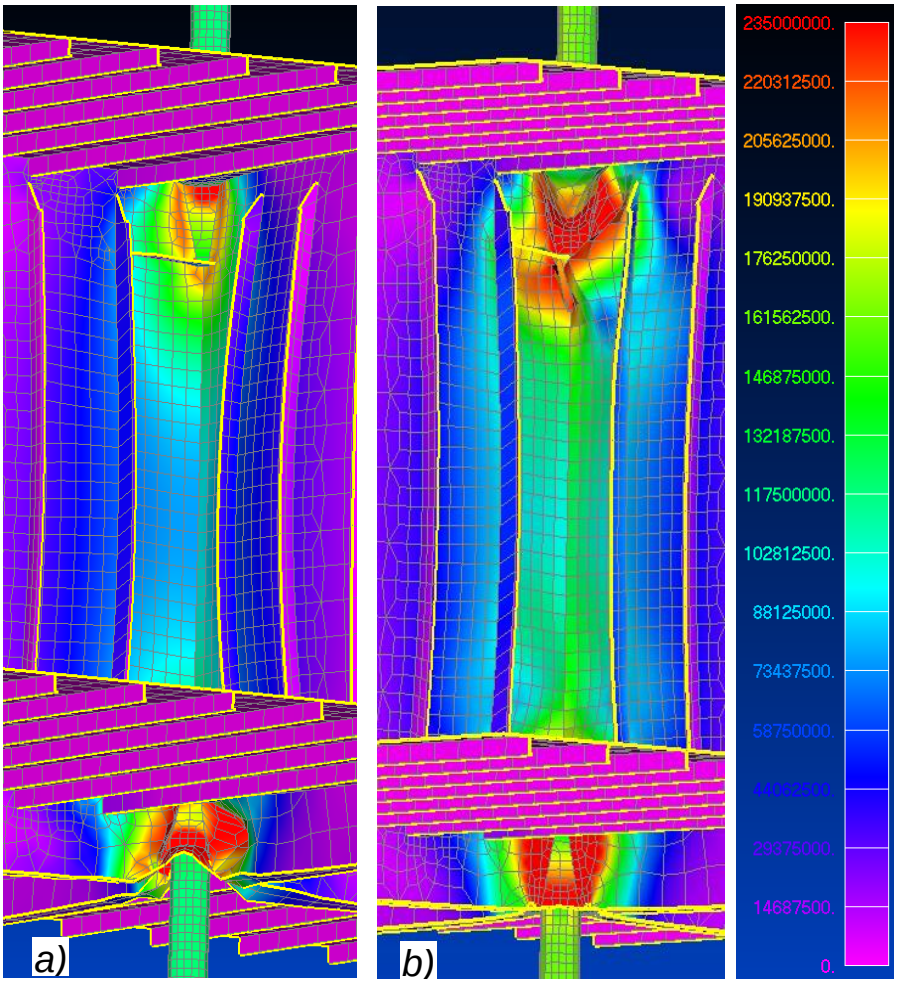

Figure 61. 10/10 bulkhead intersection GMNIA. The deformed shape and stress distribution at limit points. Von Mises Stress.

a) - deck beam webs 7.0 235 Mpa, step at the load factor = 3.35. The deck beam webs buckled.

b) - deck beam webs 10.0 355 Mpa, step at the load factor = 4.49. The bulkhead plates buckled.

Deformation patterns of the models at the limit points of the load-displacement functions for 10/10 case can be seen in Figure 61. Animations of the analyses can be found in Appendix A.

It can be noted that the load-displacement curves for the 6/6 bulkhead intersection are almost identical for analyses with deck beam webs of 7.0 mm A grade and 10.0 mm A36 grade (Figure 60). This is because the failure is induced by the bulkhead plate buckling in both cases (Figure 62).

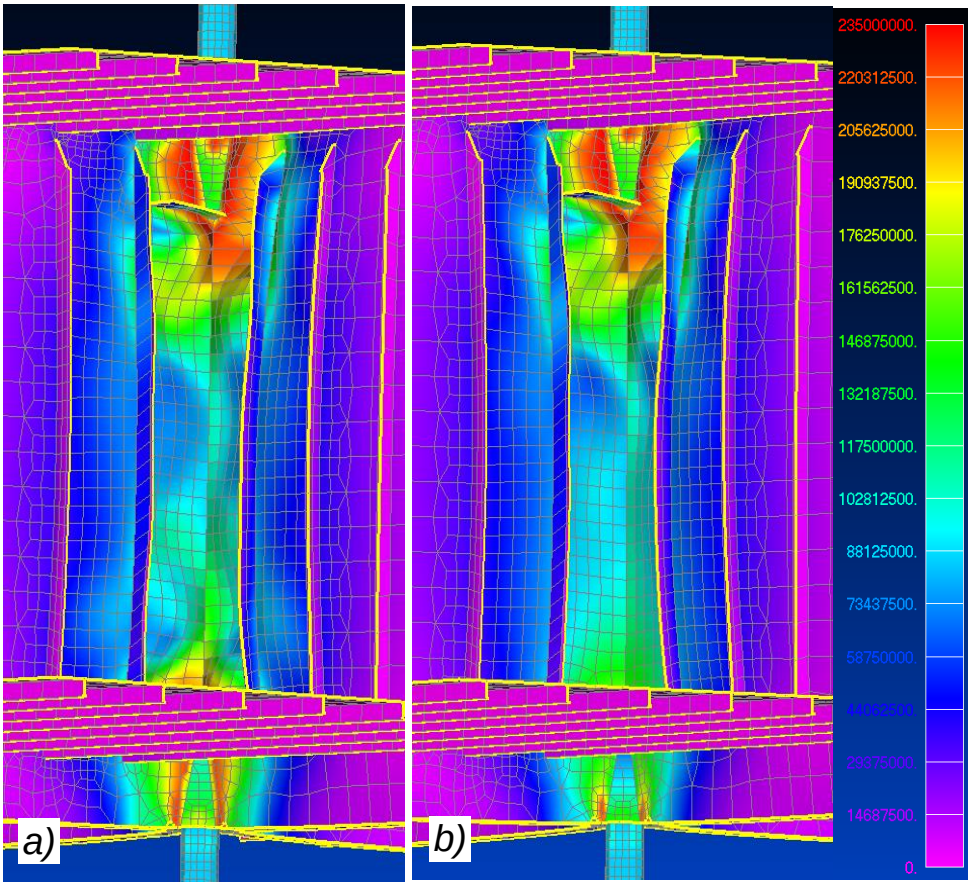

Figure 62. The deformed shape and stress distribution of GMNIA for 6/6 bulkhead intersection. The bulkhead plates buckled.
a) - deck beam webs 7.0 235 Mpa
b) - deck beam webs 10.0 355 Mpa

8.3 Findings and discussion

During the study on bulkhead intersections, it was found that due to the typical structural configuration of the pillar connection, when the pillar is approaching the bulkhead intersection from below, the loading capacity of the structure might be limited by the shearing capacity of the deck beam webs, not by the capacity of the bulkhead intersection-structure itself.

This fact is particularly critical for designers to recognize in the case of bulkhead intersections, as those consisting of two thick bulkheads or those made with high strength steel are considered very strong and capable of carrying high pillar loads and are therefore often are not subjected to any standardized capacity checking procedure.

Deck beam web failure in such cases also is not directly identifiable by global FE-analysis due to simplifications and detailing-level of the global model, as nodes of beam-elements that represent pillars are connected with nodes of the bulkhead plate's shell elements (Figure 63).

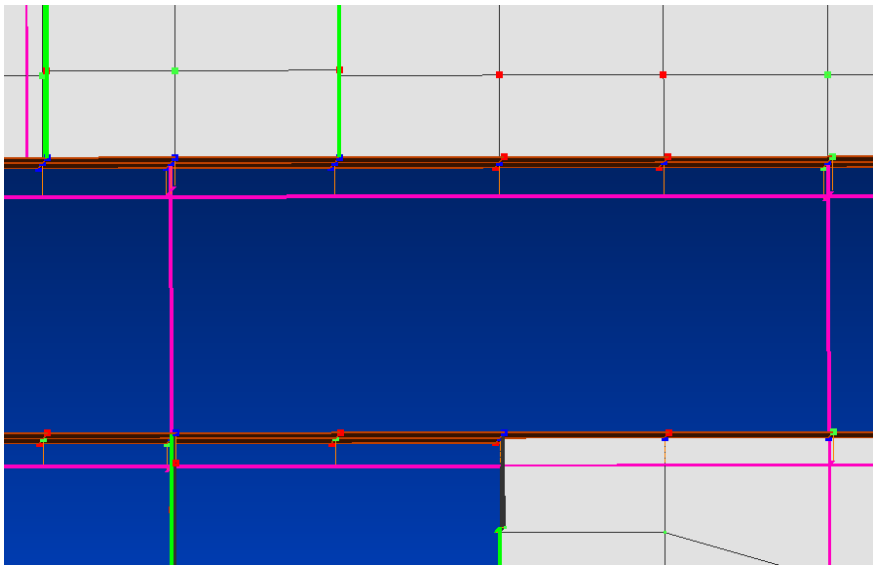

Figure 63. Simplifications in a global FE-model. Connection of pillars to the bulkheads.

9 DISCUSSION

9.1 Summary of findings and recommendations

In the present thesis, recommendations and main discussion related to the results of each research phase are provided at the end each chapter. A summary of the major findings and recommendations with reference to the relevant chapters are presented in the following.

Analyses in the thesis-related research were conducted on studied structures using Geometrically and Materially Non-linear Finite Element Method with Imperfections. After review of related literature and testing of different non-linear solution schemes, the method with displacement control was selected for the research (Section 4.2.6). The method with the selected solution scheme showed its effectiveness in solving the nonlinear equilibrium paths until collapse and also in being able to determine the post-buckling response for relatively complex structures.

The method validation study conducted on idealized structures, for which analytical solutions are well established, showed good correlation between the analytical solutions and GMNIA results, justifying the usage of the method with selected settings, solution scheme, and boundary conditions for more complex models (Section 5.1).

The studied realistic intact bulkhead structures showed relatively low imperfection sensitivity for imperfection amplitudes within typical manufacturing tolerances (Section 6.4). Different manufacturing tolerance related standards, surveys, and studies on deviations in real ship structures were considered when selecting the amplitudes for the imperfection sensitivity study. Evidently, the observed low imperfection sensitivity, among other factors, is due to the constraints provided by continuous stiffened bulkhead plate and inherent eccentricity that guide global deformations in a certain direction. Moreover, the fact that some of the studied structures experience failure governed by material yielding results in low imperfection sensitivity.

Whereas a comprehensive imperfection study with different types of initial distortions was not conducted on idealized columns, for the applied lowest eigenmode-based imperfection type, those showed much higher imperfection sensitivity compared to the realistic intact bulkhead structures (Section 5.1).

A systematic slight overestimation of the buckling capacity by the analytical Closed Form Method compared with GMNIA was observed during the study on idealized columns (Section 5.1), particularly to those with stiff flanges and high webs. It was assumed that the deviation might be due to the difference in applied imperfection shapes and amplitudes compared with those integrated in CFM though plasticity correction models. The deviation was minimized by the replacement of the Johnson-Ostenfield plasticity correction in the analytical method with correction by European buckling curves in accordance with Eurocode 3 (Section 5.1.3).

Due to the typical configuration of the studied structures, there is always an eccentricity existing between pillar- and T-column centroids. The eccentricity is often neglected during the column buckling capacity verifications with simplified analytical methods. The scale of the effect of the eccentricity was studied (Section. 5.2 and 7.1). It was shown that for T-columns with relatively low web, the eccentricity has a minor impact on the failure mode and the buckling capacity and might be neglected when checking with simplified analytical methods. However, as the height of the T-column web grows, the eccentricity begins to have an increasingly notable impact on the capacity. It was shown that, due to the column bending and shear lag, flange effectiveness decreases, and, starting from a certain point, increasing the column web height further would not give any gain in capacity for the column, which might otherwise be expected if the eccentricity is not taken into account (Sections 5.2 and 7.1.4.3). A correlation between the buckling mode changes due to the eccentricity and buckling capacity decrease was observed (Section 5.2.2, Tables 8 and 9).

The load-shedding effect was observed during non-linear analyses, which resulted in lower peak-stress values in non-linear-analyses of the same models compared with linear ones. The effect is briefly discussed in Section 7.1.3.

For realistic continuous bulkhead structures studied in Section 7.1, it was shown that when the pillar approaches the bulkhead structure with the T-column from below, the weakest part of the structure is often not the column, which is subjected to the buckling capacity verification during a standard procedure, but rather the deck beam webs (Section 7.1.4.1). This is due to the typical standardized pillar-to-bulkhead connection, as the pillar force is transferred to the bulkhead structure mainly by shear in aforementioned webs. Based on this finding, the author recommends including the deck beam web stress level and shear buckling capacity checking in a bulkhead’s capacity against the pillar forces verification procedure, along with checking of the buckling capacity of the T-columns.

Special attention must be given to places where the pillar is approaching the bulkhead intersection from below, as the similar failure mechanism of the deck beam webs is also inherent to such structures (Section 8.1). The intersections of two bulkheads, as was shown in Section 8.2, are capable of carrying very high loads; however, it must be recognized by designers that due to the standard pillar-to-bulkhead connection, in case of extreme loads, the deck beam webs may fail before the capacity of the bulkhead intersection is reached. The failure is not identifiable by global FEM analysis due to simplifications of the global FE-model (Section 8.3).

In future projects, in order to minimize the risks, it was recommended to consider applying the high strength grade steel instead of normal strength steel for all webs of deck beams positioned at intersections with pillar lines, in particular for those of lower decks. The capacity of the pillar-to-bulkhead connections when the pillar is approaching from below will thus be increased by about 50% with no increase in weight. Taking into account the typical pillar force magnitudes in large cruise ships, it was estimated that the capacity of the connection will then be sufficient to cover most of the cases, excluding the extreme ones, while connections with typical minimum deck beam web thicknesses made of normal strength steel are not sufficient against the upper bound of typical pillar force magnitudes.

It was shown that for cases when the pillar is approaching the bulkhead from above, for relatively stiff columns and due to the geometry of standardized pillar-to-bulkhead connection, the failure may occur in the upper bulkhead plate region adjacent to the pillar connection due to high shear stress (Section 7.1.4.2). A checking mechanism that will ensure that the stress level in the region of the upper pillar connection to the bulkhead would not exceed the permissible level needs to be included in the capacity verification procedure, in particular for cases with thin bulkhead plates made of normal stress steel. One feasible approach might be setting limit values of pillar forces for different typical bulkhead thicknesses and material grades.

The current simplified analytical method that is often used for estimating the capacity of the bulkhead structures positioned in the way of pillars was critically reviewed against GMNIA results. It was shown that for intact bulkhead structures, the simplified CFM method insufficiently takes into account the actual capacity of the stiffened bulkhead structure against the pillar load. For most of the cases, the method may be considered a conservative when checking the buckling capacity of the bulkhead's columns; in some cases, however, it may lead to overly conservative designs. On the other hand, analytical

methods might make it difficult to account for all possible local failure modes, including those that occur due to the inherent eccentricity.

An alternative practical approach that utilizes standardized solutions with design capacities verified with direct strength calculations, similar to those conducted during the thesis, was considered (Section 7.1.4.4). The potential to decrease the number of default standard columns to be strengthened in ship design projects was recognized, as it was demonstrated that the actual capacity of the intact bulkhead structures with standard default columns in many cases is higher than expected when relying on the simplified analytical solution. The proposed approach conforms to the trend of the standardization of structural solutions. With this approach, local failure modes as well as eccentricity effects would be naturally accounted for.

It has been demonstrated that openings in bulkheads positioned close to the pillar line may lead to different failure modes than those experienced by corresponding intact structures (Section 7.2). One feasible approach could be the development of typical strengthening solutions for openings positioned close to the pillar lines, which would guarantee, that the ultimate capacity of the structure with openings is not lower than the set design capacity for each T-column size.

For cases with extreme values of pillar loads, the solution with the closed section pillar in the middle of the bulkhead or an equivalent solution was recommended (Section 7.1.4.5).

9.2 Future work

In the present research, analyses were conducted on vertically stiffened bulkheads. While, recent trends favor more vertically stiffened bulkheads in cruise ship designs due to manufacturing reasons, horizontally stiffened bulkheads are still common in hull structures. Particularly for main longitudinal bulkheads, longitudinal stiffening is usually applied as it better contributes to longitudinal strength against global bending of the hull girder. It would be of interest to compare the behavior and capacity of otherwise identical bulkheads but with different stiffening directions. Thus, it would be beneficial to conduct analyses on longitudinally stiffened bulkheads under point loads.

Most of the analyses conducted in the study were done on bulkheads and columns made of material with a yield strength of 235 MPa. It might be beneficial to perform analyses for bulkheads made of material with a yield strength of 355 MPa, as those are very

common in hull structures. It is expected that for some of the structures, the yielding-dominant problems will then turn into buckling-dominant problems.

The lowest modes were used for elastic eigenmode-shape-based imperfections in the study. It might be of interest to check the impact of imperfection shapes that are constructed from combinations of a number of elastic buckling modes and, perhaps, applied with higher amplitudes.

The vibrational behavior of the bulkhead structures in the way of pillars was not considered in the research and might be of interest for further studies.

The solution with the T-column is considered “production-friendly” and economically more effective than the solution with the closed-section pillar positioned in the middle of the bulkhead as described in Section 7.1.4.5. As the second approach with a closed-section pillar is structurally more efficient, it might be of interest to conduct the quantitative economic justification for usage of the former one.

10 CONCLUSION

The behavior and failure mechanisms of the bulkhead structures positioned in the way of pillars under compressive point loads were studied in this thesis using Materially and Geometrically Non-linear Finite Element method with imperfections. More than 50 local FE-models for different configurations and structural member sizes were made, with the number of conducted GMNIA analyses being about double that, providing a vast coverage on the behavior of bulkheads with different typical structural arrangements existing in ship hulls.

The procedure that is based on simplified analytical methods and is often used for checking the capacity of such structures was critically reviewed against results of GMNIAs. Even though the analytical method that is included in the procedure showed good correlation with GMNIA results for the idealized columns, its direct applicability to the real ship structures remains open to discussion.

It was shown that the real intact bulkhead structure often fails with the local yielding either in the region of lower or upper pillar connection and not with column buckling. This is mostly due to the nature of the standardized pillar-to-bulkhead connections, as the pillar load is transferred to the column mostly by the shear through plated elements, the shearing capacity of which might be lower than the buckling capacity of the bulkhead structure. Thus, simply checking the structure against the buckling capacity of the column is not sufficient. Recommendations concerning the checking procedure supplementation have been made.

Concerning the applicability of the CFM to the determination of the buckling capacity of the column when the possibility of local failure is eliminated, it was shown that the load carrying capacity of the intact bulkhead structure is higher than the capacity prediction in accordance with the current simplified analytical method. Whereas some preliminary considerations have been made as to how to better account for boundary conditions existing in real intact structure when analytically estimating the column buckling capacity, the subject of developing a comprehensive analytical method that will better account for the total capacity of the stiffened bulkhead structure, compared with current approach with the effective flange, remains for the future studies.

Generally speaking, due to the complexity of the structure and wide variety of possible configurations in real structures, it is difficult and may be also impractical to try to derive a universal analytical method that would predict with sufficient accuracy the capacity,

taking into account all the different possible global and local failure modes. An alternative practical approach that relies on typical solutions, the loading capacity of which is verified with direct strength calculations, was proposed.

Impact of the inherent eccentricity in load application due to the typical configuration of the structure was considered. It was shown that for columns with low web height, the eccentricity has a low significance in terms of the column buckling capacity and might be neglected during simplified analytical checks, such as was often done before. However, with the growth of the web height, the column flange becomes increasingly ineffective and, for such columns, eccentricity should be accounted.

Effective strengthening strategies and capacity estimation methods should be failure mode dependent. Better understanding of the behavior of the typical structure and an accounting of all of the possible failure modes will decrease the risk of systematic design mistakes and thus decrease the structural failure risk levels. The number of analyses conducted during the research on typical structures, both intact and with openings, with different structural arrangements and member sizes provides a broad overview on the behavior of the structures and on their typical failure modes. Taking into account given recommendations, it would contribute to the development of more reliable capacity-verification approaches and strengthening strategies for more effective designs.

REFERENCES

ABS, 2021. Guidance notes on Nonlinear Finite Element Analysis of marine and offshore structures. American Bureau of Shipping.

Amdahl, J. 2005. TMR4205 *Buckling and Ultimate Strength of Marine Structures, Chapter 3: Buckling of Stiffened Plates.* NTNU.

Baroudi, D., 2020. *Elastic Stability of structures. Lecture notes of the course "Stability of Structures".* Otaniemi.

Basar, N.S., Stanley R.F., Rosenblatt & Son, Inc. 1978. *Survey of structural tolerances in the united states commercial shipbuilding industry.* Ship Structure Committee. Washington. D.C.

Bathe, K-J, 2014. *Finite Element Procedures.* Second edition. Watertown, MA: K.J. Bathe

Becker, A. A., 2002. *Understanding Non-linear Finite Element Analysis Through Illustrative Benchmarks.* Scottish Enterprise Technology Park, East Kilbride, Glasgow: NAFEMS Ltd

Beer, F.P., Johnston. E.R.Jr, DeWolf, J.T. and Mazurek, D.F., 2015. *Mechanics of Materials, 7th Edition.* New York: McGraw Hill Education.

Beg, D., Kuhlmann, U., Davaine, L., Braun, B. 2011. *Eurocode 3: Design of Steel Structures, Part 1-5.* Ernst & Sohn

Brodnianskya, J., Árocha, R., Belicab, A., 2014. *Unique global and local initial imperfection in the shape of the elastic buckling mode. Application for frames with Class 4 cross-sections.* EUROSTEEL 2014, September 10-12, 2014, Naples, Italy

Bruchman, D., Kihl, D.P., Adamchak, J.C. 2000. *Evaluation of the effect of construction tolerances on vessel strength.* Ship Structure Committee. Washington, DC

Buckling of transverse bulkheads. 2018. Future of the Ocean. Retrieved from: https://futureoftheocean.com/bulkheadsbuckling1 [Accessed 27.06.2021]

CEN, 2006. EN 1993-1-5. *Euocode 3: Design of steel structures. Part 1-5 General rules - Plated structural elements.* European Committee for Standardization (CEN), Brussels, Belgium

Clarkson, J. 1965. *The Elastic analysis of Flat Grillages with Particular Reference to Ship Structure.* Cambridge University Press.

Cox, H.L., 1945*. The buckling of a flat rectangular plate under axial compression and its behavior after buckling.* Aero Res Council, Rep Memo 2041.

Crocombe, A. 2001. How to tackle Non-Linear Finite Element Analysis.NAFEMS ltd.

DNV GL, 2013. *DNV-RP-C208: Recommended practice - Determination of Structural Capacity by Non-linear FE analysis Methods.* DNV GL AS.

DNV GL, 2015. DNVGL-OS-B101: Offshore standard - Metallic materials. DNV GL AS.

DNV GL, 2016. *DNVGL-CG-0138: Direct strength analysis of hull structures in passenger ships.* DNV GL AS.

DNV GL, 2018 a. *Rules for classification: Ships.* DNV GL AS.

DNV GL, 2018 b. *DNVGL-CG-0128: Class Guideline – Buckling.* DNV GL AS.

DNV GL, 2020. *DNVGL-CG-0127: Class Guideline - Finite element analysis.* DNV GL AS.

Ellobody, E., Feng, R. and Young, B., 2013. *Finite Element Analysis and Design of Metal Structures.* Oxford: Elsevier Science & Technology.

Estefen, S.F., Chujutalli J. H., Soares, G., 2016. Influence of geometric imperfections on the ultimate strength of the double bottom of a Suezmax tanker. *Engineering Structures*, 127 (2016) 287–303. Elsevier.

Evans, J.H., 1975. *Ship Structural Design Concepts.* Cornell Maritime Press. Centerville, MD.

Eyres D.J, 2001. *Ship Construction.* Fifth edition. Butterworth-Heinemann. Oxford.

Fagerberg, L., 2003. *Wrinkling of Sandwich Panels for Marine Applications.* KTH Royal Institute of Technology. Stockholm.

Falzon B., G. and Hitchings, D. 2006. *An introduction to modelling buckling and collapse*. 2-nd ed. East Kilbride, Glasgow: NAFEMS (The International Association for the Engineering analysis Community)

Faulkner, D. 1975. A review of Effective Plating to be Used in the Analysis of Stiffened Plating in Bending and Compression. *Journal of Ship Research*, 19(1), 1-17.

Hellen, T.K., & Becker, A.A., 2013. *Finite Element Analysis for Engineers – A Primer.* East Kilbride, Glasgow: NAFEMS

Hilton, E., (Ed.) 1992. *Introduction to Nonlinear Finite Element Analysis.* East Kilbride, Glasgow: NAFEMS

IACS, 2013. *Recommendation No.47. Shipbuilding and Repair Quality Standard.* International Association of Classification Societies Ltd.

Jönsson, J., Stan, T.C., 2017. European column buckling curves and finite element modelling including high strength steels. *Journal of Constructional Steel Research*, 128, 136-151.

Kelly, P., 2013. *An introduction to solid mechanics*. Lecture Notes. The University of Auckland.

Lindgaard, E., Lund, E., Rasmussen, K., 2010 Nonlinear buckling optimization of composite structures considering ‘‘worst” shape imperfections. *International Journal of Solids and Structures* 47 (2010) 3186–3202. Elsevier.

Lloyd´s Register, 2017. *ShipRight. Design and Construction. Structural Design Assessment. Procedure for Primary Structure of Passenger Ships.*

Łukasz Skotny. 2017. *How to correctly interpret results in nonlinear analysis.* Retrieved from: https://enterfea.com/nonlienar-fea-how-to-correctly-interpret-results-part-1/ [Accessed 27.06.2021]

Marguerre, K., 1937. The Effective Width of a Plate Under Compression. Translated NACA Technical Note 833, Original in *Luftfahrt Forschung*, 14(3), 121.

Meyer Turku, 2019. *Dimensional control plan in Turku Shipyard in NB1400 project.*

Meyer Turku, 2016. *Dimensional tolerances in hull structures.*

Prabu, B., Raviprakash, A., Rathinam, N. 2012. Numerical buckling analysis of thin cylindrical shells with combined distributed and local geometrical imperfections under uniform axial compression. *International Journal of Computer Aided Engineering and Technology. Vol. 4 (2012): 295-320.*

Ratcliffe A.T., 1968. *The strength of plates in compression*. PhD Thesis. Cambridge University.

RINA. 2017. *Rules for the classification of ships. Part B. Hull and stability.* Genova: RINA S.p.A.

Saha, S.K., & Culpepper M.L., 2014. *MATLAB codes for mesh perturbation and automated pre and post processing of post-bifurcation analyses via COMSOL.* Massachusetts Institute of Technology.

Sheikh, I.A., Grondin, G.Y. and Elwi, A.E., 2002. Stiffened steel plates under uniaxial compression, *Journal of Constructional Steel Research*, Volume 58, pp 1061-1080, 2002.

Siemens, 2006. *NX Nastran 11. Advanced Nonlinear Theory and Modeling Guide.* Siemens Product Lifecycle Management Software Inc.

Siemens, 2016. *Element Library Reference.* Siemens Product Lifecycle Management Software Inc.

Siemens, 2017. *Basic Nonlinear Analysis User's Guide.* Siemens Product Lifecycle Management Software Inc.

The Steel Construction Institute. 2012. *Determining the buckling resistance of steel and composite bridge structures.* Technical Report (SCI ED008). Imperial College London.

Titarenko, F. (n.d.) *Just about nonlinear finite element analysis. Bracket example.* Retrieved from: https://tech-en.netlify.app/articles/en515120/ [Accessed 27.06.2021]

Tupper, E. 1996. *Introduction to Naval Architecture*. Third edition. Butterworth-Heinemann. Oxford.

Witkowska, M., Soares, G 2015. *Ultimate strength of locally damaged panels.* Centre for Marine Technology and Ocean Engineering (CENTEC), Instituto Superior Técnico, Universidade de Lisboa, Portugal

X-Y Ni., Prusty, B.G., Hellier, A.K., 2000-2012. Buckling and post-buckling of isotropic and composite stiffened panels: a review on analysis and experiment. Transactions of the Royal Institution of Naval Architects Part A: *International Journal of Maritime Engineering* 157(January-March):A-9 - A-29

Bai, Y., 2003. Marine Structural Design. Elsevier Science. Kidlington, Oxford.

Yoo, C.H., & Lee S.C., 2011. Stability of structures. Principles and Applications. Butterworth-Heinemann. New York.

APPENDIX A. ANIMATIONS OF THE NUMERICAL SIMULATIONS

Animations of the numerical simulations can be found in the power point slideshow, attached as a separate file “Appendix_A.pptx” (38 slides)